Regulation of ESCRT endosomal recruitment by the lipid-binding protein ALIX

Larios, Jorge

UNIVERSITÉ DE GENÈVE

FACULTÉ DES SCIENCES

Section de chimie et biochimie
Département de biochimie

Professeur Jean Gruenberg
Professeur Aurélien Roux

Regulation of ESCRT Endosomal Recruitment by the Lipid-binding Protein ALIX

THÈSE

présentée à la Faculté des sciences de l'Université de Genève
pour obtenir le grade de Docteur ès sciences, mention biochimie

par

Jorge LARIOS

de

Poschiavo (GR)

Thèse N°5220

GENÈVE
Atelier de reproduction ReproMail
2018

UNIVERSITÉ
DE GENÈVE
FACULTÉ DES SCIENCES

DOCTORAT ÈS SCIENCES, MENTION BIOCHIMIE

Thèse de Monsieur Jorge LARIOS

intitulée :

«Regulation of ESCRT Endosomal Recruitment by the Lipid-binding Protein ALIX»

La Faculté des sciences, sur le préavis de Monsieur J. GRUENBERG, professeur honoraire et directeur de thèse (Département de biochimie), Monsieur A. ROUX, professeur associé et codirecteur de thèse (Département de biochimie), Monsieur T. SOLDATI, professeur associé (Département de biochimie) et Monsieur H. STENMARK, professeur (Department of Molecular Cell Biology, Institute for Cancer Research, The Norwegian Radium Hospital, Oslo, Norway), autorise l'impression de la présente thèse, sans exprimer d'opinion sur les propositions qui y sont énoncées.

Genève, le 28 mai 2018

Thèse - 5220 -

Le Doyen

N.B. - La thèse doit porter la déclaration précédente et remplir les conditions énumérées dans les "Informations relatives aux thèses de doctorat à l'Université de Genève".

A mi madre,

que ha sido una inspiración a lo largo de toda mi vida

Acknowledgements

First and foremost, I would like to express my sincere gratitude to my thesis advisors Prof. Jean Gruenberg and Prof. Aurélien Roux, for the continuous support during my Ph.D studies and research, the motivation and enthusiasm that they always expressed, and the immense knowledge shared with me. Thank you Jean for your confidence, support and for always taking time to answer my questions. Aurélien, I would like to thank you for your empathy and your scientific advice, which was always very accurate. Specially, I thank you both for giving me the space necessary to develop my creativity.

I would like to thank Prof. Thierry Soldati and Prof. Harald Stenmark for agreeing to be in my thesis committee. It is of great value to me that you have taken this time to evaluate my thesis.

To all the present and former members of the Gruenberg and Roux laboratories; thank you very much! I had the perfect friendly environment to work during these years. Cameron, thank you for answering all my questions, you became my cell biology dictionary. Thank you Nico for always being ready to help. Thank you Shem for promoting a lab collaborative spirit and always share your crazy ideas. I am also very grateful to Stefania. Thank you for the nice discussions! Special thanks to Marie-Claire for the hard work cloning all the plasmids and Marie-Hélène for taking care of the laboratory organization. Thank you Brigitte for all the help and advice regarding cell culture.

I am also grateful to my collaborators Daniel and Prof. Adibekian for their help and support. I thank the members of the Biochemistry Department, the Bioimaging Platform for their help and cooperation.

This would not have been possible without my friends! Thank you for being there and all the great moments shared. You should know that your support and encouragement was worth more than I can express here. Special thanks to Ilaria for taking time to make corrections to the thesis. Also, thank you for your easy going and cheerful personality. I would also like to thank Nicole Bok for her support and guidance.

A special thanks to Nicole Preston for her affection and kindness during my Ph.D.

I am particularly grateful to my family, for their love and endless support.

Se pasaron! Jorge

Table of Contents

Summaries

English summary of the thesis

Endocytosis is the process by which cells take up nutrients, solutes and components of the plasma membrane. Internalized cargo reaches compartments called endosomes, which are specialized for sorting of endocytosed material. One of the routes that internalized cargo follows is the pathway to the lysosome, where proteins, lipids and other macromolecules are degraded. This route is necessary for the downregulation of several transmembrane proteins, such as signaling receptors. Within this pathway, the proteins destined for degradation must be delivered to intraluminal vesicles (ILVs), which are eventually degraded with cargo in the lysosomes. Endosomes that contain intraluminal membranes are called multivesicular endosomes (MVEs).

The endosomal sorting complexes required for transport (ESCRT) is a multiprotein complex that participates in processes which require membrane deformation, such as cytokinetic abscission, virus budding and MVE biogenesis. The canonical ESCRT pathway for ILV formation requires four ESCRT complexes, ESCRT-0, -I, -II and –III, which participate in cargo sorting and membrane remodeling. ESCRT-III has been extensively described as a key player in the deformation and fission of membranes. Several ESCRT-associated proteins participate in the ESCRT pathway, one of these being the apoptosis-linked gene 2-interacting protein X (ALIX). Previous work in our lab has shown that ALIX interacts with lysobisphosphatic acid (LBPA), also called bismonoacyl glycerophosphate (BMP), a lipid that has been detected exclusively in late endosomes. ALIX also interacts with two ESCRT proteins, tumor susceptibility gene 101 (TSG101) and charged multivesicular body protein 4 (CHMP4), proteins of the ESCRT-I and –III complexes, respectively. ALIX and LBPA participate in the formation of ILVs, yet the mechanism by which they act and their link to the ESCRT machinery is unknown.

The aim of this work is to elucidate the role of ALIX in the recruitment of ESCRTs to the endosomal membranes and its effect on endosomal protein sorting.

We show that an active form of ALIX, lacking its proline rich region (ALIXΔPRR), is highly recruited (compared to full ALIX) to late endosomes. ALIXΔPRR directly recruits ESCRT-III proteins, mainly CHMP4, and this recruitment is dependent on the interaction of ALIX with

LBPA. *In vitro* experiments also show that the presence of LBPA containing membranes and ALIX alone is sufficient to recruit CHMP4. This recruitment is independent of ESCRT-0, -I and –II, and is also independent of CHMP6, a nucleation factor for CHMP4 membrane recruitment and polymerization.

The expression of ALIXΔPRR induces the accumulation of ubiquitinated proteins in endosomes. By mass spectrometry, we found several hits of transmembrane proteins accumulated in the endosomes of cells exogenously expressing ALIXΔPRR. A subset of these hits were selected and the role of ALIX with respect to the endosomal sorting of these proteins was further investigated. Furthermore, the role of ALIXΔPRR was also investigated during autophagy and exosome biogenesis.

Altogether, the data presented here underlies the importance of ALIX and LBPA in the endosomal recruitment of ESCRT-III and in the sorting of specific cargo. We describe a route that permits the recruitment of the ESCRT-III machinery to late endosomes, representing an ESCRT pathway alternative to the canonical pathway.

Résumé de la thèse en francais

L'endocytose est le procédé par lequel les cellules importent nutriments, solutés et constituants de la membrane plasmique. Une fois internalisés, les cargos rejoignent des compartiments spécialisés dans le tri du matériel endocyté, appelés endosomes. L'un des chemins que les cargos internalisés peuvent alors suivre est la voie menant au lysosome, ou protéines, lipides et autres macromolécules sont dégradés. Ce processus est nécessaire à la régulation négative de différentes protéines transmembranaires, comme les récepteurs de la signalisation cellulaire. Au sein de cette voie, les protéines devant être dégradées sont acheminées jusqu'aux vésicules intraluminales (ILVs), qui seront finalement dégradées avec leur cargos au sein des lysosomes. Les endosomes contenant des membranes intraluminales sont appelés endosomes multivésiculaires (MVEs).

Les complexes de tri endosomaux nécessaires au transport (ESCRT) sont des complexes multiprotéiques participant aux processus cellulaires qui requièrent une déformation de la membrane, comme l'abcission pendant la cytokinèse, le bourgeonnement des virus ou la biogenèse des MVE. La voie ESCRT classique impliquée dans la formation des ILVs comporte quatre complexes ESCRT, ESCRT-0, -I, -II, et –III, qui participent au tri des cargos et au remodelage de la membrane. ESCRT-III a été en particulier décrit en détail comme un acteur essentiel dans les mécanismes de déformation et de fission des membranes. Plusieurs protéines associées aux complexes ESCRT sont également impliquées dans cette voie, et notamment ALIX (ALG-2-interacting protein X). Des travaux précédents de notre groupe ont montré qu'ALIX interagissait avec l'acide lysobiphosphate (LBPA), aussi appelé bimonoacyl-glycérophosphate (BMP), un lipide exclusivement présent au niveau des endosomes tardifs. ALIX interagit également avec deux protéines ESCRT, TSG101 (tumor susceptibility gene 101) et CHMP4 (charged multivesicular body protein 4), faisant respectivement partie des complexes ESCRT-I et –III. ALIX et le LBPA sont impliqués dans la formation des ILVs, cependant leur mode d'action ainsi que leur lien précis avec la machinerie ESCRT restent inconnus.

L'objectif de cette étude est ainsi de définir le rôle joué par ALIX dans le recrutement des ESCRTs à la membrane des endosomes et dans le tri des protéines au niveau des endosomes.

Nous avons démontré qu'une forme activée d'ALIX, dépourvue de son domaine riche en proline (ALIXΔPRR), est recrutée plus efficacement au niveau des endosomes tardifs que la protéine entière. ALIXΔPRR recrute directement des protéines du complexe ESCRT-III,

principalement CHMP4, et de de façon dépendante de son interaction avec le LBPA. Des expériences *in vitro* ont aussi montré que la présence d'ALIX et de membranes contenant du LBPA est suffisante pour recruter CHMP4, indépendamment des ESCRT-0, -I et –II, mais également de CHMP6, un facteur de nucléation pour le recrutement et la polymérisation de CHMP4 à la membrane.

L'expression d'ALIXΔPRR entraîne une accumulation de protéines ubiquitinilées au niveau des endosomes. Par spectrométrie de masse, nous avons détecté plusieurs protéines transmembranaires accumulées dans les endosomes de cellules exprimant ALIXΔPRR de façon exogène. Nous avons sélectionné certaines de ces protéines pour examiner plus en détail le rôle joué par ALIX dans leur tri au niveau des endosomes. Par ailleurs, nous avons également étudié de rôle d'ALIXΔPRR dans l'autophagie et la biogenèse des exosomes.

Les données présentées dans cette étude soulignent l'importance d'ALIX et du LBPA dans le recrutement du ESCRT-III et le tri de cargos spécifiques. Nous décrivons une voie permettant le recrutement de la machinerie ESCRT-III au niveau des endosomes tardifs, constituant une alternative à la voie ESCRT classique.

Introduction

1. The endocytic pathway

Cell sensing and response to its environment is a highly regulated process. The outer leaflet of the plasma membrane, which is in direct contact with extracellular signals, has a specific content of lipids and proteins that facilitate the activation of multiple intracellular pathways. The internalization of proteins by invagination and fission of the plasma membrane, called endocytosis, is the main process used by eukaryotic cells to regulate the diversity and amount of receptors exposed to external signals. Additionally, many pathogens use the endocytic routes to mediate their internalization into cells. The internalized plasma membrane travels inside the cells as lipid vesicles that fuse with intracellular membrane compartments called endosomes (Fig 1).

1.1. The endosomal-lysosomal system

Cells have developed a complex system of endosomes that are interconnected not only between them, but also with other organelles, such as the trans-Golgi network (TGN) and the vacuole/lysosomes [for review see (Scott et al. 2014)]. Cargo proteins and lipids internalized from the plasma membrane reach a first compartment called early endosome (EE). The EE is a tubulovesicular sorting station from where endocytosed molecules can be recycled back to the plasma membrane, through a recycling endosomes/endocytic recycling compartment (RE/ERC), or targeted to lysosomes. Lysosomal compartments contain a wide variety of hydrolytic enzymes that break down molecules such as lipids, proteins and polysaccharides. Before reaching the lysosomes, EEs maturate into late endosomes (LEs) [for review see (Huotari and Helenius 2011)]. Similarly to EEs, LEs also work as a sorting station for lipids and proteins and can fuse with lysosomes for degradation of cargo. One morphological characteristic of LEs, also called MVE, is that they are packed of luminal lipids arranged as small vesicles (ILVs) [for review see (Helenius et al. 1983)]. ILVs are formed by the invagination of the limiting membrane of EEs, and they are thought to travel and accumulate in LEs. Together with the sorting of lipids to the lumen of endosomes during ILV formation, some integral membrane proteins or membrane-associated proteins can also be packed into ILVs. This process is crucial for the efficient downregulation of cell membrane

receptors by lysosomal degradation, presumably by increasing the contact of the luminal hydrolases with their substrates (Fig 1).

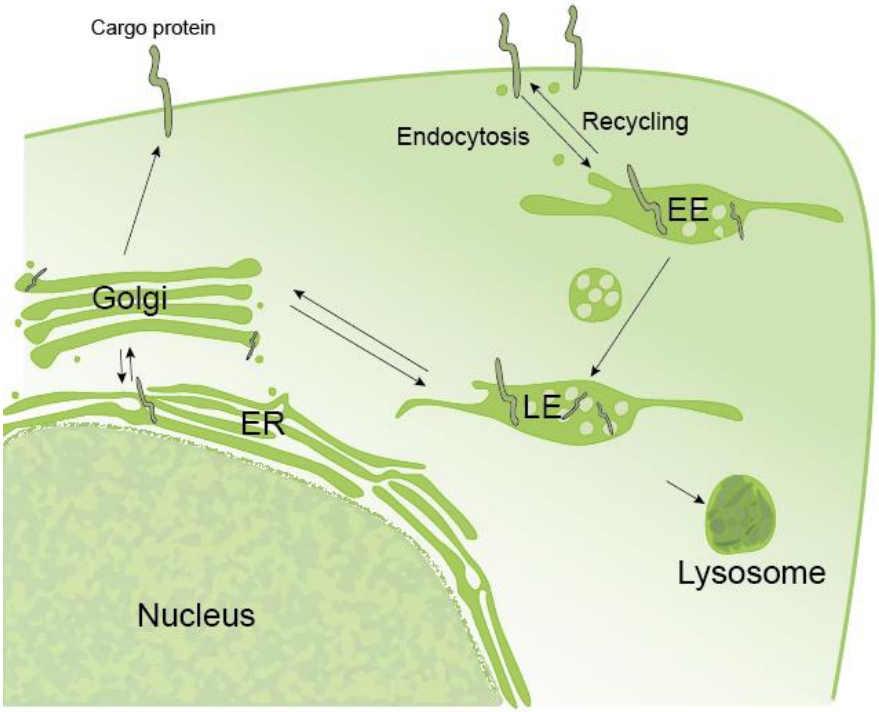

Figure 1. Membrane trafficking pathways. Trafficking routes of lipid vesicles and a transmembrane protein (cargo protein) within an eukaryotic cell. ER: Endoplasmic reticulum; EE: early endosome; LE: late endosome.

1.2. Specific lipid and protein markers in different compartments: endosomal identity

Proteins and lipids are the main components that provide identity to endosomes. The endosomal compartments are also characterized by their luminal pH. The endosomal internal pH decreases along the endocytic pathway from EEs (pH 6.0), LEs (pH 5.0) to lysosomes (pH 4.5) (Fig 2) (Yamashiro and Maxfield 1987a; Yamashiro and Maxfield 1987b). This acidification event regulates a big diversity of processes, such as enzymatic activity, cargo protein and ligand affinity, virus escape to the cytosol and the biophysical properties of lipid membranes.

Here I discuss the function of the RAB (Ras-related protein in brain) family, which are the best known proteins that confer endosomal identity and play a crucial role in the biogenesis

of the endosomal compartments. Additionally, I describe the functional and structural role of several endosomal lipids.

1.2.1. RAB GTPases

The RAB small cytosolic guanosine triphosphate hydrolases (GTPases), a family comprised of more than 70 proteins in humans, have been used as markers for the endocytic pathway due to their binding specificity for different compartments (Fig 2). For example, RAB5 and RAB7, which are the two best studied RAB proteins, bind to EEs and LEs respectively (Chavrier et al. 1990). RABs, together with their effector proteins, regulate endosomal movement along the cytoskeleton, endosomal tethering and fusion, among others [for review see (Hutagalung and Novick 2011)]. RAB GTPases switch between inactive/GDP- and active/GTP-bound forms (Ullrich et al. 1994). This process is regulated by the GTPase-activating proteins (GAP, activates the RAB enzymatic activity inducing the RAB-GDP state) and the GDP-GTP exchange factors (GEF, activates RAB proteins by the exchange of GDP-GTP). This nucleotide-exchange cycle modulates the proteins conformation and its membrane binding affinity. The activation of RAB5 (RAB5-GTP, membrane-bound conformation) by the action of the GEF Rabex-5, regulates membrane docking and fusion of EEs (Horiuchi et al. 1997). There are two key events necessary to induce endosomal fusion. The first one is the tethering of the two compartments to be fused, which allows stabilization of the membranes in close contact. The second one is the action of the fusion machinery, which generates the force to overcome the energy barrier of lipid bilayer merging. The soluble N-ethylmaleimide-sensitive factor attachment protein receptor (SNARE) proteins are the engines that drive endosomal fusion. In addition, SNARE-dependent membrane fusion requires the action of the SM (Sec1/Munc-18) family proteins, which are thought to act as chaperones and trigger SNARE fusion. Among RAB5 effectors that regulate membrane fusion there is EEA1, which has been suggested to tether EEs prior fusion (Simonsen et al. 1998; Christoforidis et al. 1999; Dumas et al. 2001; Lawe et al. 2002). Similarly, Rabenosyn-5 also interacts with RAB5 and could act as a tether (Nielsen et al. 2000). Furthermore, Rabenosyn-5 forms a complex with vacuolar protein sorting 45 (VPS45, a SM protein) which in turn stimulates SNAREs vesicle-associated protein 4 (VAMP4), Syntaxin 13, vesicle transport through interaction with t-SNAREs 1A (VTI1A) and Syntaxin 6 for membrane fusion (Bucci et al. 1992; Nielsen et al. 2000; Bethani et al. 2007; Ohya et al. 2009).

Two other endosomal tethering complexes, the CORVET (class C core endosome vacuole tethering) and the HOPS (homotypic vacuole fusion and protein sorting) complexes, have been well characterized in yeast [for review see (Kummel and Ungermann 2014)]. CORVET and HOPS mechanism of action is similar to the RAB5-dependent fusion process described before. Briefly, CORVET and HOPS complexes share a common core of four subunits (VPS11, 16, 18 and 33) and bind to specific small GTPases. CORVET interacts with the RAB5-like protein VPS21 (Peplowska et al. 2007) and HOPS binds to yeast protein two 7 (YPT7), a RAB7-like protein (Seals et al. 2000; Wurmser et al. 2000). Furthermore, both complexes share the SM protein VPS33, and thus they can regulate SNARE-dependent membrane fusion (Ostrowicz et al. 2010; Zick and Wickner 2013). The specificity of CORVET for its interaction with VPS21 makes the complex likely to act on the homotypic fusion of EEs (Balderhaar et al. 2013; Cabrera et al. 2013), while HOPS complex regulates the fusion of Golgi-derived vesicles, LEs and autophagosomes with the vacuole/lysosome (Rieder and Emr 1997; Price et al. 2000; Seals et al. 2000; Wurmser et al. 2000).

1.2.2. PtdIns

The lipid composition of endosomal membranes is also specific for different compartments. The phosphorylated derivatives of phosphatidylinositol (PtdIns), which represent not more than 1% of the total phospholipids in cells, play an important role in endosomal pathway membrane integrity [for review see (Schink et al. 2016)]. Several kinases can phosphorylate the three, four and five hydroxyl groups of inositol, giving rise to seven possible phosphorylated PtdIns (phosphatidylinositides, PIs). All of the seven PIs have been found in cells, and are located in distinct cellular membranes (Yu et al. 2004). For instance, PtdIns4P is highly enriched in Golgi membranes (Levine and Munro 2002), PtdIns(4,5)P_2 and PtdIns(3,4,5)P_3 are plasma membrane PIs (Balla et al. 2000; Gillooly et al. 2003) and PtdIns3P is mainly located in EEs (Gillooly et al. 2000) (Fig 2). PIs recruit cytosolic proteins to specific cell membranes at specific times, and by this mechanism they participate in different cell processes such as lipid signaling, cell signaling and membrane trafficking. The role of PIs in membrane trafficking includes their participation in exocytosis, endocytosis, autophagy, cell division and cell migration (Rohde et al. 2002; Oikawa et al. 2004; Blumental-Perry et al. 2006; Funderburk et al. 2010; Lorente-Rodriguez and Barlowe 2011; Cauvin and Echard 2015; Schink et al. 2016). During endosome maturation, PtdIns3P is accumulated in EEs by the action of several phosphatases that dephosphorylate the four and five positions of PIs and by the phosphorylation of the three position by the

phosphatidyilinositol-3 kinase type II (PI3K-II) or PI3K-III (VPS34) (Raiborg et al. 2013). Several cytosolic proteins contain PX (Phox homology) or FYVE (FAB1p, YOTB, VAC1p, EEA1) domains, which are PtdIns3P interacting domains, and therefore they cycle from the cytosol to EEs. One example is the FYVE domain containing protein is early endosome antigen 1 (EEA1), which by its interaction with EEs facilitates vesicle tethering and finally endosomal fusion (Simonsen et al. 1998; Christoforidis et al. 1999; Dumas et al. 2001; Lawe et al. 2002). Other PtdIns3P effectors participate in several endosomal processes, such as endosome maturation and dynamics, cargo sorting and endosome-cell localization [for review see (Schink et al. 2016)]. Similarly to EEs, LEs also contain highly enriched specific lipids. PtdIns(3,5)P_2 together with phosphatidylinositol-3-phosphate 5-kinase type III (PIKfyve, FAB1p in yeast), an enzyme that phosphorylates PtdIns3P to generate PtdIns(3,5)P_2, participate in the maturation of endolysosomes to terminal storage lysosomes (Dove et al. 2009; Bissig et al. 2017). Epsin 3 (ENT3p), ENT5p, VPS24p, and autophagy-related protein 18 (ATG18p) have been identified as PtdIns(3,5)P_2 effectors in yeast, which participate in protein trafficking in the endosomal pathway (Friant et al. 2003; Whitley et al. 2003; Eugster et al. 2004; Krick et al. 2008).

1.2.3. LBPA

Another lipid that has been shown to be a specific marker of LEs is LBPA, known also as BMP. It represents less than 1% of the total phospholipids and it is a structural isomer of phosphatidylglycerol. LBPA/BMP is highly enriched in the internal membranes (multilamellar membranes and ILVs) of LEs and has not been found in other cellular membranes (Fig 2) (Kobayashi et al. 1998). This unusual lipid comprises up to 10-15 mol% of the total endosomal lipids (Kobayashi et al. 1998). Additionally, there is evidence that this lipid can transiently reach the limiting membrane of the endosomes and get in contact with the cytosolic environment (Bissig et al. 2013). Even though its localization and some of the LBPA/BMP precursors are known, no biosynthetic enzymes have been identified, which makes the study of the functional role of this lipid more difficult. LBPA/BMP is a negatively charged and presumably cone-shaped lipid which induces the deformation of membrane bilayers (Matsuo et al. 2004). It has the intrinsic capacity to induce the formation of internal vesicles by the invagination of the limiting membrane of large liposomes *in vitro*, which also depends on acidic pH (Matsuo et al. 2004). In cells, the back fusion of the ILVs with the limiting membrane of endosomes, which also depends on LBPA/BMP, has been linked to virus infection and the anthrax toxin release to the cytoplasm (Abrami et al. 2004; Bissig et

al. 2013). Furthermore, LBPA/BMP levels are correlated with cholesterol endosomal levels, and it has been suggested that LBPA/BMP controls the cholesterol capacity of endosomes (Chevallier et al. 2008).

1.2.4. Sphingolipids

Sphingolipids are a class of lipids containing an 18-carbon amino alcohol backbone called sphingosine. They are structural molecules of cellular membranes and also participate in a high diversity of cell signaling processes [for review see (Zhou and Blom 2015)]. A subclass of sphingolipids are the ceramides, which are synthetized by the N-acylation of the sphingosine and serves as a substrate for making all other sphingolipids. About 85% of all human sphingolipids and 10-20 mol% of plasma membrane lipids, correspond to sphingomyelins (SPH), which consist of a ceramide and phosphocholine or a phophoethanolamine head group. SPH is an important source for the rapid production of ceramide, by the hydrolytic removal of the phosphocholine moiety of SPH by sphingomyelinases (SMases) (Clarke et al. 2006). Endosomal ceramide generation is linked with the formation of ILVs in cells. More specifically, ceramide has been shown to participate in the production of internal vesicles that are released as exosomes to the extracellular milieu by fusion of MVE with the plasma membrane (Trajkovic et al. 2008). Furthermore, ceramide was found enriched in purified exosomes and the exosomal production was dependent on SMases. *In vitro* experiments in giant unilamellar vesicles (GUV) containing SPH also showed the formation of ILV upon addition of SMase (Trajkovic et al. 2008).

1.2.5. Phosphatidylserine

Phosphatidylserine (PtdSer) represents 5–10% of the total phospholipids in cells. It is a negatively charged lipid, which allows electrostatic interaction with multiple proteins. PtdSer is enriched in the luminal leaflet of the endoplasmic reticulum (ER), Golgi, mitochondria and the cytosolic leaflet of the RE/ERC (Fairn et al. 2011). Some evidence suggests that PtdSer can be found also in the ILVs of late endosomes (Fairn et al. 2011). The presence of PtdSer in endosomes facilitates the recruitment of evectin-2, a protein which facilitates the RE/ERC to TGN retrograde transport of cholera toxin B subunit, TGN integral protein 38 (TGN38) and serum Golgi protein 73 (GP73) (Uchida et al. 2011; Okazaki et al. 2012). Furthermore, it was recently shown that RE/ERC PtdSer plays a role in the signaling of the growth-promoting transcription coactivator Yes-associated protein (YAP). Both nuclear localization of YAP

and YAP-dependent transcription were impaired by silencing of the RE/ERC PtdSer-flippase phospholipid-transporting ATPase IA (ATP8A1) or by masking the PtdSer in the cytoplasmic leaflet of membranes (Matsudaira et al. 2017).

1.2.6. Cholesterol

Cholesterol consists of a steroid backbone which contains a hydroxyl group and a short branched hydrophobic tail. It is an important component of mammalian cell membranes, and therefore its cellular levels are tightly regulated. For instance, high cholesterol levels found in plasma membrane regulate membrane rigidity and fluidity and also cellular processes such as cell polarization, signal transduction and membrane trafficking (Simons and Ehehalt 2002; Simons and Vaz 2004). Human cells can synthetize cholesterol by the action of multiple enzymatic reactions, especially in liver cells, but most of the cells obtain it by the internalization of serum cholesterol-rich particles, called lipoproteins. A well-studied lipoprotein cell surface receptor is the low-density lipoprotein receptor (LDLR), which binds to extracellular low-density lipoprotein (LDL) particles rich in cholesteryl esters (esterified cholesterol) (Brown and Goldstein 1975). LDL binding to LDLR triggers the internalization of the receptor. In EEs, LDL dissociates from its receptor due to the acidic pH of the compartment (Anderson et al. 1977; Davis et al. 1987). While the receptor recycles to the plasma membrane, LDL is sorted to lysosomes for its degradation and cholesterol is hydrolyzed to release free cholesterol (non-esterified cholesterol) (Anderson et al. 1982). Cholesterol export from lysosomes is mediated by the Niemann-Pick type C proteins (NPC1, NPC2) by a mechanism that is still poorly understood. A mutation in NPC1 or NPC2 genes, which is characteristic of the Niemann-Pick type C disease, causes an abnormal accumulation of cholesterol in lysosomes (Maziere et al. 1986; Liscum et al. 1989; Carstea et al. 1997; Naureckiene et al. 2000). From this pathological condition, some clear endosomal cholesterol functions were revealed. Cholesterol accumulation in LEs/lysosomes has a severe effect on endosome motility (Lebrand et al. 2002), ILV formation (Falguieres et al. 2008) and back fusion (Sobo et al. 2007).

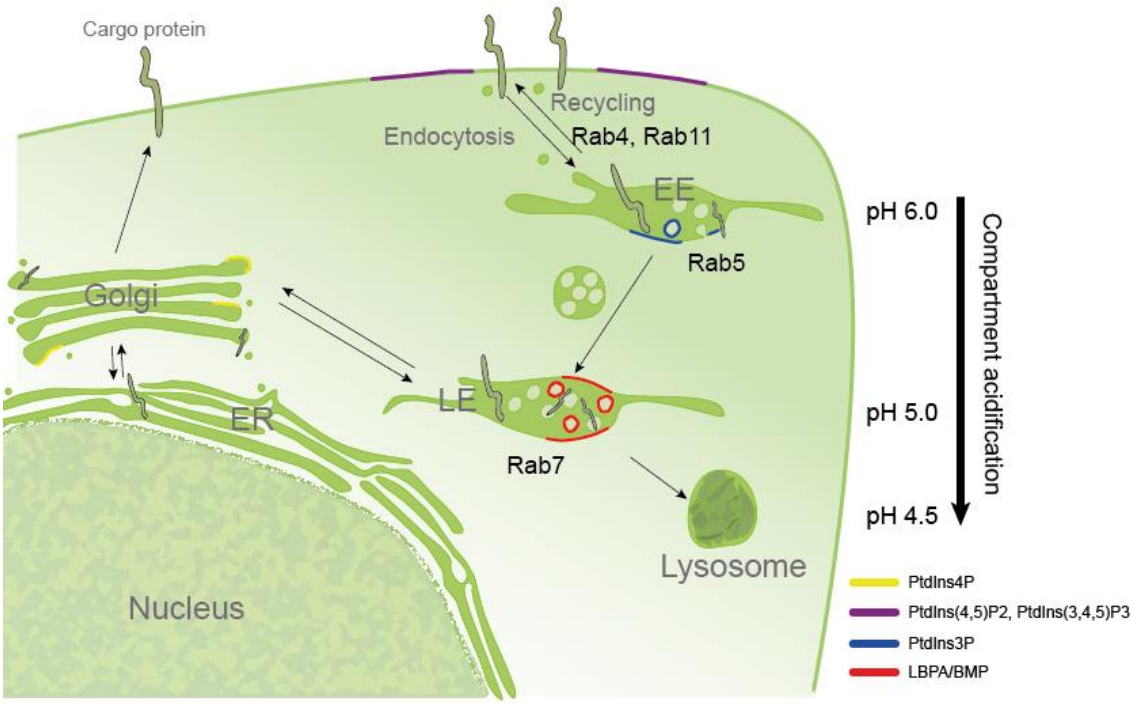

Figure 2. pH, lipids and protein content in the endosomal pathway. ER: Endoplasmic reticulum; EE: early endosome; LE: late endosome; PtdIns: phosphatidylinositol

2. The ESCRT proteins

Proteins belonging to the endosomal sorting complexes required for transport (ESCRT) are known as membrane remodeling factors which regulate events such as cytokinesis, virus budding and MVE formation, among others (Fig 3) [for review see, (Christ et al. 2017)]. They bind to the cytosolic leaflet of the lipid bilayer and form large spiral polymers which induce membrane constriction, deformation, and fission. In the endocytic pathway, ESCRTs play a crucial role in the sorting of activated, ubiquitinated receptors into ILVs, which are then transported to vacuole/lysosomes for their degradation. Here, I discuss the function of ESCRT proteins in the formation of ILV and cargo sorting, starting from their discovery in yeast, the diversity of proteins that make up this complex and their mechanism of action to induce membrane deformation and cargo sorting into ILVs.

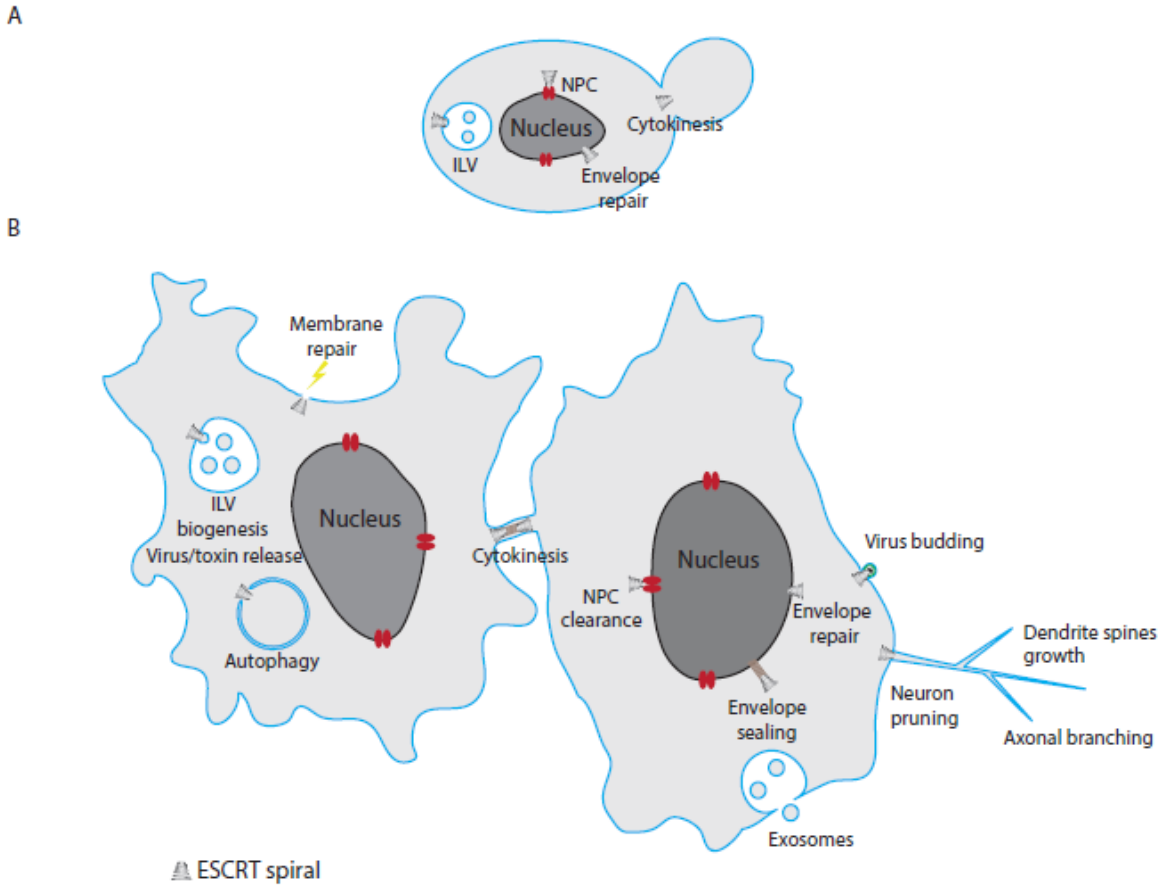

Figure 3. Overview of ESCRT functions. Yeast (A) and mammalian cell (B). The ESCRT machinery is involved in a variety of cellular events which all share a membrane deformation step away from the cytoplasm. ESCRTs are necessary for both membrane deformation and fission. The ESCRT machinery is indicated as a grey spiral. ESCRT: endosomal sorting complex required for transport; ILV: intraluminal vesicle; NPC: nuclear pore complex.

2.1. Discovery of ESCRT proteins

Genes encoding ESCRT proteins came out of pioneering genetic screens in *Saccharomyces cerevisiae*, designed to find novel components involved in vacuolar biogenesis. Amongst the mutants that have been identified and that are collectively referred to VPS mutants (Bankaitis et al. 1986; Rothman and Stevens 1986; Robinson et al. 1988; Rothman et al. 1989), the class E vps mutants comprise 13 genes coding for ESCRT and ESCRT-associated proteins (Raymond et al. 1992; Kranz et al. 2001; Bowers et al. 2004; Bowers and Stevens 2005) (Table 1). Class E mutants have a relatively normal vacuolar morphology, but show an accumulation of missorted vacuolar, late Golgi and plasma membrane proteins in an aberrant structure referred to as the Class E compartment, with some LE/MVE characteristics (Raymond et al. 1992; Davis et al. 1993; Piper et al. 1995;

Rieder et al. 1996; Odorizzi et al. 1998; Coonrod and Stevens 2010). However, class E compartments, which appear like stacks of curved cisternae, typically lack ILVs normally found in LEs (Rieder et al. 1996; Babst et al. 1997; Odorizzi et al. 1998). These findings were the first evidence that the ESCRT machinery is involved in protein sorting through endolysosomal compartments, and in biological membrane remodeling. Additionally, in mammalian cells ESCRT proteins participate in many other functions which require membrane remodeling, including cytokinetic abscission, virus budding, nuclear envelope reformation and repair, plasma membrane wound repair, microvesicle formation, microautophagy and neuron pruning [for review see (Christ et al. 2017)].

	S. cerevisiae	*H. sapiens*	*C. elegans*	*D. melanogaster*	*Aliases*
ESCRT-0	*Vps27*	*HGS*	*hgrs-1*	Hrs	*HRS*
	Hse1	*STAM1/STAM2*	stam-1	Stam	
ESCRT-I	*Vps23*	*TSG101*	*tsg-101*	Tsg101	
	Vps28	*VPS28*	*vps-28*	Vps28	
	Vps37	*VPS37A/VPS37B/VPS37C/VPS37D*	*vps-37*	Vsp37a/Vps37b	
	Mvb12	*UBAP/MVB12A/MVB12B*	*mvb-12*	Mvb12	
ESCRT-II	*Vps25*	*VPS25*	*vps-25*	Vps25	*EAP20*
	Vps22	*VPS22*	*vps-22*	Vps22/Larsen (Lsn)	*EAP30*
	Vps36	*VPS36*	*vps-36*	Vps36	*EAP45*
ESCRT-III	*Did2/Vps46*	*CHMP1A/CHMP1B*	*did-2*	Chmp1	
	Vps2	*CHMP2A/CHMP2B*	*vps-2*	Chmp2b	
	Vps24	*CHMP3*	*vps-24*	Vps24	
	Snf7	*CHMP4A/CHMP4B/CHMP4C*	*vps-32*	shrub	
	Vps60	*CHMP5*	*vps-60*	Vps60	
	Vps20	*CHMP6*	*vps-20*	Vps20	
	Chm7	*CHMP7*	T24B8.2	CG5498	
	Ist1	*IST1*	*istr-1*	CG10103	
ESCRT Associated	*Bro1*	*PDCD6IP/PTPN23*	*alx-1/ego-2*	ALiX	*ALIX/HD-PTP*
	Doa4	*UBPY/STAMBP*	*usp-50*	Usp8/CG2224	*UBPY/AMSH*
	Vta1	*VTA1*	T23G11.7	Vta1	*LIP5*
	Vps4	*VPS4A/VPS4B*	*vps-4*	Vps4	*SKD1 (VPS4B)*
		SPAST	*spas-1*	Spastin	*Spastin*
		CC2D1A/CC2D1B	Y37H9A.3	Lethal (2) Giant Discs (Lgd)	
		MITD1	Y66D12A.10	CG14985	

Table 1. List of ESCRT genes from different organisms (Stoten and Carlton 2018).

2.2. Canonical ESCRT pathway for MVE biogenesis and lysosomal cargo delivery in yeast

Soon after the discovery of ESCRTs, their role in cellular trafficking was better characterized and it was found that they assemble into five distinct complexes: ESCRT-0, -I, -II, -III and the VPS4 complex (Babst et al. 1997; Babst et al. 1998; Babst et al. 2000; Katzmann et al. 2001; Babst et al. 2002a; Babst et al. 2002b; Bilodeau et al. 2002), which function together in regulating protein trafficking towards the LE and the lysosome/vacuole (Table 1). ESCRTs recognize cargo proteins destined for degradation on the limiting membrane of endosomes, sort these cargos into membrane invaginations that form inwards and eventually detach as free ILVs in the endosome lumen (Fig 4). In yeast cells, the MVE

then fuses with the vacuole/lysosome, and the ILV together with its cargo is exposed to the hydrolytic environment of the organelle and is degraded. ESCRT complexes interact in numerous ways with each other (von Schwedler et al. 2003; Bowers et al. 2004) and with membrane proteins and lipids. Additionally, their association with lipids and cargo proteins is highly coordinated, and ESCRTs are presumably recruited in a sequential manner onto endosomal membranes (Babst et al. 2002b; Katzmann et al. 2003; Teis et al. 2008).

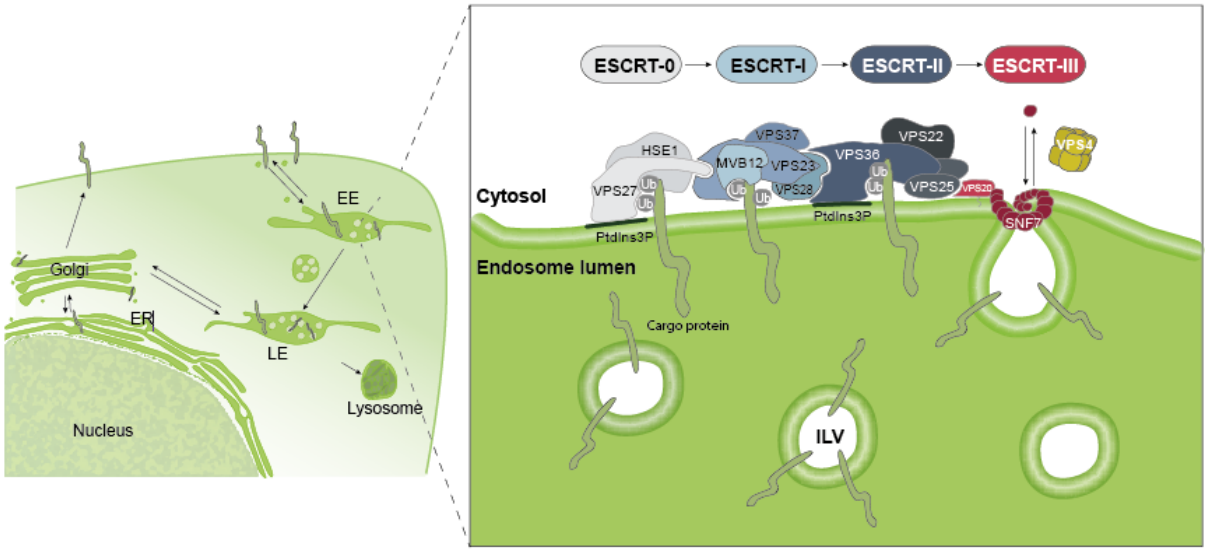

Figure 4. Canonical ESCRT pathway for ILV formation. Five protein complexes (ESCRT-0-III and VPS4) participate in the ESCRT-dependent ILV formation and vacuolar/lysosomal cargo sorting. ESCRT: endosomal sorting complex required for transport; ILV: intraluminal vesicle; Ub: ubiquitin

2.2.1. Ubiquitin: a tag for ESCRT recruitment to endosomes

It has became apparent that ubiquitin serves as the primary recognition marker for ESCRT recruitment onto endosomal membranes (Katzmann et al. 2001). Indeed, the cytosolic domain of down-regulated transmembrane proteins destined for lysosomes is initially ubiquitinated (Fig 4). Below, I discuss the importance of ubiquitin and ubiquitin ligases in several cellular processes, with a special focus on their role through the endosomal pathway.

2.2.1.1. Ubiquitination

Ubiquitin is a small 76 amino acid cytosolic protein (8.5 kDa) which is used by cells as a regulatory protein. It functions via conjugation to a large number of target proteins, a post-translational modification called ubiquitination [For review see (Clague et al. 2015)]. The ubiquitin C-terminus carboxyl group forms an isopeptide bond with the amino group of lysines in the target protein, to give rise to a monoubiquitinated protein. The ubiquitin-tagging reaction of proteins serves as a signal for protein degradation, affects the proteins activity and its cellular location and alters protein interactions. To date, more than 20 different ubiquitin-binding domains have been described, which allow information to be sensed and transmitted from ubiquitinated proteins (Piper et al. 2014). Ubiquitination depends on adenosine triphosphate (ATP) and three types of enzymes, ubiquitin-activating enzymes (E1), ubiquitin-conjugating enzymes (E2) and ubiquitin ligases (E3), which catalyze a series of reactions (Fig 5). The E3 enzymes confer substrate specificity to the ubiquitination process. For this reason, they are the largest group of proteins involved in the ubiquitin system (Deshaies and Joazeiro 2009; Rotin and Kumar 2009; Smit and Sixma 2014). The E3 enzymes are grouped in three families depending on the ubiquitin-ligase domain they contain: the homologous to E6-AP carboxyl terminus (HECT) domain E3s (29 genes in humans), the really interesting new gene (RING) domain E3s (more than 600 genes in humans) and the ring between ring fingers (RBR) domain E3s (13 genes in humans). They participate in multiple processes during protein trafficking, such as the regulation of newly synthesized membrane proteins in the secretary pathway, protein quality control through ER and Golgi, at the plasma membrane, and through the endocytic pathway. (Piper et al. 2014; Foot et al. 2017)

2.2.1.2. Role of ubiquitin in the endocytic pathway

Ubiquitination serves as an internalization signal from the plasma membrane (Egner and Kuchler 1996; Hicke and Riezman 1996). For several proteins, ubiquitin acts as a sorting signal into the clathrin-dependent internalization pathway, which is the major mechanism for the removal of cell surface proteins in most cells. There are two endocytosis adaptors which have been identified as key proteins to link ubiquitination and internalization: Epsin 1/2/3 (ENT1 and ENT2 in yeast) and epidermal growth factor receptor substrate 15 (EPS15, EDE1/END3 in yeast) (Polo et al. 2002; Shih et al. 2002; Hawryluk et al. 2006). These proteins interact with each other and also act as a bridge between some ubiquitinated endocytic cargoes and clathrin (Benmerah et al. 1995; van Delft et al. 1997; Hawryluk et al.

2006). Depletion of Epsin, EPS15 or expression of mutant proteins lacking the ubiquitin binding domain impairs the internalization process (Hawryluk et al. 2006). In mammals, ubiquitination seems to be important for the endocytosis of some cargos, such as notch ligands (Dupre et al. 2004; Wang and Struhl 2004; Sen et al. 2012). However, for other ubiquitinated proteins that are internalized from the plasma membrane, ubiquitin does not act as an internalization signal, but instead participates later in the endosomal pathway together with the ESCRT machinery (Shenoy et al. 2001; Huang et al. 2006; Huang et al. 2007).

2.2.1.3. Ubiquitin ligases in the endocytic pathway

Several ubiquitin ligases are known to play a role in the endocytic pathway. Reverses SPT-phenotype protein 5 (RSP5) is a yeast HECT E3 enzyme that is responsible for the ubiquitination of the majority of plasma membrane proteins that are sorted to ILVs for vacuolar/lysosomal degradation (Belgareh-Touze et al. 2008). Casitas B-lineage lymphoma (Cbl), a membrane-associated RING E3 ubiquitin ligase, is the best known mammalian enzyme that functions in plasma membrane protein ubiquitination (Langdon et al. 1989a; Langdon et al. 1989b). Cbl family is comprised of three members: c-Cbl, Cbl-b, and Cbl-c. Several receptor tyrosine kinases (RTKs) are ubiquitinated by Cbl, which regulates their traffic through the endocytic pathway (Mohapatra et al. 2013). Cbl substrates include EGFR, platelet-derived growth factor receptor (PDGFR), vascular endothelial growth factor receptor (VEGFR), fibroblast growth factor receptor (FGFR), and ephrin receptors (EphR) (Levkowitz et al. 1999; Miyake et al. 1999; Duval et al. 2003; Marmor and Yarden 2004; Fasen et al. 2008). Another E3 ligase family that participates in membrane protein sorting is the neural precursor cell expressed developmentally down-regulated protein 4 (NEDD4) family of HECT E3s. This family is comprised of nine members in humans (NEDD4, NEDD4-2/ NEDD4L, Atrophin-1-interacting protein 4 (AIP4), SMAD ubiquitination regulatory factor 1 (SMURF1), SMURF2, WW domain containing E3 ubiquitin protein ligase 1 (WWP1), WWP2, NEDD4-like E3 ubiquitin-protein ligase 1 (NEDL1), and NEDL2 (Yang and Kumar 2010) and cooperates in the endocytosis and degradation of multiple membrane proteins (Foot et al. 2017). The NEDD4 family downregulates various ion channels [e.g. Epithelial Na(+) channel (ENaC), nuclear chloride ion channel (NCC), cystic fibrosis transmembrane conductance regulator (CFTR)], G-protein-coupled receptors (GPCRs) [e.g. Beta-2 adrenergic receptor (β2-AR), C-X-C chemokine receptor type 4 (CXCR4), protease-activated receptor 1 (PAR1)] and RTKs (e.g. Epidermal growth factor (EGFR), Insulin-like growth factor 1 (IGF-IR),

VEGFR2). Many other E3 ligases have been identified in human cells, and are known to play a role in protein cell surface downregulation and sorting to lysosomes [see review (Foot et al. 2017) for a detailed list of E3 ligases, their cell location and function]

2.2.1.4. Ubiquitin chains

In addition to monoubiquitination, proteins are also polyubiquitinated, a process which consists in the addition of a ubiquitin chain on a single lysine residue of the target protein. These chains are made by linking the ubiquitin C-terminus with one of the seven lysines found in the ubiquitin protein sequence (K6, K11, K27, K29, K33, K48, K63). K48 and K63 are the best characterized ubiquitin-linked chains (Fig 5) (Swatek and Komander 2016). Lysine 48-linked polyubiquitin chain is the canonical signal for targeting unrequired or damaged proteins for degradation in the proteasome, which is a cytosolic protein complex with proteolytic activity (Grice and Nathan 2016). Lysine 63-linked polyubiquitin chain, on the other hand, modulates the sorting of proteins into ILVs and their lysosomal degradation (Erpapazoglou et al. 2012). Other ubiquitin lysine-linked chains do not seem to participate in this process (Erpapazoglou et al. 2012), but monoubiquitination has also been shown to be sufficient for cargo delivery into ILVs (Stringer and Piper 2011).

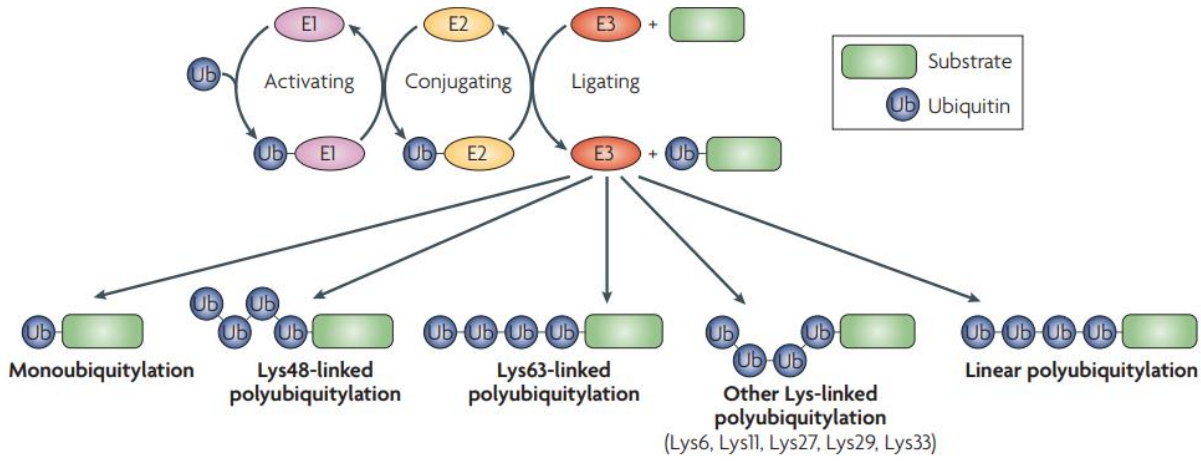

Figure 5. Enzymatic cascade that leads to substrate ubiquitylation. The activity of three enzymes is required for ubiquitylation: a ubiquitin-activating enzyme (E1), a ubiquitin-conjugating enzyme (E2) and a ubiquitin-ligating enzyme (E3), which recognizes the substrate. The completion of one ubiquitylation cycle results in a monoubiquitylated substrate. However, the cycle can be repeated to form polyubiquitylated substrates. Additional ubiquitin molecules can be ligated to a Lys residue (Lys6, Lys11, Lys27, Lys29, Lys33, Lys48 or Lys63) in a previously attached ubiquitin to form Lys-linked chains. Alternatively, ubiquitin molecules can be linked head to tail to form linear chains (Dikic et al. 2009).

2.2.2. The canonical pathway for ESCRT assembly onto endosomal membranes

The endosomal ubiquitinated cargo is recognized by the cytosolic ESCRT-0 complex [VPS27 and has symptoms of class E mutant (HSE1)], which is itself further stabilized on membranes by interactions of the VPS27 FYVE domain with PtdIns3P (Raiborg et al. 2001b; Katzmann et al. 2003). This process establishes a protein-lipid platform for cargo sorting through the recruitment and activation of other ESCRTs (Fig 4). Once ESCRT-0 is recruited, ESCRT-I [(VPS23, VPS28, VPS37 and multivesicular body sorting factor 12 (MVB12)] moves from the cytosol to endosomes through interactions with ESCRT-0 and the ubiquitinated cargo (Katzmann et al. 2003), and then ESCRT-II (VPS22, VPS25 and VPS36) is recruited via interactions with ESCRT-I. VPS36 facilitates endosomal binding by interactions of its N-terminal GLUE [GRAM-like ubiquitin-binding in ELL-associated protein of 45 kDa (EAP45)] domain with ESCRT-I, PtdIns3P and ubiquitin (Meyer et al. 2002; Alam et al. 2004; Slagsvold et al. 2005; Teo et al. 2006; Mageswaran et al. 2015). Eventually, ESCRT-III proteins [VPS2, VPS20, VPS24, VPS32/Sucrose non fermenting protein 7 (SNF7)] are sequentially recruited from cytosol to endosomes (Teis et al. 2008). In this process, the ESCRT-II protein VPS25 interacts with and activates the myristoylated ESCRT-III protein VPS20 (Teo et al. 2004; Im et al. 2009; Teis et al. 2010), which then acts as a nucleation factor for membrane-recruitment and homo-oligomerization of SNF7, the most abundant ESCRT-III protein and the key factor for membrane remodeling (Hanson et al. 2008; Teis et al. 2008; Im et al. 2009; Saksena et al. 2009; Teis et al. 2010). SNF7 polymerization into spirals on the surface of the lipid bilayer drives local membrane deformation necessary for ILV formation (Hanson et al. 2008; Saksena et al. 2009; Wollert et al. 2009; Wollert and Hurley 2010; Henne et al. 2012; Buchkovich et al. 2013; Chiaruttini et al. 2015). In the final step of ILV formation, the ESCRT-III complex recruits the ATPase associated with diverse cellular activities (AAA-ATPase) VPS4 (Babst et al. 2002a; Obita et al. 2007; Adell et al. 2014), whose enzymatic activity induces unfolding of ESCRT-III proteins, triggering their recycling to the cytosol (Babst et al. 1998; Obita et al. 2007; Stuchell-Brereton et al. 2007; Kieffer et al. 2008; Yang et al. 2015) (Fig 4). Additionally, VPS4 may also participate directly in membrane neck constriction during ILV formation (Adell et al. 2014). Finally, during the final steps of cargo delivery into the vacuole, the cargo-bound ubiquitin moiety is recycled to the cytosol by the action of degradation of alpha 4 (DOA4), an endosome-associated deubiquitinase (DUB) (Dupre and Haguenauer-Tsapis 2001; Katzmann et al. 2001; Wolters and Amerik 2015).

2.2.3. ESCRT-III-dependent membrane deformation

The first reports suggesting that ESCRT-III proteins participate in membrane remodeling were performed in mammalian cells expressing charged multivesicular body proteins 4A and 4B (CHMP4A and CHMP4B), two human homologues of SNF7. CHMP4 assembled into flat spirals at the cytosolic leaflet of the plasma membrane (Hanson et al. 2008). Furthermore, the co-expression of CHMP4 and the ATP hydrolysis-deficient VPS4 (E235Q) mutant induced the budding and tubulation of the plasma membrane, forming filopodia-like protrusions, suggesting a membrane remodeling function for the ESCRT-III proteins. Similarly, ESCRT-III spirals are found at the cytokinetic bridge of dividing cells and the neck of HIV-like budding particles, where ESCRT proteins play a crucial role in membrane constriction and fission (Guizetti et al. 2011; Cashikar et al. 2014) (Fig 6).

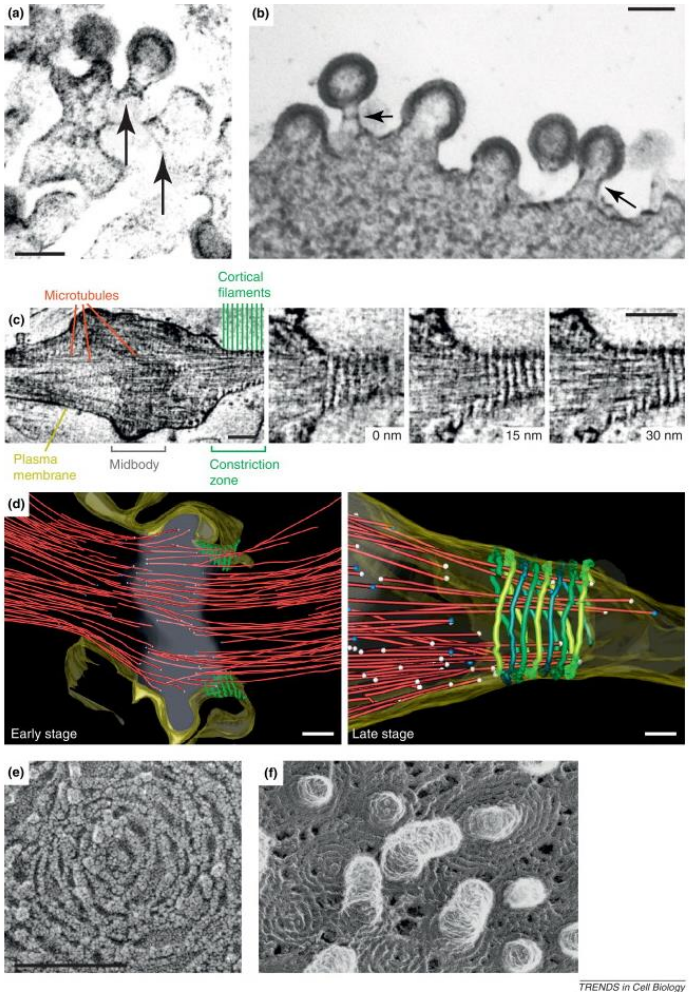

Figure 6. ESCRT-III-dependent filaments in cells. (Figure legend in next page).

2.2.3.1. ESCRT-III proteins structure

There are six ESCRT-III proteins expressed in yeast, and they all share a similar structure and a basic N-terminal and acidic C-terminal amino acid sequence. The secondary structure is comprised of three regions: 4 α-helices (h1-h4) which participate in ESCRT-III oligomerization, an auto-inhibitory h5 helix (Zamborlini et al. 2006; Shim et al. 2007; Bajorek et al. 2009; Xiao et al. 2009; Tang et al. 2015) and finally, regulatory MIT (microtubule interacting and transport) interaction motifs (MIM motifs) (Obita et al. 2007; Shim et al. 2007; Stuchell-Brereton et al. 2007; Davies et al. 2010; Adell et al. 2014). SNF7, VPS20p, VPS2p, and VPS24p are thought to form the core of ESCRT-III, whereas DOA4-independent degradation protein 2 (DID2p) and VPS60p associate with the core complex and may play regulatory roles (Babst et al. 2002a; Nickerson et al. 2006). The ESCRT-III family is expanded to 12 proteins in humans, comprised of CHMP proteins and increased sodium tolerance 1 (IST1) [for a review comparing ESCRTs from different organisms see (Stoten and Carlton 2018)].

2.2.3.2. ESCRT-III proteins "activation" for membrane interaction

Several studies suggest that the ESCRT-III proteins cycle from a "closed/inactive" to an "open/active" conformation. In the "open" form, which allows the ESCRT-III membrane oligomerization, the inhibitory h5 helix is released from the other four helices and an elongated structure is formed (Tang et al. 2015) (Fig 7). As it was mentioned previously (section 2.2.2), VPS20 (CHMP6 in mammals) accelerates the SNF7 membrane nucleation step, which allows polymerization. VPS20 has been suggested to induce the SNF7/CHMP4 "open/active" conformation (Teis et al. 2008; Saksena et al. 2009; Tang et al. 2016). Additionally, *in vitro* studies have shown that SNF7 alone have the capacity to polymerize onto negatively charged membranes, suggesting that the "active" state of the protein can also be induced by the protein-lipid interaction (Chiaruttini et al. 2015).

Figure 6. ESCRT-III-dependent filaments in cells. **(a)** Electron micrograph of thin-sectioned 293T cells transfected with HIV-1 proviral expression constructs. Arrows indicate thickened protein coats on plasma or endosomal membranes. Scale bar: 100nm. **(b)** Thin-sectioned transmission electron micrograph of HIV-1 budding particles in 293T cells, arrested at budding stage by RNAi depletion of hVPS2-1/2. Arrows indicate striations within virus bud necks. Scale bar: 100nm. **(c)** Electron tomographic Z-sections of high-pressure frozen intercellular bridge at mid-abscission stage with cortical 17-nm-diameter filaments at the constriction zone. Scale bar: 100nm. **(d)** 3D reconstructions of early- and late-stage abscission structures. Red, microtubules; green, 17-nm-diameter filaments; gray, midbody; yellow, plasma membrane; white balls, open microtubule ends; blue balls, closed microtubule ends. Scale bar: 200nm. **(e)** 3D anaglyphs of the inside of the plasma membrane of COS7 cells expressing FLAG-hSNF7-1 show curved filaments. Scale bar: 100nm. **(f)** 3D anaglyphs of cell cortex of COS7 cells co-expressing hSNF7-1 and dominant-negative VPS4B (E235Q)-GFP reveal buds and tubules of variable lengths. Scale bar: 100nm (Guizetti and Gerlich 2012).

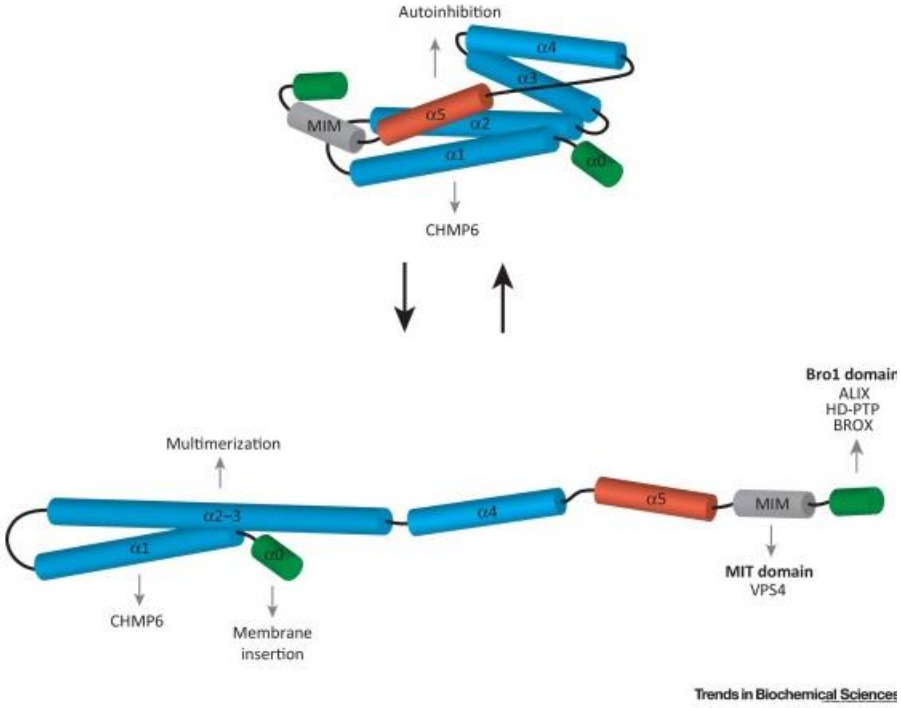

Figure 7. Dynamic CHMP4B Structure. Schematic representation of CHMP4B cycling between an inactive, closed and an activated, open conformation enabling multimerization and interaction with effectors. Abbreviations: MIM, MIT-interacting motif; MIT, microtubule interacting and transport domain (Christ et al. 2017).

2.2.3.3. ESCRT-III proteins membrane polymerization

ESCRT-III proteins are cytosolic, but they can interact with negatively charged membranes by electrostatic forces and form large polymers with variable shapes: filaments, rings, spirals, tubes or cones [for a review with the details of the structures see (Chiaruttini and Roux 2017)]. All of these structures, which are observed *in vitro* and *in vivo*, are built by single stranded ESCRT filaments which can interact laterally. The large variety of ESCRT-III structures presumably emerges from the high flexibility present in the single-stranded polymers. In addition, the possibility of the copolymerization of different ESCRTs in the same structure, or the dynamic exchange of subunits in a preformed oligomer, potentially allows the system to increase the range of ESCRT-III structures (Fig 8). The ESCRT-III dependent mechanism by which the membranes are deformed and break is not fully elucidated. Membrane buckling has been suggested as a possibility for membrane remodeling. Buckling is characterized by a sudden deflection of a structure in order to release a stressing energy. It has been suggested that membrane-bound SNF7 spirals can buckle and deform membranes. SNF7 filaments have a preferred angle of curvature, which is given by the

protein structure and the way SNF7 monomers interact. SNF7 spirals formed on flat lipid membranes have multiple angles of curvature and accumulate elastic stress, which in turn can trigger buckling of the structure and membrane deformation (Fig 8) (Chiaruttini et al. 2015).

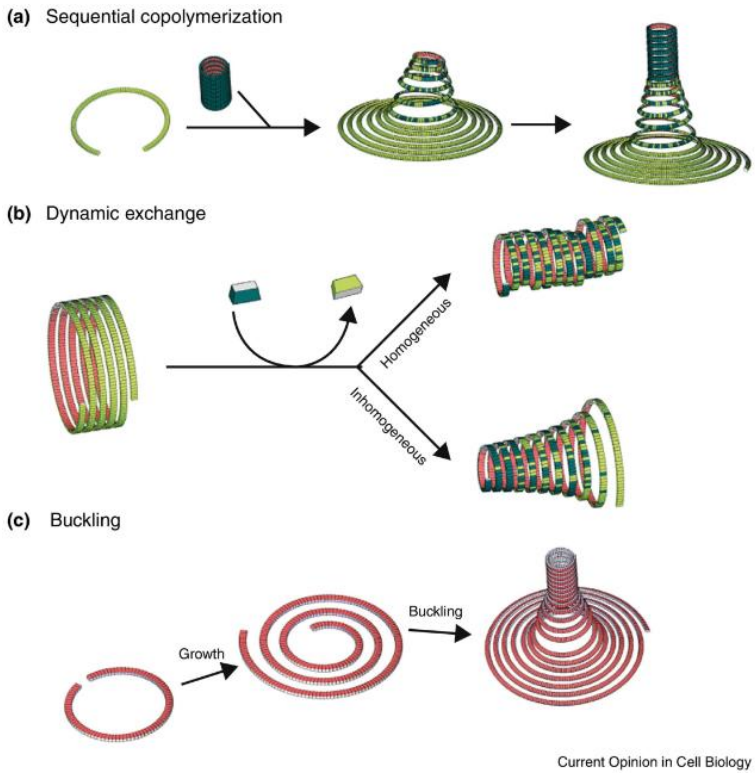

Figure 8. Flexibility in ESCRT-III polymers (a) Sequential polymerization of different subunits (first, the light green one, second, the dark green one), with different curvatures leads to the growth of a conical structure with a continuous gradient of subunits along its axis. **(b)** Dynamical exchange of subunits forming large helical tubes by subunits having a smaller radius of curvature leads to narrower cylinders if the exchange is homogeneous or narrower cones if the exchange is inhomogeneous. **(c)** Growth of a stretch filament into a spiral accumulates elastic stress, which can be released by buckling, forming a cone terminated by a tubular structure (Chiaruttini and Roux 2017).

2.2.4. BRO1 as an alternative pathway for the regulation of ESCRTs in yeast ILV formation

In addition to the ESCRT subunits, class E vps mutants also include Bro domain-containing protein 1 (BRO1), originally called VPS31, a cytosolic protein which interacts via its N-terminal domain with the ESCRT-III protein SNF7, and which also interacts with the deubiquitinase DOA4 (Odorizzi et al. 2003; Bowers et al. 2004; Kim et al. 2005; Richter et al. 2007; Wemmer et al. 2011). The interaction with SNF7 facilitates BRO1 membrane association and subsequently DOA4 recruitment (Odorizzi et al. 2003; Luhtala and Odorizzi 2004; Nikko and Andre 2007), which mediates cargo deubiquitination (Luhtala and Odorizzi 2004; Richter et al. 2007). Interestingly, BRO1 also seems to regulate early steps of the ESCRT pathway by direct physical interactions with conjugated ubiquitin, and thus may also contribute to the sorting of endosomal proteins to the vacuole (Pashkova et al. 2013).

Recent studies show that BRO1 interaction with SNF7 induces the “active” SNF7 conformation, which increases SNF7 polymerization (Wemmer et al. 2011; Tang et al. 2016), and thereby facilitates cargo sorting into ILVs (Tang et al. 2016). This process, which depends on cargo ubiquitination and the ESCRT-0 complex, is independent of ESCRT-I, -II and the SNF7 nucleation factor, VPS20 (Tang et al. 2016). Altogether, these observations suggest the existence of two parallel pathways for SNF7 polymerization during endosomal cargo sorting and membrane remodeling; the canonical pathway in which ESCRT-0, -I, -II and VPS20 recruits and “activates” SNF7, and a parallel pathway in which BRO1 induces SNF7 polymerization on the endosomal membranes (Tang et al. 2016) (Fig 9).

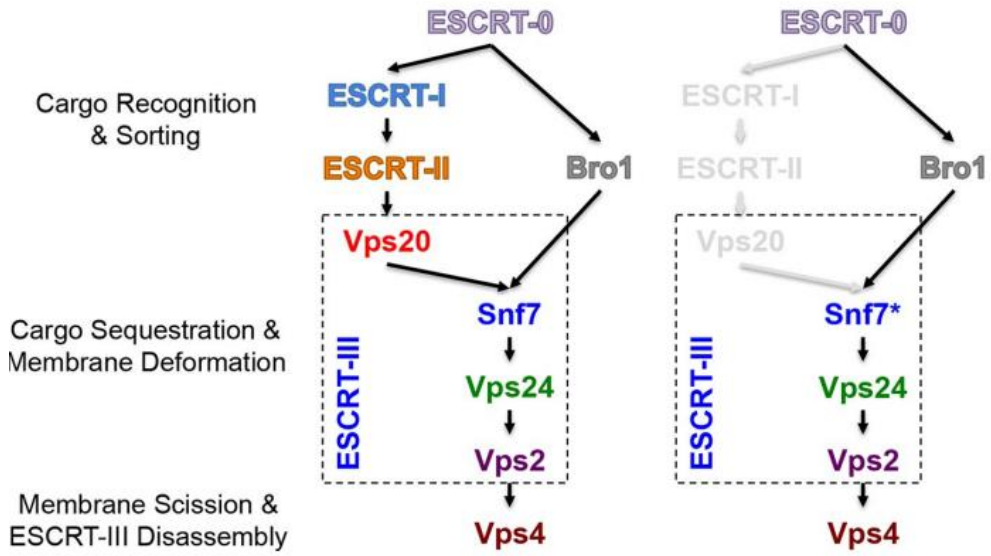

Figure 9. Conceptual models of parallel ESCRT-III SNF7 activation pathways in MVE biogenesis. Canonical ESCRT pathway (left) and BRO1-dependent pathway (right) (Tang et al. 2016).

2.3. ESCRTs in mammalian cells: ILV biogenesis

The ESCRT machinery is well conserved in all eukaryotes, indicating an early evolutionary origin, and the gene complexity is increased in multicellular organisms. All the yeast ESCRT subunits have at least one ortholog in mammals, where several ESCRT genes are duplicated (Leung et al. 2008; Michelet et al. 2010; Sun et al. 2016) (Table 1). Even though ESCRT functions in MVE biogenesis and cargo sorting are conserved in eukaryotes (Michelet et al. 2010), the regulatory mechanisms are more complex in mammalian cells than in yeast. When compared to yeast ESCRTs, mammalian subunits exhibit additional interactions with each other, as well as with other proteins and lipids. In the canonical

pathway of ILV formation, the ESCRT-0 subunit hepatocyte growth factor-regulated tyrosine kinase substrate (HRS) also interacts with clathrin in mammalian cells (Raiborg et al. 2001a; Raiborg et al. 2002), forming a bi-layered coat presumably involved in cargo sorting (Raiborg et al. 2002; Sachse et al. 2002; Sachse et al. 2004; Myromslien et al. 2006; Raiborg et al. 2006).

I will discuss below the different mammalian non-canonical mechanisms that have been reported for ILV formation and cargo protein sorting, giving special emphasis to the ESCRT-associated proteins which participate in these processes.

2.3.1. Non-canonical ESCRT pathways for ILV formation: cargo-ubiquitination independent

As mentioned above (section 2.2.1), cargo ubiquitination in the canonical ESCRT pathway is the initial step necessary for the recruitment of the early ESCRT machinery and thus for the efficient degradation of endocytosed plasma membrane receptors that need to be downregulated (Katzmann et al. 2001; Shields and Piper 2011). Consequently, multiple proteins belonging to ESCRT-0, -I and -II bind ubiquitin (Shields and Piper 2011). However, in mammalian cells, several receptors are also sorted into the lumen of the endosomes by a mechanism independent of direct cargo ubiquitination (Tanowitz and Von Zastrow 2002; Wolfe et al. 2007; Yamashita et al. 2008; daSilva et al. 2009; Dores and Trejo 2014; Mageswaran et al. 2014; Tomas et al. 2015; Dores et al. 2016) (Fig 10). A mutant of the interleukin-2 receptor β (IL-2Rβ) that cannot be ubiquitinated because it lacks all cytosolic lysine residues, is still efficiently degraded in lysosomes. Surprisingly, this mutant keeps the ability to bind the ESCRT-0 protein HRS, which normally recognizes the ubiquitinated cargo (Yamashita et al. 2008), and thus the recruitment of the remaining ESCRT subunits occurs normally. Similarly, ubiquitination is also dispensable for the negative factor (Nef)-induced degradation of the human immunodeficiency virus type 1 (HIV-1) coreceptor cluster of differentiation 4 (CD4) (daSilva et al. 2009). Finally, three GPCRs are sorted for lysosomal degradation by ubiquitin-independent mechanisms: murine δ-opioid receptor (DOR) (Tanowitz and Von Zastrow 2002), PAR1 (Wolfe et al. 2007) and P2Y purinoreceptor 1 P2Y1 (Dores et al. 2016).

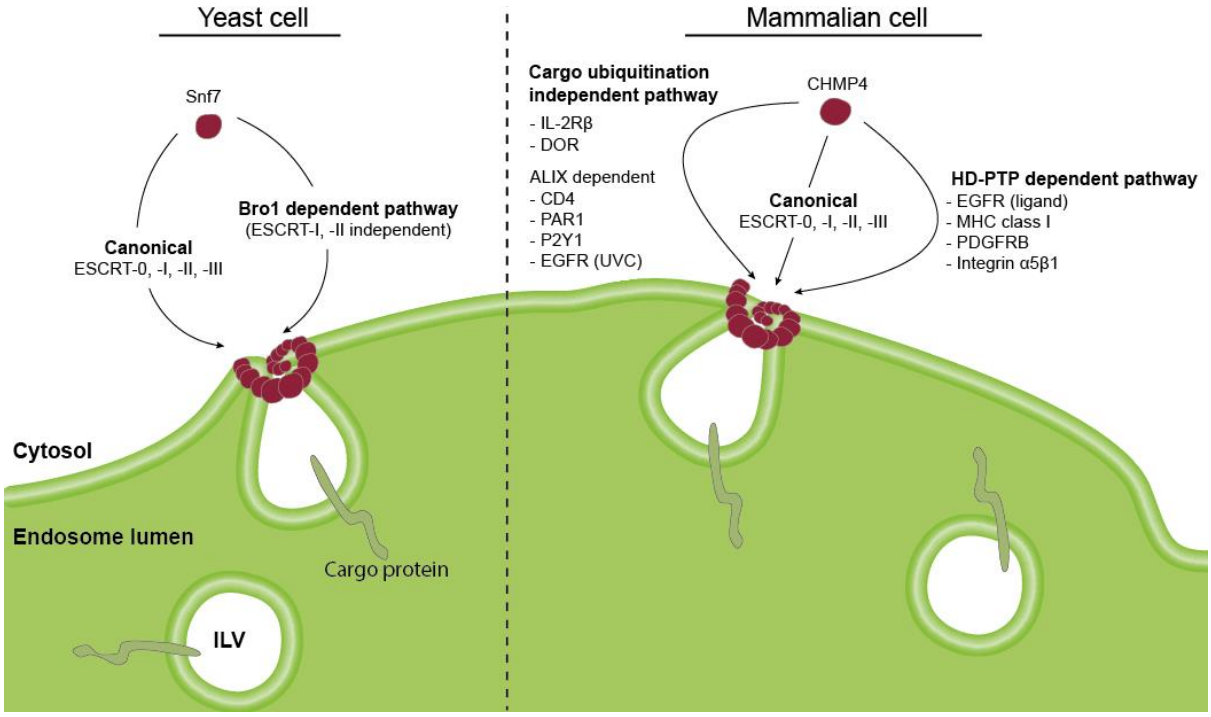

Figure 10. Different mechanisms for ESCRT-III membrane recruitment in yeast and mammalian cells. Schematic representation of the diversity of ESCRT-III membrane recruitment mechanisms for cargo sorting into ILVs. Two parallel mechanisms have been described for SNF7 membrane recruitment in yeast: the canonical ESCRT pathway and the BRO1-dependent pathway. In mammalian cells, CHMP4 membrane recruitment mechanisms are more complex than in yeast, and multiple mechanisms have been described for ILV cargo sorting. In addition to the canonical ESCRT pathway, membrane proteins in mammalian cells can be sorted into ILV independent of cargo ubiquitination or dependent on ALIX and HD-PTP. For simplicity, only SNF7/CHMP4 subunit of ESCRT-III is shown. ILV, intraluminal vesicles; UVC, ultraviolet C.

The mechanism for DOR delivery into ILVs and degradation differs from the canonical ESCRT pathway. Much like with interleukin-2 receptor subunit beta (IL-2Rβ), a DOR lysine-mutant that cannot be ubiquitinated is delivered into ILVs and degraded in lysosomes (Tanowitz and Von Zastrow 2002; Henry et al. 2011). Moreover, ligand-induced DOR degradation depends on the ESCRT proteins HRS and VPS4, but not TSG101 (Hislop et al. 2004). It has been suggested that DOR endosomal trafficking depends on G-protein coupled receptor-associated sorting protein 1 (GASP1), a GPCR interacting protein, and dysbindin, which are both involved in GPCR degradation. Dysbindin binds to GASP1 and HRS, presumably promoting the connectivity between DOR and the ESCRT machinery and thus facilitating receptor degradation. However, further studies will be needed to unravel the details of this regulatory mechanism (Marley and von Zastrow 2010).

These studies are consistent with findings of the Babst group in 2014, who reported that cargo delivery into the yeast vacuole depends on the strength of the interactions between the cargo protein and the ESCRT machinery, and not exclusively on cargo ubiquitination (Mageswaran et al. 2014). They also showed that cargo interactions with early ESCRTs (ESCRT-0, -I or -II) are not strictly required for sorting into ILVs, and that an artificial cargo that interacts with ESCRT-III, but not with any other complex, is also efficiently sorted into the yeast vacuole. Using artificial proteins that interact weakly or strongly with ESCRTs, authors conclude that in the end the strength of these interactions determines whether a candidate protein exhibits ESCRT- (strong) or cargo-like (weak) behavior, and that ubiquitin may function as temporary signal regulating the strength of cargo-ESCRT complexes interactions (Mageswaran et al. 2014).

2.3.2. ESCRT-associated proteins: BRO1-domain proteins

In recent years, several studies have identified BRO1 domain-containing proteins ALIX [official name PDCD6IP (programmed cell death 6 interacting protein)] and His domain-containing protein tyrosine phosphatase (HD-PTP), two mammalian homologs of the yeast BRO1 protein, as important regulators of ESCRT functions (Fig 11). BRO1 domain- and CAAX motif-containing protein (BROX), is a third BRO1 domain protein expressed in mammals, but its function in the ESCRT pathway is still unexplored. As BRO1, the mammalian BRO1 proteins are cytosolic and can be recruited to membranes and work in multiple membrane deformation processes. The BRO1 domain seems to be the key player that links these proteins to the ESCRT pathway, by its capacity to bind the ESCRT-III protein SNF7/CHMP4 (Katoh et al. 2003; Strack et al. 2003; von Schwedler et al. 2003; Katoh et al. 2004a; Ichioka et al. 2007). Although the BRO1 domains of the yeast BRO1, ALIX, HD-PTP and BROX do not share more than 25% of primary sequence identity, structural analysis showed that they all have the same elongated, banana-shaped structure. The latter contains a concave binding pocket which interacts with the C-terminal region of SNF7/CHMP4 (Sette et al. 2011). ALIX and HD-PTP participate in the biogenesis of MVEs (Matsuo et al. 2004; Doyotte et al. 2008) and additionally, ALIX regulates several other ESCRT-mediated processes such as virus budding (Martin-Serrano et al. 2003), cytokinesis (Carlton and Martin-Serrano 2007; Morita et al. 2007; Carlton et al. 2008; Christ et al. 2016), membrane repair (Jimenez et al. 2014; Scheffer et al. 2014), autophagy (Murrow et al. 2015), endosome-to-cytosol delivery of viral RNA (Le Blanc et al. 2005; Bissig et al. 2013) and

anthrax toxin (Abrami et al. 2004), exosome biogenesis (Baietti et al. 2012; Abrami et al. 2013) and as vehicle for viral genomes (Nour and Modis 2014).

2.3.2.1. Structural domains of the mammalian BRO1 proteins: ALIX

ALIX is an 868 amino acid protein (96 kDa) that contains two protein domains: A N-terminal BRO1 domain and a central V-shaped domain (Fisher et al. 2007). Also, ALIX has a flexible C-terminal PRR which interacts with several proteins. ALIX interaction partners are shown in Fig 11.

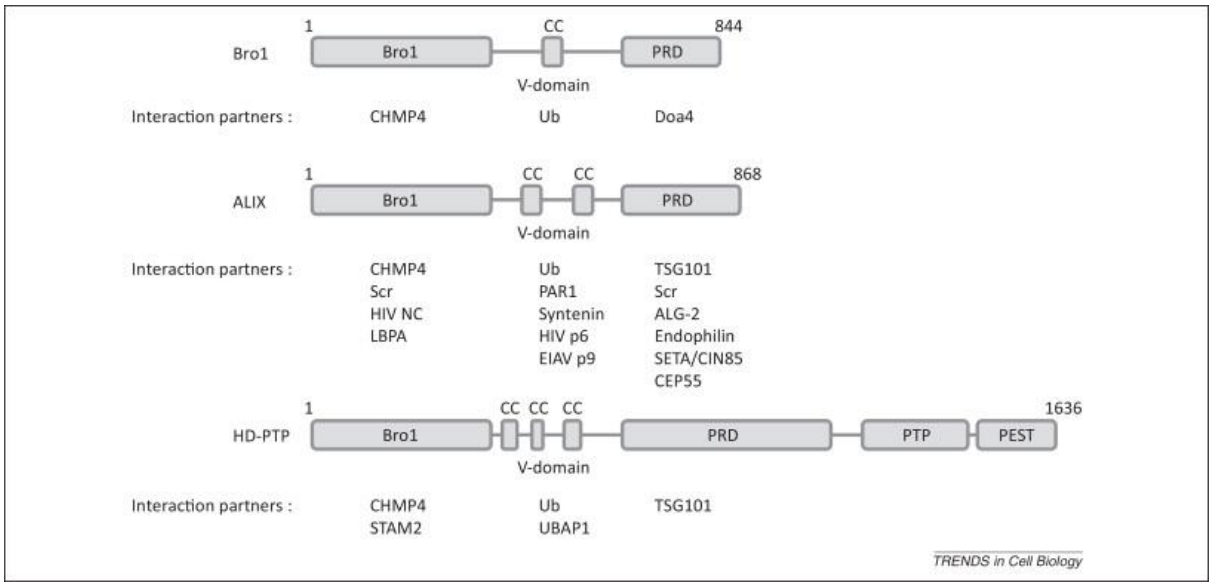

Figure 11. Schematic representation of the protein domain structures of BRO1, ALIX, and HD-PTP. BRO1, ALIX, and HD-PTP contain an N-terminal BRO1 domain which is followed by coiled-coils (CC) that build the V-domain and by a proline-rich region (PRR). Although the structural features of the BRO1 domains are highly conserved, this is less true for the V-domain and the PRR. The interaction partners of BRO1, ALIX, and HD-PTP are indicated (Bissig and Gruenberg 2014).

Apart from the interaction of ALIX BRO1 domain with the ESCRT-III protein CHMP4, ALIX can also bind to the ESCRT-I protein TSG101 through its PRR (Strack et al. 2003; von Schwedler et al. 2003). The PRR also interacts with centrosomal protein of 55 kDa (CEP55) (Carlton and Martin-Serrano 2007), a protein located at the bridge (midbody) of cells undergoing mitosis near the end of cytokinesis. ALIX and its ESCRT-interacting partners (TSG101 and CHMP4) localization at the midbody is important to coordinate cytokinetic (Carlton and Martin-Serrano 2007; Morita et al. 2007; Carlton et al. 2008; Christ et al. 2016).

Furthermore, CHMP4 membrane recruitment during cytokinesis is regulated by two parallel pathways: One dependent on CEP55, ESCRT-I, -II and CHMP6, and a second one dependent on the direct interaction between CEP55, ALIX and CHMP4 (Christ et al. 2016).

ALIX V-shaped domain binds to the late domain of HIV-1 p6 Gag and equine infectious anemia virus (EIAV) Gag p9 by recognizing the LYPX(n)L motif (Strack et al. 2003). Thus, ALIX promotes HIV-1 and EIAV budding from plasma membrane by recruiting components of ESCRT-I and ESCRT-III to the viral budding necks (Martin-Serrano et al. 2003; Strack et al. 2003; Usami et al. 2007). Moreover, the V-shaped domain and the PRR participate in ALIX dimerization, which appears to be important for HIV-1 budding (Pires et al. 2009). ALIX V-shaped domain also binds to ubiquitin, and this interaction is important for the release of HIV-1 and EIAV (Joshi et al. 2008; Dowlatshahi et al. 2012; Keren-Kaplan et al. 2013).

2.3.2.1.1. ALIX auto-inhibition by its PRR

There is clear evidence that ALIX PRR auto-inhibits both the CHMP4 and HIV-1 binding activities of ALIX (Zhou et al. 2008; Zhou et al. 2009; Zhou et al. 2010; Zhai et al. 2011; Sun et al. 2015; Sun et al. 2016). The ALIX BRO1-V construct (ALIXΔPRR) does not only have a better affinity for the HIV-1 p6 Gag protein than the full length ALIX, but is also more efficient in recovering the production of a mutant HIV-1 virus which has low interaction with the full length ALIX (Strack et al. 2003). The mechanism of auto-inhibition involves the interaction between the N-terminus of the PRR and a Src-phosphorylation site on the BRO1 domain (Zhou et al. 2010). Therefore, ALIXΔPRR possibly represents an active form of ALIX. In addition, ALIX PRR phosphorylation has been suggested to release the interaction of the PRR with the BRO1 domain, activating the ESCRT function of ALIX in cytokinesis and virus budding (Sun et al. 2016).

2.3.2.1.2. ALIX interaction with LBPA

The ALIX BRO1 domain contains a flexible loop in its convex surface, opposite to the CHMP4 interacting site, that interacts with LBPA/BMP (Bissig et al. 2013) (Fig 12). This loop does not interact with other negatively charged lipids, such as PtIns, phosphatidic acid and PtdSer. Upon binding, ALIX undergoes a conformational change that leads to the partial insertion of its LBPA-interacting region into the membrane, a process that is dependent on calcium binding (Bissig et al. 2013). The LBPA/BMP interacting loop is not conserved in other BRO1-domain containing proteins, including BRO1 itself. This interaction has been

proposed to facilitate ALIX recruitment to LEs, and also to mediate the delivery of viral nucleocapsids to the cytosol during vesicular stomatitis virus (VSV) infection (Welsch et al. 2006; Bissig et al. 2013). In addition, ALIX was suggested to participate in the formation of MVEs. ALIX-silenced cells showed a decrease in the number of ILVs per compartment when compared to a mock condition (Matsuo et al. 2004). Moreover, ALIX participates in the lysosomal degradation of some membrane receptors (discussed below). *In vitro* studies reinforced the idea of an endosomal interplay between ALIX and LBPA/BMP by showing that recombinant ALIX could regulate ILV formation of liposomes containing LBPA/BMP (Matsuo et al. 2004).

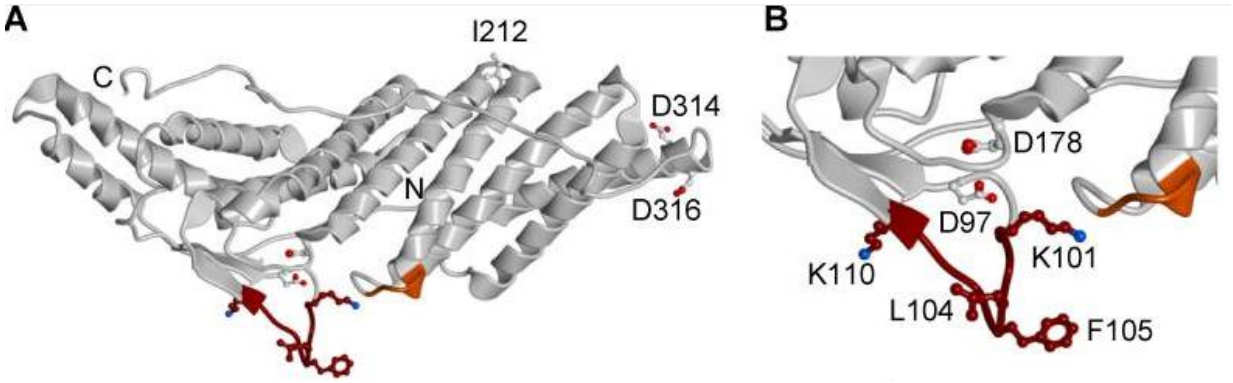

Figure 12. ALIX BRO1 domain LBPA-interacting loop. (A) Ribbon model of ALIX BRO1 domain using the atomic coordinates derived from the X-ray diffraction analysis (PDB ID: 2R03). The N- and C-termini of the BRO1 domain are marked with N and C, respectively. The LBPA/BMP interacting residues are shown in brown (101-KGSLFGGSVK-110) and orange (232-QYKD-235). The I212 residue is involved in CHMP4 interaction. D97 and D178 coordinate calcium binding. **(B)** Higher magnification view of the membrane-interacting region (Bissig et al. 2013)

2.3.2.2. Structural domains of the mammalian BRO1 proteins: HD-PTP

HD-PTP is a 1636 amino acid protein (179 kDa) which contains five domains: BRO1, V-shaped domain, PRR, a catalytically inactive tyrosine phosphatase domain and a PEST (proline-, glutamic acid-, serine-, and threonine-rich) domain (Fig 11). Similarly to ALIX, HD-PTP BRO1 domain and the PRR, interact with CHMP4 (ESCRT-III) and TSG101 (ESCRT-I), respectively (Ichioka et al. 2007). In addition, the BRO1 domain and the PRR interact with signal transducing adapter molecule (STAM) 2, which is part of ESCRT-0 (Ali et al. 2013; Lee et al. 2016). HD-PTP V-shaped domain binds directly to ubiquitin and also to K63-linked polyubiquitin chains, as for ALIX and the yeast BRO1 (Pashkova et al. 2013). In contrast to what is known for BRO1 and ALIX, until today there are no functions known for the HD-PTP interaction with ubiquitin.

2.3.2.3. BRO1 domain containing proteins function in ILV formation

In this part of the introduction I will review the functional role of the mammalian BRO1 proteins in the formation of ILV and cargo sorting to lysosomes.

2.3.2.3.1. EGFR lysosomal degradation: HD-PTP dependent

The epidermal growth factor receptor (EGFR) is a well-established example of signaling receptor downregulation triggered by ligand binding and mediated ESCRT-dependent sorting to lysosomes. Indeed, ligand-induced EGFR degradation depends on ubiquitination of its cytosolic domain (Levkowitz et al. 1998; Umebayashi et al. 2008), and on ESCRT-0, ESCRT-I and ESCRT-III (Bishop et al. 2002; Bache et al. 2004; Doyotte et al. 2005; Bache et al. 2006; Langelier et al. 2006; Razi and Futter 2006; Raiborg et al. 2008). The role of ESCRT-II in EGFR degradation has been debated (Bowers et al. 2006; Langelier et al. 2006; Malerod et al. 2007), suggesting that ESCRT-II sorting functions may be cargo-specific or redundant (Bowers et al. 2006). This may also hint at another pathway for cargo sorting into ILVs and degradation in mammalian cells, different from the canonical ESCRT pathway.

ALIX contribution in ESCRT recruitment during virus budding provided indirect evidence that ALIX might also participate in MVE biogenesis and cargo sorting. However, several studies showed that EGFR degradation was independent of ALIX, (Cabezas et al. 2005; Bowers et al. 2006; Doyotte et al. 2008) and instead, HD-PTP was shown to be important. HD-PTP was proposed to act in place of ESCRT-II during EGFR sorting into ILVs and degradation (Doyotte et al. 2008), by facilitating EGFR transfer from ESCRT-0 to ESCRT-III [together with the action of the DUB ubiquitin isopeptidase Y (UBPY)], presumably via interactions with STAM2 and the ESCRT-III subunit CHMP4 (Doyotte et al. 2008; Ali et al. 2013) (Fig 13).

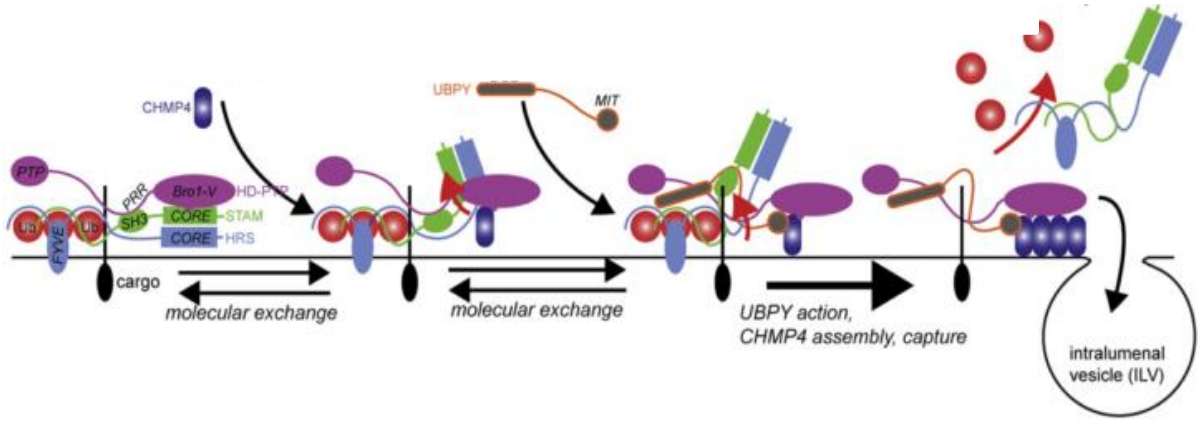

Figure 13. A model for HD-PTP and UBPY function. HD-PTP first binds EGFR and ESCRT-0. Recruitment of CHMP4B and UBPY to HD-PTP displaces STAM2/ ESCRT-0 from HD-PTP. In conjunction, STAM2 binding facilitates UBPY-dependent deubiquitination of EGFR, supporting release of ESCRT-0 from EGFR in favor of ESCRT-III (Ali et al. 2013).

2.3.2.3.2. MHC class I, Integrin α5β1, PDGFRB and TGFβR lysosomal degradation: HD-PTP dependent

Similarly to EGFR degradation, major histocompatibility complex (MHC) class I down-regulation, induced by the Kaposi's sarcoma-associated herpes virus (KSHV), also follows a non-canonical HD-PTP-dependent and ESCRT-II independent pathway (Bowers et al. 2006; Parkinson et al. 2015). HD-PTP is also involved in integrin α5β1 and platelet-derived growth factor receptor beta (PDGFRB) lysosomal degradation (Kharitidi et al. 2015; Ma et al. 2015). Additionally, the degradation and signaling of the transforming growth factor β/bone morphogenetic protein receptor (TGFβR), seems to be regulated by the interaction of HD-PTP with the TGFβR-interacting complex smad anchor for receptor activation (SARA)/Endofin, which regulates the signaling cascade of the receptor (Gahloth et al. 2017).

2.3.2.3.3. PAR1 and P2Y1 lysosomal degradation: ALIX dependent

Like HD-PTP, ALIX has also been identified as a factor necessary for the recruitment of ESCRT-III during cargo sorting into ILVs (Dores et al. 2012; Dores et al. 2015). As was mentioned previously, sorting into ILVs of the ligand-activated PAR1 and P2Y1 receptors is independent of ubiquitination (Wolfe et al. 2007; Dores et al. 2016). Furthermore, lysosomal sorting of these receptors depends on a subset of ESCRT proteins, but not on HRS (Wolfe

et al. 2007; Dores et al. 2016), reinforcing the notion that multiple pathways of cargo sorting to lysosomes may exist. Both receptors contain a cytoplasmic YPX_3L motif, which is recognized by ALIX in response to ligand-induced activation of the receptors (Dores et al. 2012; Dores et al. 2016) (Fig 14). Furthermore, the interactions between ALIX and the ESCRT-III subunit CHMP4 (von Schwedler et al. 2003) facilitate coupling of activated PAR1 to the ESCRT machinery (Dores et al. 2012). Interestingly, although PAR1 ubiquitination is dispensable, ALIX ubiquitination, which is mediated by interactions with arrestin domain-containing protein 3 (ARRDC3) and the E3 ubiquitin ligase WWP2, was shown to be important for PAR1 sorting and degradation (Dores et al. 2015).

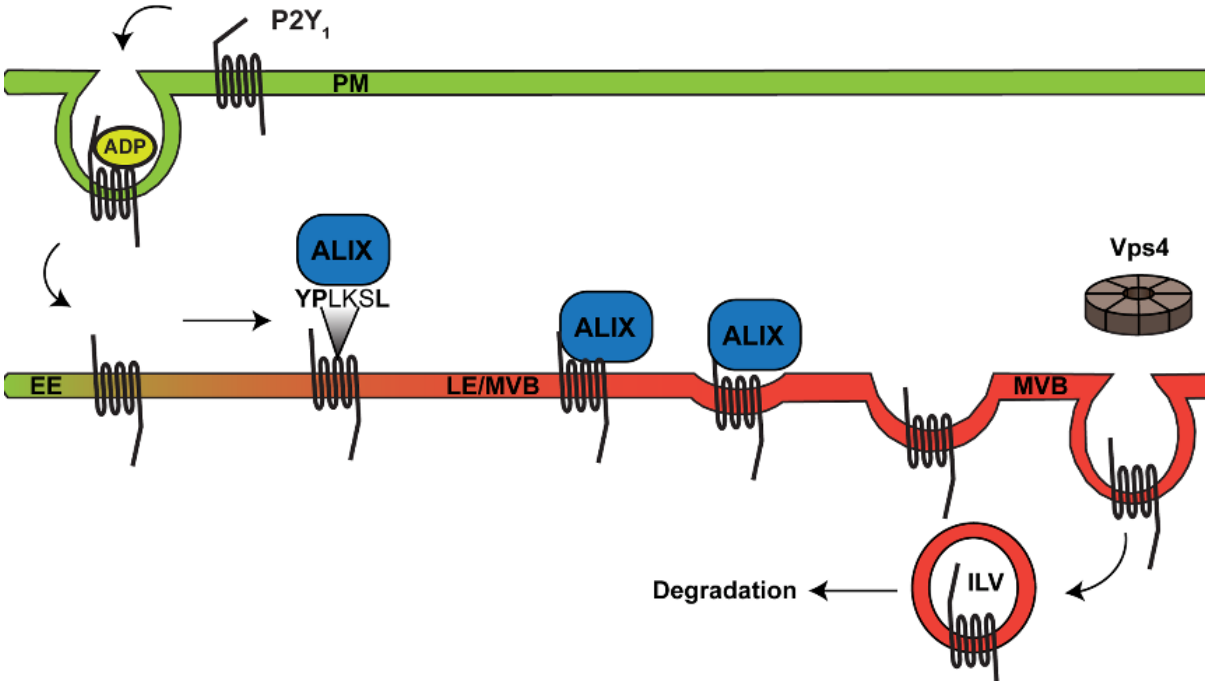

Fig 14. ALIX mediates the sorting of P2Y1 at the late endosome/MVE. ALIX interacts with a conserved YPX_3L motif of P2Y1, and facilitates sorting of the receptor at late endosomes into intraluminal vesicles (ILV) of the multivesicular body (MVB/MVE), where the receptor is eventually degraded (Dores et al. 2016).

2.3.2.3.4. CD4 lysosomal degradation: ALIX dependent

CD4 is expressed in helper T-lymphocytes and other cells of the immune system. It acts as a co-receptor for the recognition of MHC class II molecules during adaptive immune response. In addition, CD4 is the primary receptor for HIV-1 and HIV-2 and acts together with two possible co-receptors: C-C chemokine receptor type 5 (CCR5) or CXCR4. Nef is an accessory protein of HIV-1 and HIV-2 that enhances virus production and promotes disease

progression. This protein also interacts with CD4 and induces its internalization by a clathrin-mediated mechanism. Contrary to the typical plasma membrane recycling pathway followed by CD4 after endocytosis, Nef-induced internalization triggers lysosomal degradation of the receptor. CD4 degradation is independent of receptor ubiquitination and is dependent on the ESCRT proteins TSG101 and VPS4. In addition, ALIX also participates in Nef-induced CD4 degradation, presumably by acting as an adaptor for ESCRT recruitment. Nef directly interacts with the ALIX V-domain and the BRO1 domain, and they both localize in LE together with the internalized CD4 (daSilva et al. 2009; Amorim et al. 2014)

2.3.2.3.5. EGFR internalization induced by UV-light: ALIX dependent

The high flexibility of the mammalian machinery required for cargo sorting into ILVs, is also illustrated by the differences in the molecular mechanisms used during the EGF-induced and the stress-induced post-endocytic sorting of EGFR. Ultraviolet light (UV) C induces ligand-independent EGFR internalization, and its accumulation into ILVs of LBPA/BMP-containing MVEs, a process in which the receptor avoids lysosomal degradation (Tomas et al. 2015). Interestingly, in stress-induced post-endocytic sorting of EGFR, EGFR ubiquitination is not required and ALIX cooperates in EGFR sorting into ILVs, in marked contrast to EGF-induced receptor degradation, which depends on ubiquitination but not on ALIX (Umebayashi et al. 2008; Tomas et al. 2015).

2.4. ESCRT function in exosome biogenesis

Previously, I discussed the formation of MVEs and its importance for cargo degradation in lysosomes. In addition to fusion with lysosomes, MVEs can also fuse with the plasma membrane, which results in the release of ILVs to the extracellular milieu (Raposo et al. 1996). These extracellular vesicles were called exosomes, and participate in intercellular communication by transferring membrane and cytoplasmic components between cells. During the past few years, secreted vesicles were demonstrated to be involved in physiological processes such as coagulation, inflammation, angiogenesis, waste management and physiopathological processes like tumor progression, neurodegeneration and cardiovascular diseases [for review see (Simons and Raposo 2009)]. The capacity to secrete exosomes differs from cell type to cell type and can occur on a constitutive or inducible basis (Raposo et al. 1997; Zitvogel et al. 1998). The mechanism involved in MVE fusion with plasma membrane has not been fully elucidated; however, RAB proteins

(RAB11, RAB35, RAB27A and RAB27B) are known to regulate this process (Savina et al. 2005; Hsu et al. 2010; Ostrowski et al. 2010). Exosomes contain specific lipid and protein content, which arise from the plasma membrane, the endocytic pathway and the cytosol (Thery et al. 1999; Thery et al. 2001; Wubbolts et al. 2003; Subra et al. 2007). The ESCRT-I protein TSG101 and ALIX, were found enriched in exosomes (Thery et al. 2001), which made ESCRTs a possible machinery involved in exosome biogenesis. A gene silencing-based screening targeting 23 ESCRT and ESCRT-associated proteins, showed that only a subset of these proteins (HRS, STAM1, TSG101, ALIX, VPS4B) participate in the secretion of exosomes (Colombo et al. 2013), implying that a pathway different from the canonical ESCRT pathway is presumably involved in exosome biogenesis. As it was discussed previously (section 1.2.4), a mechanism for exosomes formation independent of ESCRTs, but dependent on ceramide, has been described (Trajkovic et al. 2008). Additionally, the late endosomal protein CD63 was also suggested to participate in cargo sorting into ILVs destined for secretion as exosomes (van Niel et al. 2011).

2.4.1. ALIX function in exosome biogenesis

The interaction of three proteins, syndecan, syntenin and ALIX, has been shown to be important for the recruitment of the ESCRT-III machinery on the limiting membrane of endosomes for exosome biogenesis (Fig 15) (Baietti et al. 2012; Ghossoub et al. 2014; Roucourt et al. 2015; Iavello et al. 2016). Syndecan, a transmembrane heparan sulfate proteoglycan, interacts with PDZ (PSD-95, Discs Large, Zo-1 domain) domains of the cytosolic protein syntenin (Grootjans et al. 2000). In addition, syntenin N-terminal domain interacts with ALIX via three LYP(X)nL motifs (Baietti et al. 2012). Gain and loss of function experiments established that syndecan, syntenin and ALIX work together to control the exosomal release of CD63, Heat Shock Protein 70 (HSP70) and their own exosomal secretion. Moreover, the cleavage of heparan sulfate chains in syndecan, which is catalyzed by heparanase intracellularly, is necessary for syndecan-syntenin-ALIX exosome formation (Roucourt et al. 2015). This pathway is also dependent on the ESCRT-I component TSG101, ESCRT-II VPS22 and ESCRT-III proteins CHMP4A,B,C and CHMP2A, but not CHMP3 and CHMP6 (Baietti et al. 2012). Furthermore, neutral SMase2, which catalyzes sphingomyelin breakdown and ceramide production, might also regulate syndecan-syntenin-ALIX-dependent pathway (Baietti et al. 2012). Phospholipase D2 (PLD2) and the adenosine 5′-diphosphate (ADP)-ribosylation factor 6 (ARF6) small GTPase, which regulates syntenin-syndecan recycling to the plasma membrane (Zimmermann et al. 2005), are necessary for

syntenin exosome production (Ghossoub et al. 2014). The PLD2 and ARF6 mechanism for exosome production is unknown. However, ARF6 is known to stimulate phospholipase D2 (PLD2) activity (Hiroyama and Exton 2005), inducing an increase in the cone-shaped lipid phosphatidic acid, which might control ILV formation.

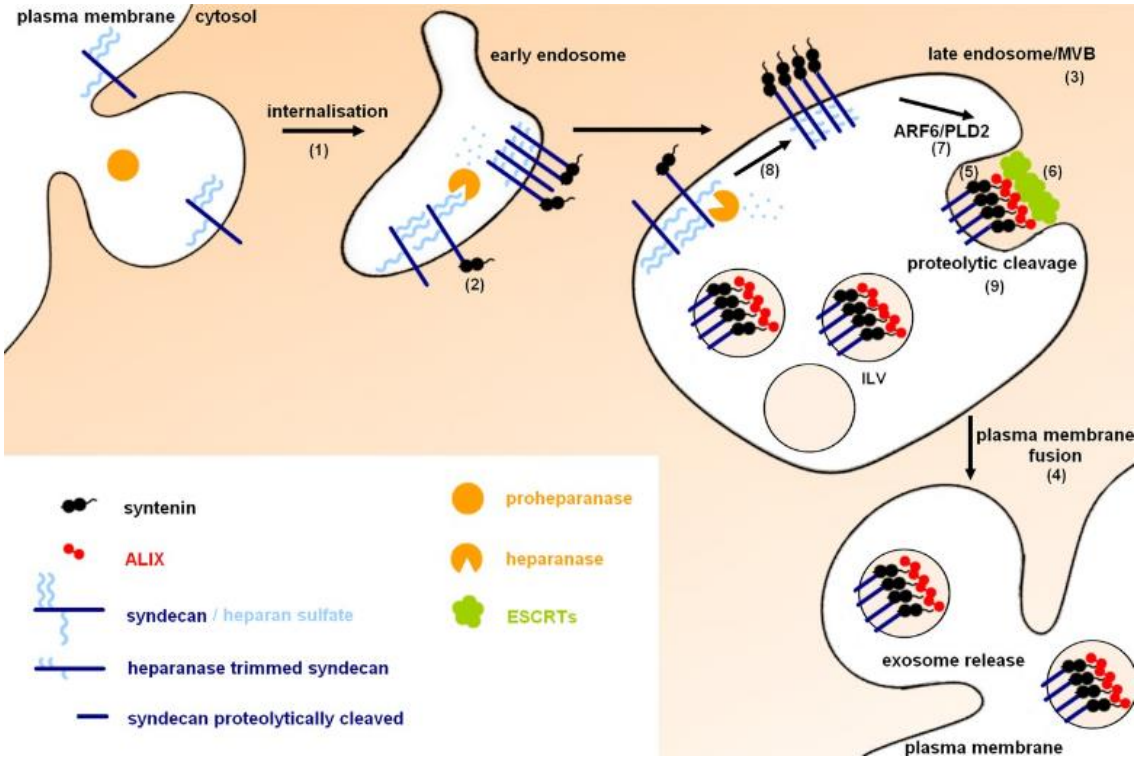

Fig 15. Syndecan–syntenin-ALIX and associated regulators in exosome biogenesis (Friand et al. 2015)**.**

3. Aim of the project

The ESCRT-associated protein ALIX acts in multiple ESCRT-mediated processes, such as virus budding, cytosolic release of the viral capsid, cytokinesis, membrane repair, autophagy and exosome biogenesis. The capacity of ALIX to interact with the ESCRT proteins TSG101 and CHMP4 facilitates the recruitment of the ESCRT machinery during virus budding, cytokinesis and membrane repair. Additionally, some evidence shows that ALIX participates in ILV formation and cargo sorting to lysosomes. ALIX association with endosomes depends on the interaction of its BRO1 domain with LBPA/BMP. As it was discussed before, LBPA/BMP induces ILV formation in large acidic liposomes, a process which is regulated by ALIX. Therefore, it is tempting to think that ALIX could serve as a nucleation factor for the ESCRT proteins, through its ability to bind both the LBPA/BMP endosomal membranes and the ESCRT proteins (CHMP4 and TSG101). In other words, LBPA/BMP and ALIX may play a direct role in ESCRT-dependent ILV formation and cargo sorting within LEs.

The aim of this study is to investigate the role of ALIX in the recruitment of ESCRTs to the endosomal membranes and its effect on endosomal protein sorting. Some of the raised questions regarding the link between ALIX and the ESCRTs endosomal function are the following:

Is ALIX regulating the ESCRTs endosomal association?

1. If ALIX associates with LE, can ALIX also recruit ESCRTs to this compartment?
2. Which ESCRT proteins are regulated by ALIX?
3. What is the mechanism by which ALIX regulates the ESCRT endosomal interaction?
4. Is ALIX-LBPA/BMP interaction important for ALIX-dependent recruitment of ESCRTs?

Is ALIX participating in cargo sorting in the MVE?

1. Which proteins traffic through endosomes in an ALIX-dependent manner? Is this pathway cargo-specific?
2. Is ALIX affecting other endosomal processes which also require ESCRTs

Results

1. Regulation of ESCRT Endosomal Recruitment by the Lipid-binding Protein ALIX

Jorge Larios, Vincent Mercier, Daniel Abegg, Alexander Adibekian, Aurélien Roux, Jean Gruenberg.

(in preparation)

Regulation of ESCRT Endosomal Recruitment by the Lipid-binding Protein ALIX

Jorge Larios[1], Vincent Mercier[1], Daniel Abegg[2], Alexander Adibekian[2], Aurélien Roux[1, 3], Jean Gruenberg[1,3]

(1) Department of Biochemistry, 30 quai E. Ansermet, 1211 Geneva 4. Switzerland.
(2) Department of Chemistry, The Scripps Research Institute, 130 Scripps Way, Jupiter, FL 33458, USA.
(3) To whom correspondence should be addressed. Department of Biochemistry, 30 quai E. Ansermet, 1211 Geneva 4. Switzerland.

Tel: +41-22-379-3464; Fax +41-22-379-6470; e-mail: jean.gruenberg@unige.ch

Running head: ALIX-dependent ESCRT recruitment to endosomes.

SUMMARY

The endosomal sorting complexes required for transport (ESCRT) is a multiprotein complex that participates in processes which require membrane deformation, such as cytokinetic abscission, virus budding and multivesicular body (MVB) biogenesis. MVBs contain intraluminal vesicles (ILV), the formation of which plays a key role in the delivery of ubiquitinated cargo to the lysosomes for degradation. The canonical ESCRT pathway for MVB formation requires four complexes, ESCRT-0, -I, -II and –III, which participate in cargo sorting and membrane remodeling. Amidst these complexes, ESCRT-III has been extensively described as a key player in the deformation and fission of membranes. ALIX is an ESCRT-associated protein known to interact with TSG101 (ESCRT-I), CHMP4 (ESCRT-III), and a late endosomal lipid, LBPA. ALIX and LBPA participate in the formation of ILVs, yet the mechanism by which they act and their link to the ESCRT machinery is unknown. Here, we show that an active form of ALIX, lacking its proline rich region (ALIXΔPRR), recruits ESCRT-III proteins, mainly CHMP4, to late endosomes, in an LBPA-dependent manner. This recruitment occurs independently of ESCRT-0, -I and –II, and of CHMP6. Additionally, ALIXΔPRR induces the accumulation of ubiquitinated proteins, providing evidence that the endosomal sorting of several specific transmembrane proteins depends on ALIX. Altogether, we illustrate the importance of ALIX and LBPA in the recruitment of ESCRT-III proteins and in the sorting of specific cargo. We describe a route that permits the recruitment of the ESCRT-III machinery to late endosomes, representing an ESCRT pathway alternative to the canonical pathway.

INTRODUCTION

Signaling receptors and other cell surface proteins that need to be downregulated are endocytosed into early endosomes, from where they are sent to the lysosomes for degradation. First, in the endosomes, they are sorted from molecules that are destined to be recycled to the plasma membrane or transported to the trans-Golgi network (Scott et al. 2014). Second, they are selectively incorporated into ILVs within multivesicular regions of the early endosome. This nascent endosomal carrier vesicle (ECV)/MVB then matures and transports endocytosed materials towards late endosomes and lysosomes (Scott et al. 2014). There, ILVs are degraded together with their signaling receptor cargo. However, ILVs can also have different fates, such as secretion into the extracellular milieu as exosomes (Kowal et al. 2014).

Sorting of proteins targeted for lysosomal degradation into ILVs depends on the addition of ubiquitin (Kolling and Hollenberg 1994; Hicke and Riezman 1996; Katzmann et al. 2001) by triggering the sequential recruitment of ESCRTs onto the endosomal membranes (Babst et al. 2002a; Babst et al. 2002b; Katzmann et al. 2003; Teis et al. 2008; Saksena et al. 2009). ESCRTs are organized in four complexes, ESCRT-0, -I, -II and –III (Williams and Urbe 2007), with ESCRT-0, -I and –II having multiple ubiquitin-binding domains (Shields and Piper 2011). In addition to cargo sorting, ESCRTs are also believed to play a direct role in membrane remodeling processes leading to ILV formation. Specifically, ESCRT-III is recruited to the membrane by ESCRT-II (Babst et al. 2002b), which acts as a nucleator and activator of ESCRT-III polymerization (Teis et al. 2010). Membrane polymerization of the ESCRT-III protein CHMP4 (SNF7 in yeast) in spiral-shaped structures (Chiaruttini and Roux 2017), has been suggested to be the main contributor for membrane deformation not only in ILV biogenesis, but also in other ESCRT mediated processes (Wollert et al. 2009; Chiaruttini et al. 2015). Consistently, ESCRT-III, is proposed to be a general fission machinery for budding processes with the same orientation away from the cytoplasm, as it is required for cytokinesis (Carlton and Martin-Serrano 2007; Morita et al. 2007; Mierzwa et al. 2017), virus budding (Garrus et al. 2001; Martin-Serrano et al. 2001; Strack et al. 2003), plasma membrane (Jimenez et al. 2014; Scheffer et al. 2014) and nuclear envelope repair (Denais et al. 2016; Raab et al. 2016), nuclear envelope reassembly following mitosis (Olmos et al. 2015; Vietri et al. 2015; Olmos et al. 2016; Gu et al. 2017) and autophagy (Filimonenko et al. 2007; Lee et al. 2007).

In addition to the classical ESCRT-0, -I, -II pathway, other mechanisms for ESCRT-III recruitment have been suggested (Jimenez et al. 2014; Scheffer et al. 2014 Vietri, 2015 #44; Christ et al. 2016; Tang et al. 2016; Gu et al. 2017). In yeast, the ESCRT-associated protein BRO1 interacts with SNF7 (Kim et al. 2005), and together with ESCRT-0, induces SNF7 polymerization on membranes in an ESCRT-I and –II independent manner (Tang et al. 2016). In mammals, there are three BRO1-domain containing proteins, which all interact with SNF7/CHMP4: HD-PTP, ALIX and BROX (Katoh et al. 2003; Strack et al. 2003; Ichioka et al. 2007; Ichioka et al. 2008). By linking ESCRT-0 and –III, HD-PTP may participate in the ILV sorting and lysosomal targeting of EGFR in an ESCRT-II independent mechanism (Doyotte et al. 2008; Ali et al. 2013). Similarly, ALIX is believed to mediate the ubiquitin-independent sorting of specific G protein-coupled receptors (GPCRs) into ILVs for degradation (Dores et al. 2012; Dores et al. 2016). ALIX is also required for other ESCRT-dependent processes such as HIV budding (Strack et al. 2003), plasma membrane repair (Jimenez et al. 2014), cytokinetic abscission (Carlton and Martin-Serrano 2007; Morita et al. 2007; Christ et al. 2016) and autophagy (Murrow and Debnath 2015).

ALIX has an N-terminal BRO1 domain, a central V-shaped domain and a flexible C-terminal PRR (Fisher et al. 2007). ALIX BRO1 domain interacts with CHMP4 (Katoh et al. 2003; Strack et al. 2003), and the PRR binds TSG101 in ESCRT-I (Strack et al. 2003). In addition, the PRR region interacts with the BRO1 domain, keeping ALIX in a closed, auto-inhibited conformation (Strack et al. 2003; Zhou et al. 2008; Zhou et al. 2009; Zhou et al. 2010; Zhai et al. 2011). The V-domain binds to the YPX_3L motif present in the cytosolic region of the GPCRs PAR1 and P2Y1 and is required for their lysosomal degradation (Dores et al. 2012; Dores et al. 2016). We previously reported that the BRO1 domain interacts with lysobisphosphatidic acid/bis(monoacylglycero)phosphate (LBPA/BMP) (Bissig et al. 2013), an unconventional phospholipid found only in late endosomes and not detected in other cellular membranes (Kobayashi et al. 1998). LBPA participates in the specific recruitment of ALIX to late endosomes (Matsuo et al. 2004; Bissig et al. 2013). While these interactions have been partially characterized, their importance for the lysosomal degradation of specific membrane proteins remains unclear. In particular, whether the ALIX pathway acts as a bypass for specific cargo degradation is unknown. Here, we studied ALIX-dependent mechanisms of ESCRTs recruitment to endosomes. We find that ALIXΔPRR massively recruits CHMP4 to the late endosomes, through an ALIX-LBPA interaction. The massive recruitment of CHMP4 is correlated with the accumulation of ubiquitinated proteins in late endocytic compartments, and an abnormal endosomal accumulation of specific transmembrane proteins.

RESULTS

ALIX is confined to late endosomes containing LBPA

ALIX-PRR presumably functions as an auto-inhibitory domain that can interact with the BRO1 domain via the flexible V-domain (Zhou et al. 2008). When expressed in HeLa cells, both full-length ALIX and ALIX without the PRR (ALIXΔPRR) tagged with mCherry, showed both a cytosolic and punctate distribution (Fig 1B). However, the proportion of ALIXΔPRR in punctae was more important than wild-type ALIX. Because the deletion of the auto-inhibitory domain in ALIXΔPRR could promote membrane association, we studied the possible colocalization of ALIXΔPRR punctae with endosomal structures. ALIXΔPRR-mCherry colocalized to a very large extent with the late endosomal lipid LBPA, contrary to the poor colocalization with the early endosomal marker EEA1 (Fig 1C; quantification in Fig 1D), consistent with the notion that ALIX membrane-association is LBPA dependent (Matsuo et al. 2004; Bissig et al. 2013). Thus, the PRR of ALIX is inhibitory to its association with late endosomal membranes.

ALIX recruits ESCRT-III on late endosomes

Since ESCRT-III binds to ALIX through the BRO1 domain (Katoh et al. 2003), we investigated whether ALIXΔPRR-mCherry was able to interact with ESCRT-III *in vivo*. To this end, we used cells stably expressing GFP-CHMP4B at low levels (Poser et al. 2008) equivalent to endogenous protein levels (Fig 2B). In these cells, GFP-CHMP4B was found primarily in the cytosol and nucleoplasm (Fig 2A), but also on intracellular punctae. Upon ALIXΔPRR expression, the intensity (Fig 2C) and number (Fig 2C-D) of CHMP4B-labeled punctae increased severalfold, and CHMP4B then co-localized with ALIXΔPRR-mCherry. Triple-labeling experiments confirmed that CHMP4B was recruited onto late endosomes containing both ALIXΔPRR and LBPA (Fig 2E). Consistent with these observations, both CHMP4B and GFP-CHMP4B also increased severalfold on light membranes (endosomal-enriched fraction) prepared from cells expressing ALIXΔPRR-mCherry (Fig 2G-H), when compared to the post-nuclear supernatant (Fig 2F). Moreover, overexpression of the RAB7 effector RILP (RAB-interacting lysosomal protein), which clusters late endosomes at the microtubule-organizing center (MTOC) (Cantalupo et al. 2001), also clustered ALIXΔPRR in the perinuclear region of Hela cells (Fig 3A). These punctae contained RILP itself, GFP-CHMP4B, ALIXΔPRR and the late endocytic marker LAMP1 (Fig 3C). We also investigated

whether ALIX also recruited other ESCRT-III subunits onto endosomes. CHMP1A-V5 and CHMP1B-Flag exhibited primarily a cytosolic distribution without ALIX (Fig 4A-B). Much like CHMP4B, both proteins were efficiently recruited onto endosomes containing ALIXΔPRR-mCherry (Fig 4C-D). Similarly, both CHMP4A and CHMP3 were enriched in light membrane fractions prepared from cells expressing ALIXΔPRR (Fig 4E-F; our antibodies against CHMP4A and CHMP3 do not work by immunofluorescence). Additionally, VPS22 and VPS4B, other ESCRT components, were also increased in light membranes upon ALIXΔPRR expression. It has been previously described that a dynamic subunit turnover in ESCRT-III assembly is necessary to induce membrane deformation, which is regulated by VPS4 (Adell et al. 2014; Adell et al. 2017; Mierzwa et al. 2017). Fluorescence of GFP-CHMP4B and ALIXΔPRR-mCherry on endosomes was partially recovered after photobleaching, showing that the binding of both proteins to the compartments is dynamic, and suggesting that VPS4 participates in the remodeling of the endosomal ESCRT-III polymers formed by ALIXΔPRR expression (Fig S1). Altogether, these data demonstrate that ALIXΔPRR causes the constitutive recruitment of ESCRT subunits on the late endosomes containing both LBPA and LAMP1, and that the process is highly selective.

ESCRT-III membrane association depends on LBPA and ESCRT-III binding sites of ALIX

Given that it was previously established that ALIX binding to ESCRT-III is abolished by the I212D mutation in ALIX BRO1 domain (Fisher et al. 2007; McCullough et al. 2008), we investigated whether this binding site was required for CHMP4B recruitment. In contrast to ALIXΔPRR, the ALIXΔPRR-I212D mutant exhibited a strictly cytosolic distribution in cells expressing GFP-CHMP4B (Fig 5A) and was thus unable to recruit GFP-CHMP4B onto endosomal membranes, as monitored by fluorescence microscopy (Fig 5A; quantification in Fig 5B) and subcellular fractionation (Fig 5C-D, quantification in Fig 5E). These observations indicate not only that ALIX recruits ESCRT-III highly specifically, but also that interactions with ESCRT-III are necessary to stabilize ALIX onto endosomal membranes.

Similarly, we previously showed that ALIX association to LBPA-containing membranes depends on a flexible loop on the side of the BRO1 domain opposite to the ESCRT-III binding site, and that mutation of the exposed hydrophobic residues L104 and F105 to glutamines (ALIXΔPRR-QQ) abolishes membrane association (Bissig et al. 2013). Much like ALIXΔPRR-I212D, ALIXΔPRR-QQ remained strictly cytosolic in cells expressing GFP-CHMP4B (Fig 5A), as expected (Bissig et al. 2013), and was unable to recruit GFP-

CHMP4B onto endosomes, as monitored by fluorescence microscopy (Fig 5A; quantification in Fig 5B) and subcellular fractionation (Fig 5C-D, quantification in Fig 5E). Hence, intact binding sites for both LBPA and ESCRT-III are required for the ALIX-dependent recruitment of ESCRT-III onto late endosomal membranes *in vivo*.

Both LBPA and ALIX are necessary to support ESCRT-III binding *in vitro*

Having shown that LBPA is required for ALIX binding to endosomes and that ALIX membrane association in turn mediates ESCRT-III recruitment *in vivo*, we then investigated whether the process could be reconstituted *in vitro* using purified components. In these experiments, giant unilamellar vesicles (GUV) were prepared with a phospholipid composition mimicking the one of endosomes, enriched in LBPA (Kobayashi et al. 1998) and labeled with trace amounts of N-rhodamine PE (DOPC:DOPE:PI:LBPA:Rhod-PE-4.99:2:1:2:0.01 molar ratio). We then used our previously established method to prepare supported bilayers upon GUV deposition onto glass (Chiaruttini et al. 2015; Mierzwa et al. 2017). Supported bilayers were then sequentially incubated with purified recombinant ALIX BRO1 domain, and then with purified recombinant Alexa-488 CHMP4B (Fig S2).

In the absence of LBPA, no CHMP4B was bound onto the bilayer, whether ALIX-BRO1 was present or not. However, hardly detectable levels of CHMP4B could be recruited in the presence of ALIX-BRO1, when PS, another negatively-charge lipid, replaced LBPA in the same molar ratio (DOPC:DOPE:PI:DOPS - 5:2:1:2). By contrast, CHMP4B was massively recruited onto LBPA-containing bilayers, but only when ALIX-BRO1 was present (Fig 6A, quantification in Fig 6C). CHMP4B recruitment occurred with relatively rapid kinetics *in vitro*, with an apparent t1/2 of approximately 5 min (Fig 6B, boxed area in Fig 6A). Altogether, these observations demonstrate that CHMP4B recruitment onto the bilayer can be fully recapitulated *in vitro*, provided that LBPA and ALIX-BRO1 are present.

Other ESCRT or ESCRT-related proteins are dispensable for the ALIX-dependent membrane association of CHMP4B

Our *in vivo* (Fig 4-5) and *in vitro* (Fig 6) analysis strongly suggests that CHMP4B recruitment onto late endosomal membranes strictly depends on LBPA and ALIX. We thus decided to investigate whether other factors, which had been previously linked to ESCRT-III physically or functionally, also played a role in ALIX-dependent CHMP4B membrane association. In particular, we tested the possible role of the ESCRT-0 subunits STAM1/2 and

the ESCRT-I subunit TSG101, which binds ALIX, as well as the role of VPS22, which initiates ESCRT-III polymerization on membranes, and of the ESCRT-III subunit CHMP3 and CHMP6. Finally, we tested the possible involvement of other BRO1 domain-containing proteins HD-PTP and BROX (Fig 7). Each individual protein except ALIX was depleted using a pool of siRNA target sequences to limit the danger of off-target effects, while ALIX was depleted using a well-characterized single siRNA (Bissig et al. 2013). After knock-down, each protein was reduced 5-10 times, except perhaps STAM1, which was reduced approximately 3 times (Fig 7C).

ALIXΔPRR was fully capable of redistributing GFP-CHMP4B from cytosol to endosomal membranes upon depletion of any individual protein candidate (Fig 7A). Indeed, CHMP4B-GFP exhibited the same characteristic punctate pattern as shown in Fig 1, after each KD much like in mock-treated controls (Fig 7A) and the quantification confirmed that none of the KDs had any effect of GFP-CHMP4B membrane association (Fig 7B). Only a slight increase in GFP-CHMP4B recruitment was observed in CHMP3 KD cells, which could be related to CHMP3 function in ESCRTs membrane disassembly. Altogether, our *in vitro* and *in vivo* data show that the extensive recruitment of ESCRT-III onto late endosomal membranes strictly depends on LBPA and ALIX and does not require other factors. We conclude that, in addition to the canonical mechanism dependent on ESCRT-0, ESCRT-I and ESCRT-II, ALIX functions as an alternative mechanism to recruit ESCRT-III selectively onto late endosomes containing LBPA.

ALIX participates in the endosomal sorting of cargo proteins

If ALIX provides an alternative mechanism for ESCRT-III recruitment, this ALIX-ESCRT-III pathway is likely used by cargo proteins trafficking to the late endosomes. Relatively little is known about the possible role of ALIX in protein sorting into multivescular endosomes. ALIX does not seem to play a role in the downregulation of the EGF receptor, a canonical ESCRT cargo protein (Cabezas et al. 2005), but is involved in the ubiquitin-independent, ESCRT-dependent sorting of two GPCRs to the lysosomes (Dores et al. 2012; Dores et al. 2016).

As a first step to investigate the possible role of ALIX in cargo sorting, we followed the fate of proteins originally biotinylated at the cell surface. We used a membrane-impermeable biotinylation reagent containing a disulfide bridge, so that biotinylated proteins remaining at the cell surface at the end of the incubation period could be released upon reduction. After

18h incubation, labeling with streptavidin-Cy5 showed that the biotinylated proteins distributed within structures dispersed over the cell cytoplasm (Fig 8A-B). These elements correspond primarily to early and recycling endosomes, as previously shown (Steinman et al. 1983). Endocytosed biotinylated proteins were also found in structures labelled with ALIXΔPRR-mCherry (Fig 8A-B), presumably corresponding to endocytosed proteins sent to late endosomes and lysosomes (Scott et al. 2014). Interestingly, careful observations showed that biotinylated proteins accumulated significantly in the ALIXΔPRR-containing endosomes, when compared to untransfected cells (Fig 8B; quantification in Fig 8C). Since EGF receptor degradation in cells challenged with EGF was not perturbed by ALIXΔPRR expression, we concluded that the expression of ALIXΔPRR did not induce a general block of the late endosomal pathway, but rather of specific cargos labelled for degradation (Fig S3).

As protein sorting into the ILVs occurs mostly upon ubiquitination (Kolling and Hollenberg 1994; Hicke and Riezman 1996; Katzmann et al. 2001), we investigated whether ubiquitinated proteins were present in ALIXΔPRR-containing late endosomes. Strikingly, immunofluorescences revealed that conjugated ubiquitin accumulated within endosomes containing both ALIXΔPRR and GFP-CHMP4B (Fig 8D-F), and conjugated ubiquitin was hardly detected, if at all, in cells that did not express ALIXΔPRR (Fig 8E). In addition, cell fractionation showed accumulation of ubiquitinated proteins in light membranes in cells expressing ALIXΔPRR (Fig S4). These observations demonstrate that massive recruitment of ALIXΔPRR and ESCRT-III causes the selective accumulation of specific ubiquitinated cargoes, including cell surface proteins, in late endosomes. Presumably, the constitutive recruitment of ESCRT-III mediated by ALIXΔPRR leads to unbalanced ESCRT-III kinetics, eventually leading to cargo capture and accumulation within the endosome.

Cargo proteins which follow an ALIX-dependent sorting in endosomes

Having shown that ALIXΔPRR expression affects the sorting of ubiquitinated proteins in endosomes, we designed a strategy to identify the missorted proteins. After ALIXΔPRR expression in HeLa cells, or the transfection of an empty vector (control), a subcellular fractionation was carried out and the protein content of the endosomal-enriched fractions was processed by mass spectrometry and label-free quantification (Fig 9A). As expected, several proteins were accumulated in the ALIXΔPRR endosomes when compared with the control condition (Fig 9 and Fig S5). Multiple transmembrane proteins and proteins linked to ubiquitination, autophagy, endosome and actin function were identified (Fig 9B). The top hits

were in majority ESCRTs, and ESCRT-III proteins showed the highest accumulation upon ALIXΔPRR expression, with a 15-fold increase for CHMP4B, 7-fold increase for CHMP2A-B and at least 2.5-fold increase in other ESCRT-III proteins (Fig 9C). As CHMP6 (VPS20 in yeast) has been proposed to initiate CHMP4/SNF7 polymerization onto endosomal membranes, we wondered if ALIXΔPRR could affect its endosomal-association. CHMP6 was more difficult to detect by mass spectrometry and was only identified in the ALIXΔPRR transfected condition. Surprisingly, western blot analysis of the light membranes did not show any difference in CHMP6 levels between ALIXΔPRR and the control condition (Fig S6), suggesting a specific ALIX-dependent and CHMP6-independent pathway for ESCRT-III endosomal recruitment. Although autophagy-linked proteins were accumulated, the basal number of LC3 or P62 autophagosomes was not affected by ALIXΔPRR expression (Fig S7), which implies that the general basal autophagy pathway is not affected. Within the list of proteins accumulated in endosomes by ALIXΔPRR expression, 55 corresponded to transmembrane proteins. Endosomal EGFR levels were not affected by ALIXΔPRR expression, which was corroborated by western blot (Fig S3), suggesting ALIX participation in the endosomal sorting of specific cargo.

DISCUSSION

ALIX recruits the ESCRT proteins to late endosomes

There is accumulating evidence that ALIX binds to endosomes and plays an important role in ILV formation and back-fusion (Matsuo et al. 2004; Falguieres et al. 2008; Bissig et al. 2013). We previously demonstrated that the ALIX BRO1 domain contains a lipid-binding loop that interacts with LBPA/BMP, and this interaction is important for ALIX binding to endosomes (Bissig et al. 2013). Our results show that ALIXΔPRR binds more efficiently to endosomes than the full length protein, and that more than 70% of the endosome-associated ALIX localizes to LBPA/BMP-positive late endosomes. ALIXΔPRR has been suggested to be an ALIX “active” form, in which the BRO1 domain is no longer blocked by the flexible PRR and is more accessible to interact with CHMP4 (Zhou et al. 2009; Zhou et al. 2010). Likewise, ALIX V-domain interaction with the HIV-1 p6 Gag late domain is also increased in ALIXΔPRR (Strack et al. 2003; Zhou et al. 2008). From this piece of evidence and other structural analysis, a model for ALIX “activation” has been proposed, in which the PRR loses its interaction with the BRO1 domain and the V-domain elongates allowing ALIX dimerization (Pires et al. 2009). Thus, one may hypothesize that ALIXΔPRR BRO1 domain is also more exposed for the interaction with LBPA, or that the global protein conformation has a better interaction with the lipid membrane, resulting in an increase in endosomal ALIX. Additionally, the mechanism by which ALIX dissociates from membranes is unknown, so the dynamics of ALIXΔPRR membrane dissociation could also be different than the full length protein.

Using fluorescence microscopy, biochemistry analysis and mass spectrometry, we find that ALIXΔPRR expression induces massive ESCRT protein recruitment to endosomes. ESCRT-III proteins are accumulated the most on endosomes upon ALIXΔPRR expression, where CHMP4B expression is increased 15 times. In addition, both CHMP4B and ALIXΔPRR localize to late endosomes. Several studies show that the AAA-ATPase VPS4, which regulates ESCRT-III polymers disassembly and remodeling, plays a crucial role during ESCRT-dependent membrane deformation and fission (Adell et al. 2014; Adell et al. 2017; Mierzwa et al. 2017). Even though CHMP4B is highly redistributed from the cytosol to endosomes in ALIXΔPRR expressing cells, we show that GFP-CHMP4B fluorescence is partly recovered after photobleaching, which indicates that endosomal ESCRT-III turns over CHMP4B subunits with cytoplasmic pools. Furthermore, ALIXΔPRR expression also induces

the endosomal recruitment of VPS4A and VPS4B, which further supports that ESCRT-III recruited proteins are functional and could participate in endosomal membrane deformation.

Mechanism for ALIX-dependent ESCRT-III endosomal recruitment

ALIX has been shown to participate in the recruitment of ESCRT-III proteins during virus budding, cytokinesis and plasma membrane repair (Strack et al. 2003; Carlton and Martin-Serrano 2007; Morita et al. 2007; Jimenez et al. 2014) and has been suggested to participate in an alternative pathway for ESCRT-III activation and membrane polymerization (McCullough et al. 2008; Pires et al. 2009; Jimenez et al. 2014; Meng et al. 2015; Christ et al. 2016). Furthermore, the ALIX yeast homolog, BRO1, induces ESCRT-III protein SNF7 “activation” and membrane polymerization during cargo sorting into ILVs. Two parallel pathways were proposed for ESCRT-III endosomal recruitment in yeast: one dependent on ESCRT-I/II (canonical pathway) and a second one dependent on ESCRT-0/BRO1 (Tang et al. 2016). Our results show that ALIXΔPRR-dependent CHMP4B recruitment to endosomes is coordinated by the dual capacity of ALIX BRO1 domain to interact with CHMP4 and LBPA; in this regard, it is important to highlight that CHMP4 and LBPA interact with opposite regions in the BRO1 domain, which suggests that both interactions might take place at the same time. Interestingly, our results show that CHMP6 (VPS20 in yeast), which has been proposed to act as the initial nucleation factor for membrane recruitment and polymerization of SNF7/CHMP4 (Teis et al. 2008; Saksena et al. 2009; Tang et al. 2015), is not recruited to endosomes upon ALIXΔPRR expression. In addition, silencing of ESCRT-0, -I, -II or ESCRT-III proteins (CHMP3 and CHMP6) did not prevent CHMP4B endosomal recruitment induced by ALIXΔPRR expression. Our *in vitro* experiments clearly show that ALIX BRO1 strongly recruits CHMP4B to lipid bilayers containing LBPA, and that ALIX binding is specific to this lipid and not to other negatively charged lipids, which confirms our previous results (Bissig et al. 2013). All this strongly suggests that ALIX directly recruits CHMP4 to LBPA-containing endosomes, as an alternative pathway for the canonical ESCRT-0, -I, -II-dependent ESCRT-III recruitment, as it was previously shown for cytokinesis (Christ et al. 2016).

ALIX participates in the endosomal sorting of specific transmembrane proteins

Endosomal sorting and degradation of two GPCRs, PAR1 and P2Y1, the primary HIV-1 receptor, CD4, and EGFR (UVC-induced internalization) are regulated by ALIX (Dores et al.

2012; Tomas et al. 2015; Dores et al. 2016). We find that ALIXΔPRR expression induces the accumulation of plasma membrane proteins in endosomes. In addition, high levels of ubiquitinated proteins localize to ALIXΔPRR and CHMP4B positive endosomes in ALIXΔPRR expressing cells. Interestingly, the accumulation of ubiquitinated proteins by the knock down or overexpression of ESCRT proteins HRS, TSG101 and VPS28 has been previously described (Bishop et al. 2002). Our mass spectrometry analysis of endosomal-enriched fraction show that several transmembrane proteins accumulate in endosomes isolated from ALIXΔPRR expressing. However, EGFR and other proteins that are sorted in endosomes do not accumulate, suggesting that ALIX regulates the sorting of a specific pool of proteins. Furthermore, the global integrity of the endosomal pathway is not affected, which is supported by the results showing that ligand-induced EGFR degradation is not affected in ALIXΔPRR expressing cells.

The evidence presented elucidates a role for ALIX in a non-canonical ESCRT-III endosomal recruitment. We showed that ALIX recruits ESCRT-III proteins, primarily CHMP4, in an LBPA dependent and ESCRT-0, -I, –II, and CHMP6 independent manner. Furthermore, data provides evidence that ALIX participates in the endosomal sorting of ubiquitinated cargo, as shown by accumulation of transmembrane and ubiquitinated proteins in endosomes in the presence of ALIX lacking its PRR.

MATERIALS AND METHODS

Cells, Antibodies and Reagents

We obtained HeLa-MZ cells from Marino Zerial (MPI-CBG, Dresden), HeLa Kyoto cells stably expressing GFP-CHMP4B from Anthony Hyman (MPI-CBG, Dresden) (Poser et al. 2008), and HeLa Kyoto cells stably expressing CHMP1A-V5 or CHMP1B-FLAG from Harald Stenmark (Christ et al. 2016). All cells were grown in Minimum Essential Media Eagle (MEM) (Sigma-Aldrich, St. Louis, MO) supplemented with 10% fetal bovine serum (FBS) (Thermo Fisher Scientific, Waltham, MA), 1% MEM Non-Essential Amino Acids (Thermo Fisher Scientific, Waltham, MA), 2 mM L- Glutamine (Thermo Fisher Scientific, Waltham, MA), 100 µg/mL penicillin and 100 units/mL streptomycin (Thermo Fisher Scientific, Waltham, MA) in a 37 °C, 5% CO_2 incubator. HeLa Kyoto cells stably expressing GFP-CHMP4B were additionally supplemented with 0.5 mg/mL Geneticin (Millipore, Billerica, MA) and cells expressing CHMP1A-V5 or CHMP1B-FLAG were maintained with 0.5 µg/mL puromycin (Thermo Fisher Scientific, Waltham, MA).

The anti-LBPA monoclonal antibody (6C4) has been described (Kobayashi et al. 1998) and the anti-RAB5 monoclonal antibody was a gift from Reinhard Jahn (Göttingen, Germany). The antibodies against STAM1 (12434-1-AP), HD-PTP (10472-1-AP), TSG101 (14497-1-AP), CHMP6 (16278-1-AP) and CHMP3 (15472-1-AP) were from Proteintech (Chicago, IL), against FLAG (F3165) and tubulin (T9026) from Sigma-Aldrich (St. Louis, MO), against CHMP4A (H-52) and VPS22 (EAP30 C-11) from Santa Cruz Biotechnology (Dallas, TX), against P62 (ab109012), CHMP4B (ab105767) and BROX (ab193008) from Abcam (Cambridge, UK), against EEA1 (ALX-210-239-C100) and conjugated ubiquitin (FK2) from Enzo Life Sciences (Farmingdale, NY), against Lamp1 (D2D11) from Cell Signaling Technology (Danvers, MA), against V5 (R960-25) from Thermo Fisher Scientific (Waltham, MA), against EGFR (20-ES04, for western blot) from Fitzgerald (Acton, MA), against EGFR (555996, for immunofluorescence) from BD biosciences (Franklin lakes, NJ), against LC3 (M152-3) from MBL international (Woburn, MA) and against ALIX (pab0204) from Covalab (Villeurbanne, France). The Cy2-, Cy3-, and Cy5-conjugated fluorescent antibodies were from Jackson ImmunoResearch (West Grove, PA) and the peroxidase-conjugated secondary antibodies from Bio-Rad Laboratories (Hercules, CA). Streptavidin-Cy5, EZ-Link Sulfo-NHS-SS-Biotin, Alexa Fluor 488 TFP ester, Ni-NTA Agarose, 7 kDa MWCO Zeba Spin Desalting Columns and Hoechst 33342 were from Thermo Fisher Scientific (Waltham, MA).

MBPTrap HD 5 mL columns, Glutathione Sepharose 4B and Dextrin Sepharose High Performance were from GE Healthcare (Anaheim, CA). The cOmplete Protease Inhibitor Cocktail was from Roche (Basel, Switzerland). Restriction enzymes were obtained from New England Biolabs (Ipswich, MA).

LBPA [(S,S) Bisoleoyl-lysobisphosphatidic acid] was from Echelon Biosciences (Salt Lake City, UT). DOPC, DOPE, DOPS, Liver PI and lissamine rhodamine B sulfonyl (18:1 Rhod PE) were from Avanti Polar Lipids (Alabaster, AL). The lysosomotropic reagent L-leucyl-L-leucine methyl ester (LLOMe) was from Sigma-Aldrich (St. Louis, MO). Other reagents and chemicals were obtained from Sigma-Aldrich (St. Louis, MO).

Plasmids, RNA Interference and Transfection

RILP plasmids were obtained from C. Bucci (Lecce, Italy). pmCherry vector was obtained from Clontech (Mountain View, CA). Myc-ALIX-mCherry plasmid was generated by cloning ALIX cDNA into a pCMV-Tag3C vector (Agilent Technologies, Santa Clara, CA) using *XhoI* site. Then, the mCherry cDNA was cloned in ALIX C-terminus using *XhoI* and *ApaI* sites. A mutagenesis in ALIX stop codon was generated using the following primers: forward, CTATCCACAGCAGTTACCTCGAGGGGGGGCCC and reverse, GGGCCCCCCCTCGAGGTAACTGCTGTGGATAG. The Myc-ALIXΔPRR-mCherry plasmid was generated by replacing ALIX cDNA from the Myc-ALIX-mCherry plasmid, cloned in *XhoI* site, with the ALIXΔPRR cDNA (ALIX BRO1 domain and V-domain, which corresponds to the first 702 amino acids). The following primers were used to generate the mutants Myc-ALIXΔPRR-I212D-mCherry, Myc-ALIXΔPRR-QQ-mCherry (mutation LF 104/105 to QQ) and the siRNA resistant Myc-ALIXΔPRR-mCherry mutant: I212D forward primer, GATAAGATGAAAGATGCCGACATAGCTAAGCTGGCAAATC and reverse, GATTTGCCAGCTTAGCTATGTCGGCATCTTTCATCTTATC. LF104/105QQ forward primer, GCTTTTGATAAAGGTTCCCAGCAAGGAGGGTCTGTAAAATTGG and reverse, CCAATTTTACAGACCCTCCTTGCTGGGAACCTTTATCAAAAGC. siRNA resistant forward primer, GCCAAGCCGCTCGTCAAATTCATCCAGCAGACGTAC and reverse, GTACGTCTGCTGGATGAATTTGACGAGCGGCTTGGC. The CHMP4B expression plasmid for recombinant protein purification was generated by replacing SNF7 from pMBP-HIS2-SNF7 plasmid (Addgene no. 21492) for the CHMP4B cDNA, using BamHI and NotI sites. Before cloning CHMP4B into the plasmid, a silent mutation was generated in the CHMP4B sequence in order to remove an internal BamHI cutting site. The primers used for the mutation were the following: forward, AACTGGGCTGGGTCCATGTAACCAGCTTTCTTG

and reverse, CAAGAAAGCTGGTTACATGGACCCAGCCCAGTT. The ALIX BRO1 domain plasmid for recombinant protein production was generated by cloning the BRO1 domain (1-359 amino acids) into a pGEX-6P-2 vector.

The siRNA sequences against STAM1, STAM2, TSG101, VPS22, CHMP3, CHMP6, HD-PTP and BROX were from siTOOLs Biotech (Planegg, Germany). For each gene, a pool of 30 different siRNA sequences was designed. A pool of 30 siRNA sequences, which do not interact with human genes, was used as a negative control. Each pool was used at a low 3 nM concentration in order to reduce the danger of off-target effects in knockdown experiments. The single siRNA sequence against ALIX (AAGCCGCTGGTGAAGTTCATC) had been previously characterized and its effects are fully rescued by RNAi-resistant ALIX (Bissig et al. 2013); the negative control siRNA (AllStars) was from Qiagen (Hilden, Germany). Single siRNAs were used at 20 nM. The sequences are listed in the 5′-to-3′ direction.

DNA and siRNA were transfected in cells according to the manufacturer's instructions using FuGENE HD (Promega Corporation, Madison, WI) and Lipofectamine RNAiMAX (Thermo Fisher Scientific, Waltham, MA), respectively. Unless indicated otherwise, experiments were performed after transfection with DNA for 7 h and siRNA for 72 h.

Fluorescent light microscopy: Immunofluorescence and cell surface biotinylation

Immunofluorescence was performed after fixing cells grown on glass coverslips, or directly in 96-well dish plates for high throughput microscopy, for 20 min with 3% PFA in PBS. All steps of the immunofluorescence procedure were performed at room temperature. When indicated, cells were permeabilized for 5 min with 0.01% saponin in PBS prior to PFA fixation. After fixation, cells were incubated for 45 min in 1% fish skin gelatin, 0.1% saponin in PBS, followed by 30 min incubation with the primary antibody in 1% fish gelatin in PBS. After washing the primary antibody with PBS, the cells were incubated for 30 min with the secondary antibody (Cy2-, Cy3-, or Cy5-conjugated fluorescent antibodies) in 1% fish gelatin in PBS, followed by PBS washes. The cells were mounted in Mowiol 40-88 medium containing 10 µg/mL Hoechst and imaged with a Zeiss 700 confocal microscope (Carl Zeiss AG; Oberkochen, Germany) using a 63x objective. For high throughput microscopy, 96-well plates were imaged with an ImageXpress Micro XLS Widefield High-content microscope (Molecular Devices; CA, USA) or an ImageXpress Micro Confocal High-content microscope (Molecular Devices; CA, USA) (used in the widefield mode) using a 40x objective.

To biotinylate the cell surface, cells grown on glass coverslips were washed with ice cold PBS 0.9 mM $CaCl_2$, 0.5 mM $MgCl_2$ (PBS^{++}) and incubated for 30 min with 1.5 mg/mL EZ-Link Sulfo-NHS-SS-Biotin in PBS^{++} at 4 °C. The cells were washed once with 50 mM glycine in PBS^{++}, followed by three washes with PBS^{++} at 4 °C. Fresh medium was added to the cells and the Myc-ALIXΔPRR-mCherry plasmid was transfected for 18 h. Cells were washed four times with PBS^{++} at 4 °C and incubated twice 20 min with 50 mM Tris pH 8.6, 75 mM NaCl, 0.9 mM $CaCl_2$, 0.5 mM $MgCl_2$ and 50 mM sodium 2-mercaptoethanesulfonate (MesNA). After washing the cells with 5 mg/mL iodoacetamide in ice cold PBS^{++} and three washes with PBS^{++}, cells were fixed with 3% PFA in PBS for 20 min at 4 °C.

GUV electroformation

GUV electroformation was performed as described in (Chiaruttini et al. 2015). Briefly, lipids were mixed in chloroform at a final concentration of 1 mg/mL. Then, 20 µL lipids were spread on two indium tin oxide coated glass slides. After 1 h incubation in a vacuum oven at 30 °C, a rubber ring was placed between the two slides and the space between the glasses was filled with 500 mM sucrose solution (500 mOsmol). GUVs were formed by applying 1 V AC-current (10 Hz sinusoidal) for 1 h at room temperature.

Live imaging of protein binding to supported lipid bilayers

Supported lipid bilayers were prepared in a glass bottom flow chamber sticky-slide VI 0.4 from ibidi (Planegg, Germany). The chamber was filled with 150 µL of 20 mM Hepes pH 8, 250 mM NaCl (500 mOsmol) and 10 µL of GUVs. After mixing, in order to obtain a lipid bilayer attached to the glass, the solution was incubated for 10 min followed by 3 washes with 120 µL ALIX buffer: 25 mM Hepes pH 7.4, 0.3 mM BAPTA, 0.3 mM NTA, 0.3 mM HEDTA and 686 µM $CaCl_2$ (20 µM free calcium, calculated using WEBMAXC STANDARD software: http://www.stanford.edu/~cpatton/webmaxcS.htm). The chamber was incubated for 10 min with a mix of 4 mg/mL casein in 20 mM Hepes pH 8 and ALIX buffer (volume ratio, 1:1), followed by 15 washes with ALIX buffer. When ALIX BRO1 domain was added, the protein was incubated for 40 min in ALIX buffer at a final concentration of 3.7 µM, and the unbound protein was removed with ALIX buffer. The chamber was placed in an inverted microscope assembled by 3i (Intelligent Imaging Innovation, Denver, USA) and Nikon (Eclipse C1, Nikon, Tokyo, Japan) for imaging. One of the entries of the chamber was connected to a syringe pump. The other entry was used to add CHMP4B-488, which was

incubated for 25 min in ALIX buffer at a final concentration of 0.64 µM. The chamber was imaged every minute during the incubation with CHMP4B-488 and a 2-µm-thick volume stack (1 µm above and below the supported membrane) was acquired. The stacks were converted into 2D images by maximum intensity projection.

Image analysis

CHMP4B clusters were quantified in ALIXΔPRR-mCherry expressing cells using CellProfiler (Kamentsky et al. 2011). Briefly, the cell periphery was selected manually and the images were processed with the enhanced edges module. The object identification module was used to identify and quantify the CHMP4B clusters per cell. Coloc 2 plugin from ImageJ (National Institutes of Health, Bethesda, MD) was used for colocalization analysis.

LC-MS/MS sample preparation

Protein concentration was determined using the Bradford assay (Bio-Rad Laboratories, Hercules, CA). Samples were denatured with 6 M urea in 50 mM NH_4HCO_3 , reduced with 10 mM TCEP for 30 min and alkylated with 25 mM iodoacetamide for 30 min in the dark. Samples were diluted to 2 M urea with 50 mM NH_4HCO_3, and digested with trypsin (1 µL of 0.5 µg/µL) in the presence of 1 mM $CaCl_2$ for 12 hours at 37 °C. Samples were acidified to a final concentration of 5% acetic acid, desalted over a self-packed C18 spin column and lyophilized. Samples were analyzed by LC-MS/MS (see below) and the MS data was processed with MaxQuant (see below).

LC-MS/MS analysis

Peptides were resuspended in water with 0.1% formic acid (FA) and analyzed using Proxeon EASY-nLC 1000 nano-UHPLC coupled to QExactive Plus Quadrupole-Orbitrap mass spectrometer (Thermo Fisher Scientific, Waltham, MA). The chromatography column consisted of a 30 cm long, 75 µm i.d. microcapillary capped by a 5 µm tip and packed with ReproSil-Pur 120 C18-AQ 2.4 µm beads (Dr. Maisch HPLC GmbH, Ammerbuch, Germany). LC solvents were 0.1% FA in H_2O (Buffer A) and 0.1% FA in MeCN (Buffer B). Peptides were eluted into the mass spectrometer at a flow rate of 300 nL/min over a 240 min linear gradient (3-35% Buffer B) at 55 °C. Data was acquired in data-dependent mode (top-20,

NCE 30, R = 17’500) after full MS scan (R = 70’000, m/z 400-1’300). Dynamic exclusion was set to 10 s, peptide match to prefer and isotope exclusion was enabled.

MaxQuant analysis

The MS data was analyzed with MaxQuant 1 (V1.5.2.8) and searched against the human proteome (Uniprot) and a common list of contaminants (included in MaxQuant). The first peptide search tolerance was set at 20 ppm, 10 ppm was used for the main peptide search and fragment mass tolerance was set to 0.02 Da. The false discovery rate for peptides, proteins and sites identification was set to 1%. The minimum peptide length was set to 6 amino acids and peptide re-quantification, label-free quantification (MaxLFQ) and “match between runs” were enabled. The minimal number of peptides per protein was set to two. Methionine oxidation was searched as a variable modification and carbamidomethylation of cysteines was searched as a fixed modification.

Other experimental procedures

Subcellular fractionation was carried out by flotation in sucrose gradients as described (Muriel et al. 2017). Cell lysis was performed with 50 mM Tris, pH 7.4, 1% NP-40, 0.25% sodium deoxycholate, 150 mM NaCl, 1mM EDTA, 1mM PMSF, 1 µg/mL aprotinin, 1 µg/mL leupeptin, 1 µg/mL pepstatin. Western blot analysis was preformed using WesternBright ECL from Advansta (Menlo Park, CA).

ACKNOWLEDGEMENTS

We are grateful to members of the Gruenberg and Roux laboratories for fruitful discussion. We also thank Marie-Claire Velluz, Marie Hélène Beuchat and Brigitte Bernadets for technical support. Support to JG was from the Swiss National Science Foundation, the Swiss Sinergia program, the Polish-Swiss Research Programme (PSPB-094/2010), the NCCR in Chemical Biology and LipidX from the Swiss SystemsX.ch initiative, evaluated by the Swiss National Science Foundation.

REFERENCES

Adell MA, Vogel GF, Pakdel M, Muller M, Lindner H, Hess MW, Teis D. 2014. Coordinated binding of Vps4 to ESCRT-III drives membrane neck constriction during MVB vesicle formation. *J Cell Biol* **205**: 33-49.

Adell MAY, Migliano SM, Upadhyayula S, Bykov YS, Sprenger S, Pakdel M, Vogel GF, Jih G, Skillern W, Behrouzi R et al. 2017. Recruitment dynamics of ESCRT-III and Vps4 to endosomes and implications for reverse membrane budding. *Elife* **6**.

Ali N, Zhang L, Taylor S, Mironov A, Urbe S, Woodman P. 2013. Recruitment of UBPY and ESCRT exchange drive HD-PTP-dependent sorting of EGFR to the MVB. *Curr Biol* **23**: 453-461.

Babst M, Katzmann DJ, Estepa-Sabal EJ, Meerloo T, Emr SD. 2002a. Escrt-III: an endosome-associated heterooligomeric protein complex required for mvb sorting. *Dev Cell* **3**: 271-282.

Babst M, Katzmann DJ, Snyder WB, Wendland B, Emr SD. 2002b. Endosome-associated complex, ESCRT-II, recruits transport machinery for protein sorting at the multivesicular body. *Dev Cell* **3**: 283-289.

Bishop N, Horman A, Woodman P. 2002. Mammalian class E vps proteins recognize ubiquitin and act in the removal of endosomal protein-ubiquitin conjugates. *J Cell Biol* **157**: 91-101.

Bissig C, Lenoir M, Velluz MC, Kufareva I, Abagyan R, Overduin M, Gruenberg J. 2013. Viral infection controlled by a calcium-dependent lipid-binding module in ALIX. *Dev Cell* **25**: 364-373.

Cabezas A, Bache KG, Brech A, Stenmark H. 2005. Alix regulates cortical actin and the spatial distribution of endosomes. *J Cell Sci* **118**: 2625-2635.

Cantalupo G, Alifano P, Roberti V, Bruni CB, Bucci C. 2001. Rab-interacting lysosomal protein (RILP): the Rab7 effector required for transport to lysosomes. *EMBO J* **20**: 683-693.

Carlton JG, Martin-Serrano J. 2007. Parallels between cytokinesis and retroviral budding: a role for the ESCRT machinery. *Science* **316**: 1908-1912.

Chiaruttini N, Redondo-Morata L, Colom A, Humbert F, Lenz M, Scheuring S, Roux A. 2015. Relaxation of Loaded ESCRT-III Spiral Springs Drives Membrane Deformation. *Cell* **163**: 866-879.

Chiaruttini N, Roux A. 2017. Dynamic and elastic shape transitions in curved ESCRT-III filaments. *Curr Opin Cell Biol* **in press**.

Christ L, Wenzel EM, Liestol K, Raiborg C, Campsteijn C, Stenmark H. 2016. ALIX and ESCRT-I/II function as parallel ESCRT-III recruiters in cytokinetic abscission. *J Cell Biol* **212**: 499-513.

Denais CM, Gilbert RM, Isermann P, McGregor AL, te Lindert M, Weigelin B, Davidson PM, Friedl P, Wolf K, Lammerding J. 2016. Nuclear envelope rupture and repair during cancer cell migration. *Science* **352**: 353.

Dores MR, Chen B, Lin H, Soh UJ, Paing MM, Montagne WA, Meerloo T, Trejo J. 2012. ALIX binds a YPX(3)L motif of the GPCR PAR1 and mediates ubiquitin-independent ESCRT-III/MVB sorting. *J Cell Biol* **197**: 407-419.

Dores MR, Grimsey NJ, Mendez F, Trejo J. 2016. ALIX Regulates the Ubiquitin-Independent Lysosomal Sorting of the P2Y1 Purinergic Receptor via a YPX3L Motif. *PLoS One* **11**: e0157587.

Doyotte A, Mironov A, McKenzie E, Woodman P. 2008. The Bro1-related protein HD-PTP/PTPN23 is required for endosomal cargo sorting and multivesicular body morphogenesis. *Proc Natl Acad Sci U S A* **105**: 6308-6313.

Falguieres T, Luyet PP, Bissig C, Scott CC, Velluz MC, Gruenberg J. 2008. In vitro budding of intralumenal vesicles into late endosomes is regulated by Alix and Tsg101. *Mol Biol Cell* **19**: 4942-4955.

Filimonenko M, Stuffers S, Raiborg C, Yamamoto A, Malerod L, Fisher EM, Isaacs A, Brech A, Stenmark H, Simonsen A. 2007. Functional multivesicular bodies are required for autophagic clearance of protein aggregates associated with neurodegenerative disease. *J Cell Biol* **179**: 485-500.

Fisher RD, Chung HY, Zhai Q, Robinson H, Sundquist WI, Hill CP. 2007. Structural and biochemical studies of ALIX/AIP1 and its role in retrovirus budding. *Cell* **128**: 841-852.

Garrus JE, von Schwedler UK, Pornillos OW, Morham SG, Zavitz KH, Wang HE, Wettstein DA, Stray KM, Cote M, Rich RL et al. 2001. Tsg101 and the vacuolar protein sorting pathway are essential for HIV-1 budding. *Cell* **107**: 55-65.

Gu M, LaJoie D, Chen OS, von Appen A, Ladinsky MS, Redd MJ, Nikolova L, Bjorkman PJ, Sundquist WI, Ullman KS et al. 2017. LEM2 recruits CHMP7 for ESCRT-mediated nuclear envelope closure in fission yeast and human cells. *Proc Natl Acad Sci U S A* **114**: E2166-E2175.

Henne WM, Buchkovich NJ, Zhao Y, Emr SD. 2012. The endosomal sorting complex ESCRT-II mediates the assembly and architecture of ESCRT-III helices. *Cell* **151**: 356-371.

Hicke L, Riezman H. 1996. Ubiquitination of a yeast plasma membrane receptor signals its ligand-stimulated endocytosis. *Cell* **84**: 277-287.

Ichioka F, Kobayashi R, Katoh K, Shibata H, Maki M. 2008. Brox, a novel farnesylated Bro1 domain-containing protein that associates with charged multivesicular body protein 4 (CHMP4). *FEBS J* **275**: 682-692.

Ichioka F, Takaya E, Suzuki H, Kajigaya S, Buchman VL, Shibata H, Maki M. 2007. HD-PTP and Alix share some membrane-traffic related proteins that interact with their Bro1 domains or proline-rich regions. *Arch Biochem Biophys* **457**: 142-149.

Jimenez AJ, Maiuri P, Lafaurie-Janvore J, Divoux S, Piel M, Perez F. 2014. ESCRT machinery is required for plasma membrane repair. *Science* **343**: 1247136.

Kamentsky L, Jones TR, Fraser A, Bray MA, Logan DJ, Madden KL, Ljosa V, Rueden C, Eliceiri KW, Carpenter AE. 2011. Improved structure, function and compatibility for CellProfiler: modular high-throughput image analysis software. *Bioinformatics* **27**: 1179-1180.

Katoh K, Shibata H, Suzuki H, Nara A, Ishidoh K, Kominami E, Yoshimori T, Maki M. 2003. The ALG-2-interacting protein Alix associates with CHMP4b, a human homologue of yeast Snf7 that is involved in multivesicular body sorting. *J Biol Chem* **278**: 39104-39113.

Katzmann DJ, Babst M, Emr SD. 2001. Ubiquitin-dependent sorting into the multivesicular body pathway requires the function of a conserved endosomal protein sorting complex, ESCRT-I. *Cell* **106**: 145-155.

Katzmann DJ, Stefan CJ, Babst M, Emr SD. 2003. Vps27 recruits ESCRT machinery to endosomes during MVB sorting. *J Cell Biol* **162**: 413-423.

Kim J, Sitaraman S, Hierro A, Beach BM, Odorizzi G, Hurley JH. 2005. Structural basis for endosomal targeting by the Bro1 domain. *Dev Cell* **8**: 937-947.

Kobayashi T, Stang E, Fang KS, de Moerloose P, Parton RG, Gruenberg J. 1998. A lipid associated with the antiphospholipid syndrome regulates endosome structure and function. *Nature* **392**: 193-197.

Kolling R, Hollenberg CP. 1994. The ABC-transporter Ste6 accumulates in the plasma membrane in a ubiquitinated form in endocytosis mutants. *EMBO J* **13**: 3261-3271.

Kowal J, Tkach M, Thery C. 2014. Biogenesis and secretion of exosomes. *Curr Opin Cell Biol* **29**: 116-125.

Lee JA, Beigneux A, Ahmad ST, Young SG, Gao FB. 2007. ESCRT-III dysfunction causes autophagosome accumulation and neurodegeneration. *Curr Biol* **17**: 1561-1567.

Maejima I, Takahashi A, Omori H, Kimura T, Takabatake Y, Saitoh T, Yamamoto A, Hamasaki M, Noda T, Isaka Y et al. 2013. Autophagy sequesters damaged lysosomes to control lysosomal biogenesis and kidney injury. *EMBO J* **32**: 2336-2347.

Martin-Serrano J, Zang T, Bieniasz PD. 2001. HIV-1 and Ebola virus encode small peptide motifs that recruit Tsg101 to sites of particle assembly to facilitate egress. *Nat Med* **7**: 1313-1319.

Matsuo H, Chevallier J, Mayran N, Le Blanc I, Ferguson C, Faure J, Blanc NS, Matile S, Dubochet J, Sadoul R et al. 2004. Role of LBPA and Alix in multivesicular liposome formation and endosome organization. *Science* **303**: 531-534.

McCullough J, Fisher RD, Whitby FG, Sundquist WI, Hill CP. 2008. ALIX-CHMP4 interactions in the human ESCRT pathway. *Proc Natl Acad Sci U S A* **105**: 7687-7691.

Meng B, Ip NC, Prestwood LJ, Abbink TE, Lever AM. 2015. Evidence that the endosomal sorting complex required for transport-II (ESCRT-II) is required for efficient human immunodeficiency virus-1 (HIV-1) production. *Retrovirology* **12**: 72.

Mierzwa B, Chiaruttini N, Redondo-Morata L, Moser von Filseck J, König J, Larios J, Poser I, Müller-Reichert T, Scheuring S, Roux A et al. 2017. Dynamic subunit turnover in

ESCRT-III assemblies is regulated by Vps4 to mediate membrane remodelling during cytokinesis. *Nature Cell Biology* **in press**.

Morita E, Sandrin V, Chung HY, Morham SG, Gygi SP, Rodesch CK, Sundquist WI. 2007. Human ESCRT and ALIX proteins interact with proteins of the midbody and function in cytokinesis. *EMBO J* **26**: 4215-4227.

Muriel O, Scott CC, Larios J, Mercier V, Gruenberg J. 2017. In Vitro Polymerization of F-actin on Early Endosomes. *J Vis Exp*.

Murrow L, Debnath J. 2015. ATG12-ATG3 connects basal autophagy and late endosome function. *Autophagy* **11**: 961-962.

Olmos Y, Hodgson L, Mantell J, Verkade P, Carlton JG. 2015. ESCRT-III controls nuclear envelope reformation. *Nature* **522**: 236-239.

Olmos Y, Perdrix-Rosell A, Carlton JG. 2016. Membrane Binding by CHMP7 Coordinates ESCRT-III-Dependent Nuclear Envelope Reformation. *Curr Biol* **26**: 2635-2641.

Pires R, Hartlieb B, Signor L, Schoehn G, Lata S, Roessle M, Moriscot C, Popov S, Hinz A, Jamin M et al. 2009. A crescent-shaped ALIX dimer targets ESCRT-III CHMP4 filaments. *Structure* **17**: 843-856.

Poser I, Sarov M, Hutchins JR, Heriche JK, Toyoda Y, Pozniakovsky A, Weigl D, Nitzsche A, Hegemann B, Bird AW et al. 2008. BAC TransgeneOmics: a high-throughput method for exploration of protein function in mammals. *Nat Methods* **5**: 409-415.

Raab M, Gentili M, de Belly H, Thiam H-R, Vargas P, Jimenez AJ, Lautenschlaeger F, Voituriez R, Lennon-Duménil A-M, Manel N et al. 2016. ESCRT III repairs nuclear envelope ruptures during cell migration to limit DNA damage and cell death. *Science* **352**: 359.

Saksena S, Wahlman J, Teis D, Johnson AE, Emr SD. 2009. Functional reconstitution of ESCRT-III assembly and disassembly. *Cell* **136**: 97-109.

Scheffer LL, Sreetama SC, Sharma N, Medikayala S, Brown KJ, Defour A, Jaiswal JK. 2014. Mechanism of Ca(2)(+)-triggered ESCRT assembly and regulation of cell membrane repair. *Nat Commun* **5**: 5646.

Scott CC, Vacca F, Gruenberg J. 2014. Endosome maturation, transport and functions. *Semin Cell Dev Biol* **31**: 2-10.

Shields SB, Piper RC. 2011. How ubiquitin functions with ESCRTs. *Traffic* **12**: 1306-1317.

Steinman RM, Mellman IS, Muller WA, Cohn ZA. 1983. Endocytosis and the recycling of plasma membrane. *J Cell Biol* **96**: 1-27.

Strack B, Calistri A, Craig S, Popova E, Göttlinger HG. 2003. AIP1/ALIX Is a Binding Partner for HIV-1 p6 and EIAV p9 Functioning in Virus Budding. *Cell* **114**: 689-699.

Tang S, Buchkovich NJ, Henne WM, Banjade S, Kim YJ, Emr SD. 2016. ESCRT-III activation by parallel action of ESCRT-I/II and ESCRT-0/Bro1 during MVB biogenesis. *Elife* **5**.

Tang S, Henne WM, Borbat PP, Buchkovich NJ, Freed JH, Mao Y, Fromme JC, Emr SD. 2015. Structural basis for activation, assembly and membrane binding of ESCRT-III Snf7 filaments. *Elife* **4**.

Teis D, Saksena S, Emr SD. 2008. Ordered assembly of the ESCRT-III complex on endosomes is required to sequester cargo during MVB formation. *Dev Cell* **15**: 578-589.

Teis D, Saksena S, Judson BL, Emr SD. 2010. ESCRT-II coordinates the assembly of ESCRT-III filaments for cargo sorting and multivesicular body vesicle formation. *EMBO J* **29**: 871-883.

Tomas A, Vaughan SO, Burgoyne T, Sorkin A, Hartley JA, Hochhauser D, Futter CE. 2015. WASH and Tsg101/ALIX-dependent diversion of stress-internalized EGFR from the canonical endocytic pathway. *Nat Commun* **6**: 7324.

Vietri M, Schink KO, Campsteijn C, Wegner CS, Schultz SW, Christ L, Thoresen SB, Brech A, Raiborg C, Stenmark H. 2015. Spastin and ESCRT-III coordinate mitotic spindle disassembly and nuclear envelope sealing. *Nature* **522**: 231-235.

Williams RL, Urbe S. 2007. The emerging shape of the ESCRT machinery. *Nat Rev Mol Cell Biol* **8**: 355-368.

Wollert T, Wunder C, Lippincott-Schwartz J, Hurley JH. 2009. Membrane scission by the ESCRT-III complex. *Nature* **458**: 172-177.

Zhai Q, Landesman MB, Chung HY, Dierkers A, Jeffries CM, Trewhella J, Hill CP, Sundquist WI. 2011. Activation of the retroviral budding factor ALIX. *J Virol* **85**: 9222-9226.

Zhou X, Pan S, Sun L, Corvera J, Lee YC, Lin SH, Kuang J. 2009. The CHMP4b- and Src-docking sites in the Bro1 domain are autoinhibited in the native state of Alix. *Biochem J* **418**: 277-284.

Zhou X, Pan S, Sun L, Corvera J, Lin SH, Kuang J. 2008. The HIV-1 p6/EIAV p9 docking site in Alix is autoinhibited as revealed by a conformation-sensitive anti-Alix monoclonal antibody. *Biochem J* **414**: 215-220.

Zhou X, Si J, Corvera J, Gallick GE, Kuang J. 2010. Decoding the intrinsic mechanism that prohibits ALIX interaction with ESCRT and viral proteins. *Biochem J* **432**: 525-534.

LEGENDS OF THE FIGURES

Figure 1 Subcellular distribution of ALIXΔPRD

(A). Outline of ALIX organization into three structural domains: the BRO1 domain, the V-domain and the auto-inhibitory proline rich region (PRR). Experiments were typically carried out using an ALIX mutant lacking this auto-inhibitory region (ALIXΔPRR).

(B). HeLa-MZ cells were transfected with ALIX-mCherry or ALIXΔPRR-mCherry, and imaged by confocal microscopy. Scale bar: 10 µm.

(C-D). HeLa-MZ cells were transfected with ALIXΔPRR-mCherry, double-labeled with antibodies against LBPA and EEA1, and processed for triple-channel immunofluorescence microscopy (C). Each individual channel is shown on the left and merged micrographs of ALIXΔPRR-mCherry with EEA1 or LBPA on the right. The boxed area is shown in higher magnification. The fraction of endosomes containing ALIXΔPRR-mCherry that colocalizes with EEA1 or LBPA was quantified by calculating the Manders overlap coefficients (D). Box plot, median (box central line); 25% and 75% percentiles (box edges); 10% and 90% percentiles (whiskers); outliers (black circles). ***p < 0.001; n = 50 cells from three independent experiments. Scale bar: 10 µm.

Figure 2 ALIXΔPRR recruits the ESCRTIII protein CHMP4B to late endosomes

(A-B). HeLa Kyoto cells stably expressing GFP-CHMP4B (HeLa GFP-CHMP4B cells) were imaged (A) by confocal microscopy and analyzed by western blotting (B) using anti-CHMP4B antibody. (A) Scale bar: 10 µm.

(C-D). HeLa GFP-CHMP4B cells transfected with ALIXΔPRR-mCherry were imaged (C) by confocal microscopy. The number of CHMP4B granules was quantified (D) in cells expressing ALIXΔPRR-mCherry (ΔPRR) as compared to untransfected cells (-). Box plot, median (box central line); 25% and 75% percentiles (box edges); 10% and 90% percentiles (whiskers); outliers (black circles). ***p < 0.001; n = 90 cells from three independent experiments (C) Scale bar: 10 µm. The pearson correlation coefficient for ALIX and CHMP4B in (C): 0.72, n=50 cells.

(E). HeLa GFP-CHMP4B cells transfected with ALIXΔPRR-mCherry were stained with anti-LBPA antibody and analyzed by triple-channel fluorescence microscopy. The boxed areas show higher magnification views. Scale bar: 10 µm.

(F-H). HeLa GFP-CHMP4B cells transfected for 18 h with ALIXΔPRR (ΔPRR) or an empty vector as control (ctrl) were fractionated by flotation in a sucrose density gradient. The post-nuclear supernatant (PNS in F) and the light membranes (LM in G) were analyzed by western blotting using antibodies against CHMP4B and ALIX, as well as tubulin and RAB5 (equal loading controls). The relative amounts of CHMP4B in LM fractions was quantified by densitometry (H), using RAB5 intensity for the normalization of the CHMP4B signal. Boxes, mean; bars, ± SD (*n* = 3); ctrl vs ΔPRR, *p < 0.05.

Figure 3 ALIX-induced endosomal recruitment of CHMP4B colocalize with RILP

(A). HeLa-MZ cells transfected with ALIXΔPRR-mCherry and GFP-RILP were analyzed by double-channel fluorescence microscopy. The boxed area in the merged micrograph is shown in higher magnification.

(B-C). HeLa GFP-CHMP4B cells transfected with RILP alone (B) or with RILP together with ALIXΔPRR-mCherry (C), were labeled with antibodies against Lamp1 and analyzed by double (B) and triple (C) channel fluorescence confocal microscopy. The boxed area is shown in higher magnification. Scale bar (A-C): 10 µm.

Figure 4 ALIXΔPRR recruits multiple ESCRT proteins

(A-D). HeLa cells stably expressing CHMP1B-Flag (A and C) or CHMP1A-V5 (B and D) were transfected (C-D) or not (A-B) with ALIXΔPRR-mCherry. The cells were labeled with antibodies against the Flag (A and C) and V5 (B and D) epitopes and analyzed by single (A-B) or double (C-D) channel confocal microscopy. The boxed areas are shown in higher magnification. Scale bar: 10 µm.

(E-F). HeLa GFP-CHMP4B cells transfected with ALIXΔPRR for 18 h were fractionated by flotation in a sucrose density gradient as in Fig 2F. The PNS and the LM fractions were analyzed by western blotting with antibodies against ALIX, VPS4B, CHMP1A, CHMP4A, VPS22 and CHMP3. RAB5 was used as an equal loading control. The relative amounts of each protein in LM was quantified by densitometry (F), using RAB5 intensity to normalize each signal. Boxes, mean; bars, ± SD (*n* = 3); *p < 0.05, **p < 0.01, ***p < 0.001.

Figure 5 CHMP4B recruitment to endosomes depends on ALIX BRO1 domain

(A-B). HeLa GFP-CHMP4B cells transfected with ALIXΔPRR-mCherry, ALIXΔPRR-I212D-mCherry and ALIXΔPRR-QQ-mCherry as indicated, were analyzed by double channel confocal microscopy. The boxed areas are shown in higher magnification. Scale bar: 10 µm. The number of CHMP4B granules was quantified (B) as in Fig 2D. Box plot, median (box central line); 25% and 75% percentiles (box edges); 10% and 90% percentiles (whiskers); outliers (black circles). *p < 0.05; n = 90 cells from three independent experiments.

(C-E). HeLa GFP-CHMP4B cells transfected with ALIXΔPRR (ΔPRR), ALIXΔPRR-I212D (ΔPRR-I212D), ALIXΔPRR-QQ (ALIXΔPRR-QQ) or an empty vector as control (ctrl) were fractionated by flotation in a sucrose density gradient as in Fig 2F. The PNS (C) and LM (D) fractions were analyzed by western blotting with antibodies against CHMP4B and ALIX. Tubulin and RAB5 were used as loading controls for PNS and LM, respectively. The relative amounts of CHMP4B in LM were quantified by densitometry, using RAB5 intensity to normalize the signal. Boxes, mean; bars, ± SD (*n* = 3); ***p < 0.001.

Figure 6 ALIX BRO1 domain recruits CHMP4B to artificial membranes *in vitro*

(A-C). Supported bilayers were prepared with the following lipid composition: DOPC:DOPE:PI (PC:PE:PI, 6.99:2:1 mol), DOPC:DOPE:PI:DOPS (PC:PE:PI:PS, 4.99:2:1:2 mol) and DOPC:DOPE:PI:LBPA (PC:PE:PI:LBPA, 4.99:2:1:2 mol), and all were labeled with trace (0.01 mol) amounts of N-Rhodamine PE (red). The supported bilayers were preincubated (A, right column) or not (A, left column) with ALIX BRO1 domain for 40 min, subsequently incubated for 25 min with CHMP4B-488 (green), and analyzed by time-lapse double channel confocal microscopy. Each panel in A corresponds to a view in the green (CHMP4B-488) channel after 40min incubation, while the boxed areas corresponds to smaller view of the same field in the red channel (N-Rhodamine PE). The time-course of CHMP4B-488 association to LBPA-containing bilayers pre-incubated with ALIX is shown in (B), corresponding to a magnified view of the area marked with a white square in the bottom right panel in (A). The intensity of CHMP4B-488 fluorescence was quantified on the lipid supported bilayers after 25 min incubation (C). Box plot, median (box central line); 25% and 75% percentiles (box edges); 10% and 90% percentiles (whiskers); outliers (black circles). ***p < 0.001; n = 20 lipid patches from two independent experiments. ns: not significant. Scale bar (A): 30 µm.

Figure 7 CHMP4B recruitment induced by ALIXΔPRR expression is independent of other ESCRT proteins

(A-B). HeLa GFP-CHMP4B (green) cells were transfected with a siRNA resistant mutant of ALIXΔPRR-mCherry (red), treated with siRNAs against the indicated proteins and analyzed by double channel confocal microscopy. Two negative control siRNAs were used. siCtrl 1 corresponds to a pool of siRNA sequences used as a control for the siRNA pools used against STAM1+2, TSG101, VPS22, CHMP3, CHMP6, HD-PTP and BROX. siCtrl 2 corresponds to a single siRNA sequence used as a control for the single siRNA used to knockdown endogenous ALIX. Scale bar: 10 µm. The number of CHMP4B granules was quantified (B) as in Fig 2D. Box plot, median (box central line); 25% and 75% percentiles (box edges); 10% and 90% percentiles (whiskers); outliers (black circles). *$p < 0.05$; n = 83 cells from three independent experiments. ns: not significant.

(C). The knockdown efficiency of the different condition in (A-B) was analyzed by western blotting using antibodies against the indicated proteins. Tubulin was used as an equal loading control.

Figure 8 ALIXΔPRR expression induces plasma membrane cargo and ubiquitinated proteins intracellular accumulation

(A). The proteins of HeLa cell surface were labeled with biotin using a reagent cleavable upon reduction, and the cells were then transfected with ALIXΔPRR-mCherry. After 18 h, the biotin still present on the cell surface was removed with the reducing agent MesNa. The cells were then fixed, permeabilized, labeled with streptavidin-Cy5 to detect internalized biotin and analyzed by double channel confocal microscopy. Scale bar: 10 µm. The boxed area is shown in higher magnification. Scale bar: 2 µm.

(B-C). The nuclei of HeLa cells treated as in (A) were stained with Hoechst (B). The intensity of the streptavidin-Cy5 labeling (internalized biotinylated proteins) was then quantified (C) in cells expressing ALIXΔPRR-mCherry (ΔPRR) and compared with non-transfected cells (-). Box plot, median (box central line); 25% and 75% percentiles (box edges); 10% and 90% percentiles (whiskers); outliers (black circles). ***$p < 0.001$; n = 95 cells. Scale bar (B): 10 µm

(D). HeLa GFP-CHMP4B cells were transfected with ALIXΔPRR-mCherry, permeabilized with saponin 0.01% in PBS prior to PFA fixation, labeled with an antibody against conjugated ubiquitin, and analyzed by triple channel fluorescence microscopy. Scale bar: 10 µm. The

boxed area is shown in higher magnification. Arrows point at endosomes containing ALIXΔPRR, CHMP4B and conjugated ubiquitin. Scale bar 1 μm.

(E-F). The nuclei of HeLa cells treated as in (D) were stained with Hoechst, to illustrate the accumulation of ubiquitinated proteins in cells expressing ALIXΔPRR-mCherry, when compared to non-transfected cells. Scale bar: 10 μm (E). The ubiquitin intensity per cell was quantified (F) in cells expressing ALIXΔPRR-mCherry (ΔPRR) and compared with non-transfected cells (-).

Figure 9 ALIXΔPRR expression induces the endosomal accumulation of multiple transmembrane proteins and proteins involved in endosomal cargo sorting

(A). Schematic representation of the steps followed for the identification of proteins accumulated in endosomes upon ALIXΔPRR expression. HeLa GFP-CHMP4B cells were transfected with ALIXΔPRR or an empty vector (control) and were fractionated by flotation in a sucrose density gradient**.** The LM (endosome-enriched fraction) was analyzed by mass spectrometry and label-free quantification. For each protein identified, the average ratio ALIXΔPRR/control was calculated from the signal obtained from two independent experiments.

(B). 189 proteins were accumulated in endosomes upon ALIXΔPRR expression (quantification ratio ALIXΔPRR/control, >1.4). From this list, proteins were categorized in four groups: transmembrane proteins, ub-linked proteins, autophagy and other proteins that participate in endosomal and actin-associated functions.

(C). Table with a list of all the ESCRT and ESCRT-associated proteins, and their mass spectrometry quantification values for two independent experiments (ratio ALIXΔPRR/control). In addition to the massive recruitment of several ESCRT-III proteins to endosomes, ALIXΔPRR expression seems to induce the recruitment of ESCRT-0 proteins, TSG101 and other ESCRT-associated proteins. -: not detected by mass spectrometry; +: detected only in the ALIXΔPRR condition.

SUPPLEMENTARY MATERIALS AND METHODS

Recombinant protein purification

Human CHMP4B was expressed in bacteria and purified as described (Mierzwa et al. 2017). Briefly, pMBP-HIS2-CHMP4B was expressed in *Escherichia coli* Rosetta cells. At OD_{600nm}=0.7, protein expression was induced with 0.5 mM IPTG for 3 h at 30 °C. Bacteria were lysed and sonicated in lysis buffer containing 20 mM Hepes pH 8, 100 mM NaCl, 1% Triton X-100, and cOmplete Protease Inhibitor Cocktail at 4 °C. The fusion protein 6xHis-MBP-CHMP4B was purified by affinity chromatography using an MBPTrap HP 5 mL column. The column was first washed with 20 mM Hepes pH 8, 250 mM NaCl, 0.1% Triton X-100, followed by a second wash with 20 mM Hepes pH 8 and proteins bound to the column were eluted in 20 mM Hepes pH 8, 10 mM maltose. The 6xHis-MBP region was removed by cleavage with TEV protease, followed by incubation with Ni-NTA Agarose resin and with Dextrin Sepharose media. CHMP4B fluorescent-labeling was performed by incubating the protein with Alexa Fluor 488 TFP ester in a 1:2 molar ratio (protein:dye), in the presence of 100 mM $NaHCO_3$ pH 9, 1h at room temperature. The free dye was removed by overnight dialysis against 20 mM Hepes pH 8 at 4 °C, using a membrane of 12–14 kDa MWCO, followed by size-exclusion chromatography using 7 kDa MWCO Zeba Spin Desalting Columns. Finally, the protein was centrifuge at 100,000 g for 10 min, 4 °C. The supernatant was aliquoted, snap frozen using liquid N_2 and stored at -80 °C.

Human ALIX BRO1 domain was expressed and purified from *Escherichia coli* Rosetta cells transformed with the pGEX-ALIX BRO1 domain. At OD_{600nm}=0.5, protein expression was induced with 0.4 mM IPTG for 18 h at 18 °C. Bacteria were lysed and sonicated in lysis buffer containing PBS, 1 mM EDTA, 1 mM DTT, 1% Triton X-100, and cOmplete Protease Inhibitor Cocktail at 4 °C. The lysate was centrifuged at 10,000 g for 30 min at 4 °C and the supernatant was filtered through a 0.22 µm filter. The lysate was incubated with Glutathione Sepharose beads for 2 h at 4 °C. The beads were first washed with PBS, followed by a second wash with 50 mM Tris pH 7.5, 150 mM NaCl, 1 mM EDTA and 1 mM DTT. ALIX BRO1 domain was release from the Glutathione Sepharose beads by the cleavage of GST-ALIX BRO1 domain using PreScission protease. The supernatant was loaded into a size-exclusion chromatography Zeba Spin Desalting Column (7 kDa MWCO) for buffer exchange. The final buffer was 25 mM Hepes pH 7.4, 0.3 mM BAPTA, 0.3 mM NTA and 0.3 mM

HEDTA. After centrifugation at 100,000 g for 10 min, 4 °C, the supernatant was aliquoted, snap frozen using liquid N_2 and stored at -80 °C.

EGF treatment and EGFR degradation analysis: biochemistry and microscopy assays

HeLa cells stably expressing GFP-CHMP4B were transfected for 18 h with myc-ALIXΔPRR or an empty pCMV-Tag3C vector as a control, and then incubated for 3 h in serum-free medium, followed by 1 h incubation with 10 µg/mL cycloheximide in serum-free medium. Then, cells were treated for 1 h, 2 h or 4 h with 100 ng/mL EGF, 10 µg/mL cycloheximide in serum-free medium. All the treatments were performed in a 37 °C, 5% CO_2 incubator. Cells were harvested, lysed, and analyzed by SDS-PAGE and western blot. EGFR degradation measured by immunofluorescence was performed in HeLa-MZ cells transfected 18 h with myc-ALIXΔPRR-mCherry, and then incubated for 3 h in serum-free medium, followed by 1 h incubation with 10 µg/mL cycloheximide in serum-free medium. Then, cells were treated for 15 min, 60 min, 120 min or 240 min with 100 ng/mL EGF, 10 µg/mL cycloheximide in serum-free medium. All the treatments were performed in a 37 °C, 5% CO_2 incubator.

Basal autophagy levels analysis

HeLa MZ cells were transfected for 18 h with myc-ALIXΔPRR-mCherry or pmCherry vector as a control. In addition, cells were treated for 4 h with 500 µM LLOMe, a lysosomotropic reagent which has been shown to recruit the autophagy machinery to lysosomes (Maejima et al. 2013). All the treatments were performed in a 37 °C, 5% CO_2 incubator.

FRAP

HeLa GFP-CHMP4B cells were transfected with ALIXΔPRR-mCherry for 8 h and were treated or not with 10 µM nocodazole for 2 h (to depolymerize microtubules and avoid endosome movement) and rinsed using FluoroBrite DMEM Media (Thermo Fisher Scientific, Waltham, MA) before imaging. Endosomes were imaged using a 100x 1.4 NA oil DIC Plan-Apochromat VC objective (Nikon; Tokyo, Japan) with a Nikon A1 scanning confocal

microscope. Photobleaching were performed in circular regions with 4 iterations of 488 nm at 100% laser intensity.

Image analysis

High throughput image analysis was performed using custom module editor MetaXpress software, from Molecular Devices (CA, USA). Briefly, cells were segmented and the nucleus, cytoplasm and granules (endosomal EGFR, LC3 or P62) were identified. The average intensity of the granules per cell or the number of granules was quantified in cells expressing ALIXΔPRR-mCherry and compared with non-expressing cells.

For FRAP analysis, background fluorescence was subtracted to ROIs intensity values. Those values were subsequently normalized by a non-bleached area and the value of intensity of the first frame after bleaching was subtracted. Finally, FRAP curves were normalized with the pre-bleach fluorescence intensity value.

LEGENDS OF THE SUPPLEMENTARY FIGURES

Fig S1 Endosomal assembly of ALIXΔPRR and CHMP4B is dynamic

(A-B). HeLa GFP-CHMP4B cells were transfected with ALIXΔPRR-mCherry. Fluorescence recovery after photobleaching (FRAP) of endosomes containing GFP-CHMP4B (green) and ALIXΔPRR-mCherry (red) was analysed. White circles indicate photobleached regions. The first column (time: 0 s) corresponds to the time before photobleaching. Fluorescence recovery curves of endosomes for GFP-CHMP4B and ALIXΔPRR-mCherry were calculated (B). Dots, mean; shaded area, ± SD (n = 17 endosomes).

(C-D). HeLa GFP-CHMP4B cells were transfected with ALIXΔPRR-mCherry and analyzed as in A and B. Cells were treated with 10 µM nocodazole for 2 h (to avoid endosomes movements) prior FRAP. Dots, mean; shaded area, ± SD (n = 28 endosomes).

Fig S2 Recombinant CHMP4B and ALIX BRO1 domain protein purification

(A-B). A typical SDS-PAGE gel of recombinant human CHMP4B purification was stained with Coomassie brilliant blue (A). The gel compares aliquots taken at sequential steps of the purification: 1. Bacterial lysate expressing His-MBP-CHMP4B. 2. Protein elution from an MBPTrap column which shows the His-MBP-CHMP4B purified protein. 3. Protein fragments obtained after the incubation with TEV protease (His-MBP and CHMP4B). During the final step of the protein purification procedure, the protein was centrifuged to remove protein aggregates. Aliquots of the supernatant (4) and resuspended pellet (5) are shown. The same gel was exposed to UV light at 320 nm wavelength (B). Fluorescently labeled CHMP4B-488 is visible in wells 4 and 5.

(C). A typical SDS-PAGE gel of the purification of human ALIX BRO1 domain was stained with Coomassie brilliant blue. The gel compares aliquots taken at sequential steps of the purification: 1. Bacterial lysate expressing GST-ALIX BRO1 domain. 2. GST-ALIX BRO1 domain purified with Glutathione Sepharose beads. 3. Protein fragments obtained after the incubation with PreScission protease (ALIX BRO1 domain and GST). During the final step of the protein purification procedure, the protein was centrifuged to remove protein aggregates. An aliquot of the supernatant (4) and the resuspended pellet (5) are shown.

Fig S3 ALIXΔPRR does not affect ligand-induced EGFR degradation or its endosomal levels

(A-B). HeLa GFP-CHMP4B cells were transfected for 18 h with myc-ALIXΔPRR or an empty vector as a control (Ctrl). Cells were sequentially incubated at 37 °C for 3 h in serum-free medium, for 1 h with 10 µg/mL cycloheximide, and finally for 1, 2 or 4 h with 100 ng/mL EGF. Samples were collected and analyzed by western blotting with antibodies against EGFR, ALIX and myc. Tubulin was used as an equal loading control. The relative amounts of EGFR in control cells (ctrl) and in cells expressing myc-ALIXΔPRR (ΔPRR) were quantified by densitometry (B), using tubulin intensity to normalize the signal. Circles, mean; bars, ± SD (*n* = 3). There is no significant difference between Ctrl and ΔPRR for the different time points. **(C-D).** Ligand-induced EGFR degradation was analyzed by high throughput microscopy in HeLa-MZ cells transfected with ALIXΔPRR-mCherry. CHX (10 µg/mL) and EGF (100 ng/mL) incubation was performed as in (A), and an additional 15 min time point was included. After fixation, cells were labeled with an antibody against EGFR and processed for triple-channel immunofluorescence microscopy. Each row represents the imaged area obtained from one 96-well plate, EGFR (green), ALIXΔPRR-mCherry (red) and nuclear staining Hoescht (blue) (C). For each time point, a total of 12000 cells were imaged and ALIXΔPRR-mCherry positive (ΔPRR) or negative (no ΔPRR) cells were segmented using mCherry signal (D, cell segmentation image). Similarly, the endosomal EGFR was also segmented (EGFR granules) and the average EGFR granule intensity per cell was plotted for each time point (D). As at time 0 min, EGFR is mostly at the plasma membrane, 15 min was used as the first time point to measure EGFR endosomal signal. Circles, mean; bars, ± SD. There is no significant difference between non-transfected and ALIXΔPRR-mCherry transfected cells for the different time points.

(E-F). HeLa GFP-CHMP4B cells transfected for 18 h with ALIXΔPRR (ΔPRR) or an empty vector as a control (ctrl) were fractionated by flotation in a sucrose density gradient as in Fig 2F. The total cell lysate and LM (E) were analyzed by western blotting with antibodies against EGFR and ALIX. RAB5 was used as equal loading control. The relative amounts of EGFR in total cell lysate and LM was quantified by densitometry (F), using RAB5 intensity to normalize the signal. Boxes, mean; bars, ± SD (*n* = 3); ns: not significant.

Fig S4 ALIXΔPRR expression induces intracellular accumulation of ubiquitinated proteins

(A-B). HeLa GFP-CHMP4B cells transfected with ALIXΔPRR (ΔPRR) or an empty vector as a control (ctrl) were fractionated by flotation in a sucrose density gradient as in Fig 2F. The PNS and the LM fractions were analyzed by western blotting (A) with antibodies against conjugated ubiquitin and ALIX. RAB5 was used as an equal loading control. The relative amounts of conjugated ubiquitin in PNS and LM was quantified by densitometry (B), using RAB5 intensity to normalize the signal. Boxes, mean; bars, ± SD (*n* = 3); **p < 0.01.

Fig S5 ALIXΔPRR expression induces the accumulation of multiple proteins in the endosomes

List of proteins detected by mass spectrometry in light membranes of HeLa GFP-CHMP4B cells transfected with ALIXΔPRR or an empty vector (control). Proteins were quantified for two independent experiments (A and B) by label-free mass spectrometry quantification, and the ratio ALIXΔPRR/control (A, B and mean) is shown in the table. Transmembrane proteins: green; ESCRT and ESCRT-associated proteins: blue; Ubiquitination-linked proteins: red. ---: not detected by mass spectrometry; +++: detected by mass spectrometry only in ALIXΔPRR transfected cells.

Fig S6 CHMP6 endosomal levels are not affected by ALIXΔPRR expression

(A-B). HeLa GFP-CHMP4B cells transfected with ALIXΔPRR for 18 h were fractionated by flotation in a sucrose density gradient as in Fig 2F. The PNS and the LM fractions were analyzed by western blotting with antibodies against CHMP6 and ALIX. RAB5 was used as an equal loading control (A). The relative amount of CHMP6 in LM was quantified by densitometry (B), using RAB5 intensity to normalize each signal. Boxes, mean; bars, ± SD (*n* = 3); ns: not significant.

Fig S7 Basal number of autophagosomes is not affected by ALIXΔPRR expression

(A-C). Basal autophagy was analyzed by high throughput microscopy in HeLa MZ cells. Four conditions were analyzed: Non treated cells (-), ALIXΔPRR-mCherry or mCherry transfected cells and 4 h treatment with 500 µM L-leucyl-L-leucine methyl ester (LLOMe), as a lysosomal autophagy positive control. After fixation, cells were labeled with an antibody

against LC3 (green, A) or P62 (green, C) and processed for triple-channel immunofluorescence microscopy. Each row represents the imaged area obtained from one 96-well plate. Nuclear staining, Hoechst, is shown in blue. An amplified view of LC3- or P62-labeled cells is shown in the bottom row (A, C). Cells were segmented as explained in Fig S2. ALIXΔPRR-mCherry or mCherry transfected cells were classify in three groups according to their mCherry signal intensity: no expression, low expression and high expression. For each condition, approximately 35000 cells were analyzed, and the average number of LC3 or P62 granules per cell was quantified (B, D). Boxes, mean; bars, ± SD. ***$p < 0.001$; ns: not significant. Scale bar: 10 µm.

SUPLEMMENTARY REFERENCES

Maejima I, Takahashi A, Omori H, Kimura T, Takabatake Y, Saitoh T, Yamamoto A, Hamasaki M, Noda T, Isaka Y et al. 2013. Autophagy sequesters damaged lysosomes to control lysosomal biogenesis and kidney injury. *EMBO J* **32**: 2336-2347.

Mierzwa B, Chiaruttini N, Redondo-Morata L, Moser von Filseck J, König J, Larios J, Poser I, Müller-Reichert T, Scheuring S, Roux A et al. 2017. Dynamic subunit turnover in ESCRT-III assemblies is regulated by Vps4 to mediate membrane remodelling during cytokinesis. *Nature Cell Biology* **in press**.

Larios et al., **Figure 1**

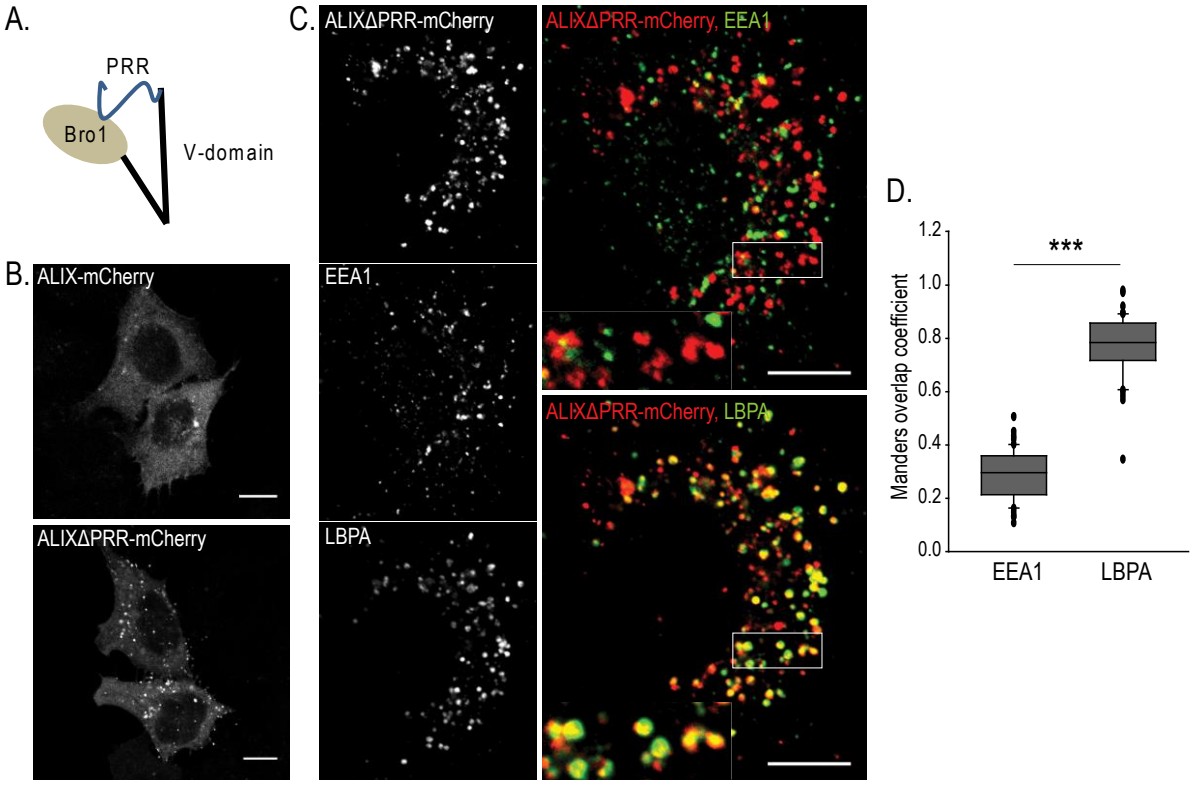

Larios et al., **Figure 2**

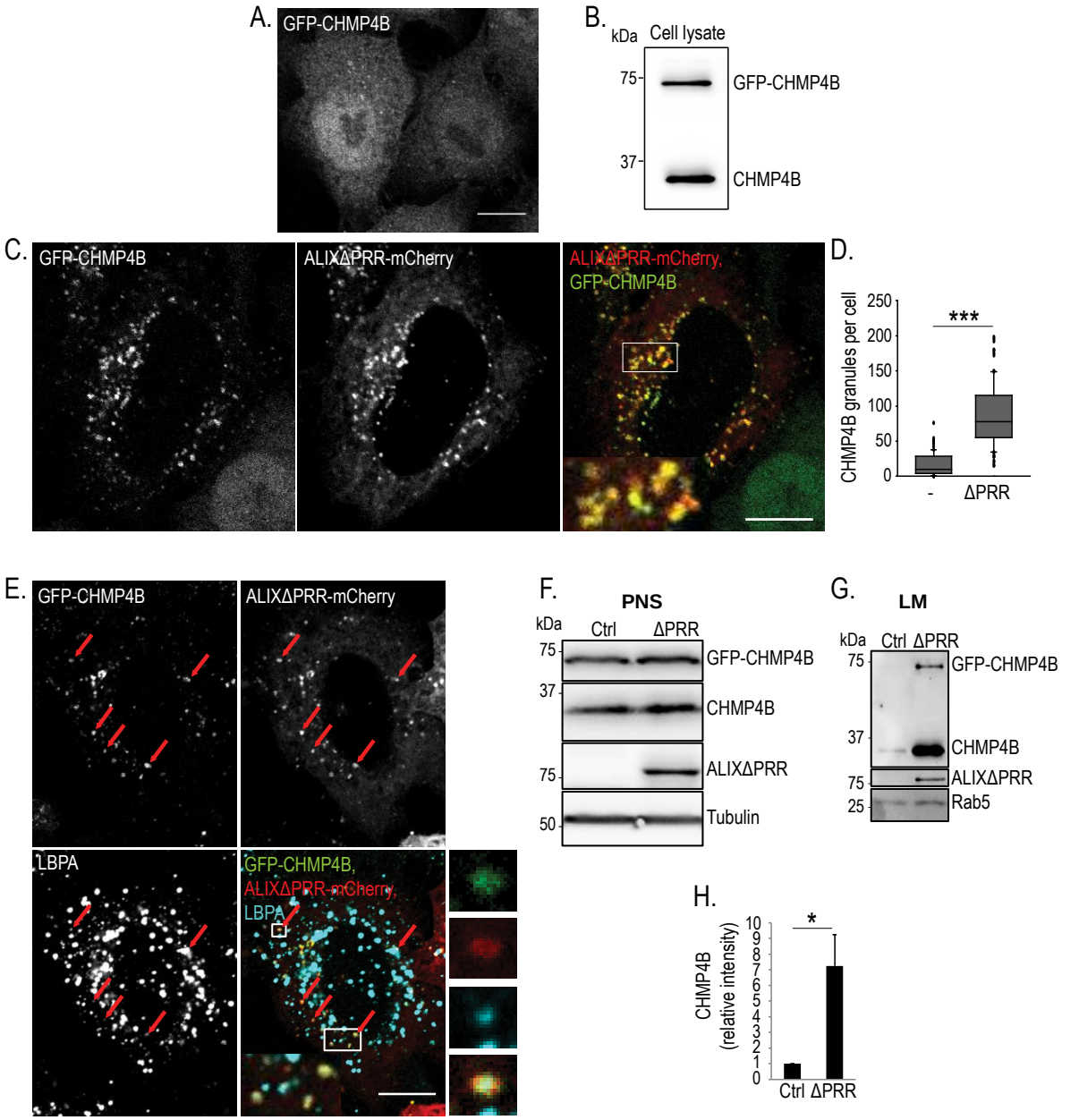

Larios et al., **Figure 3**

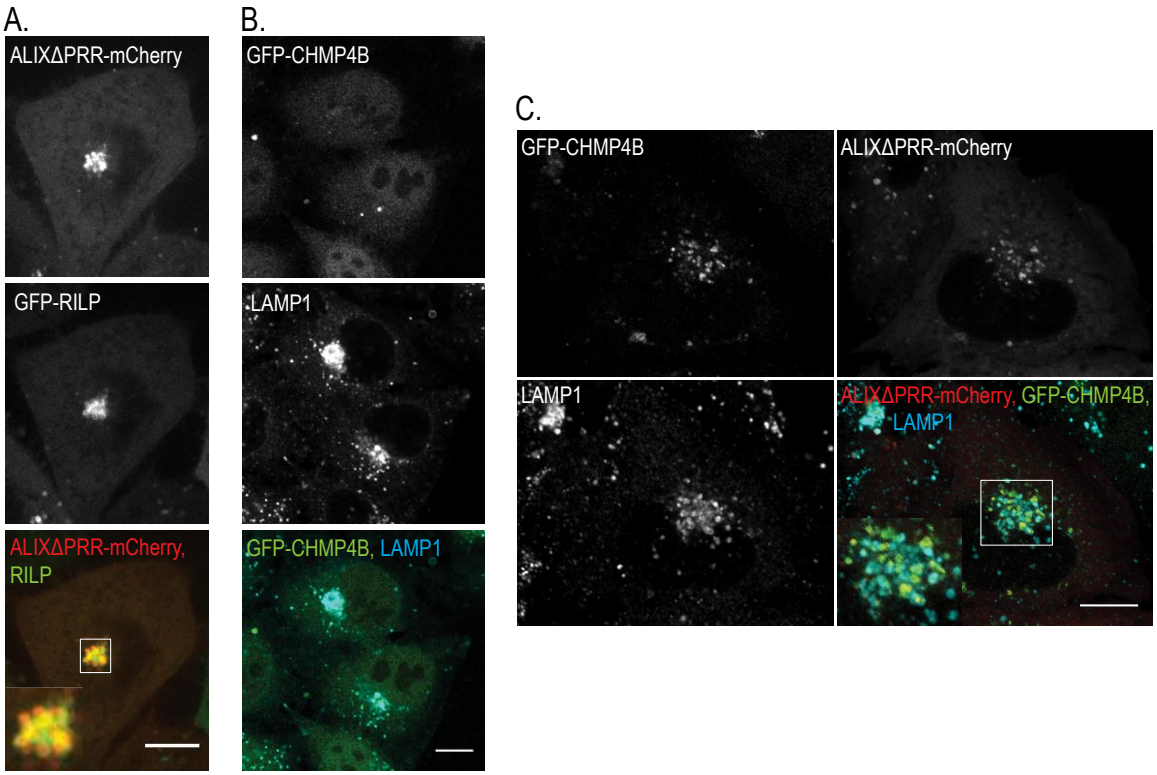

Larios et al., **Figure 4**

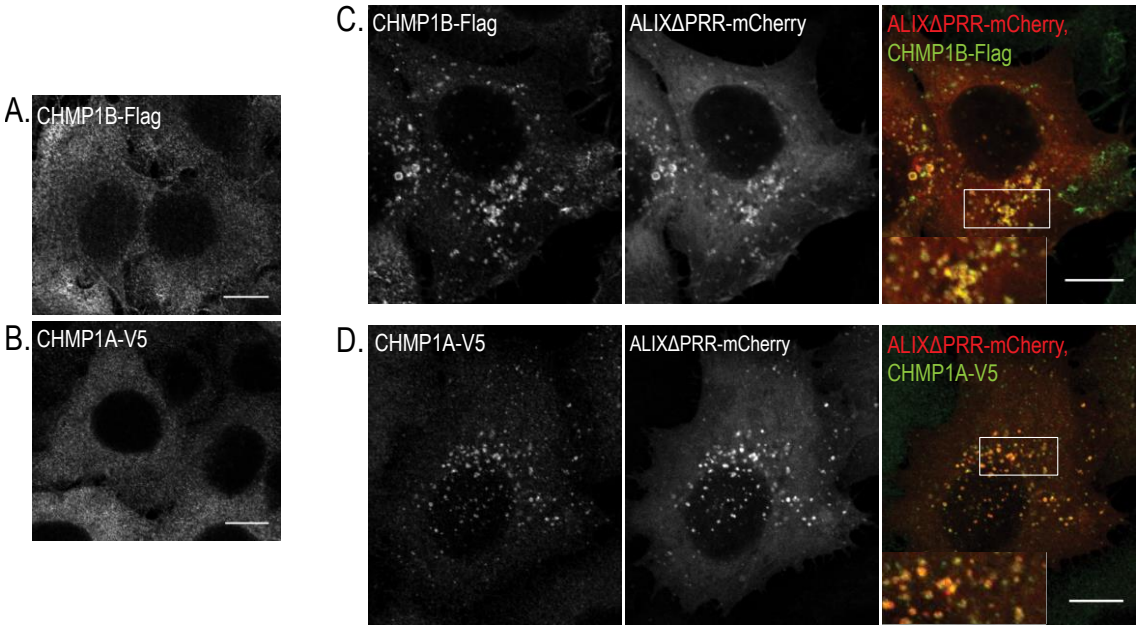

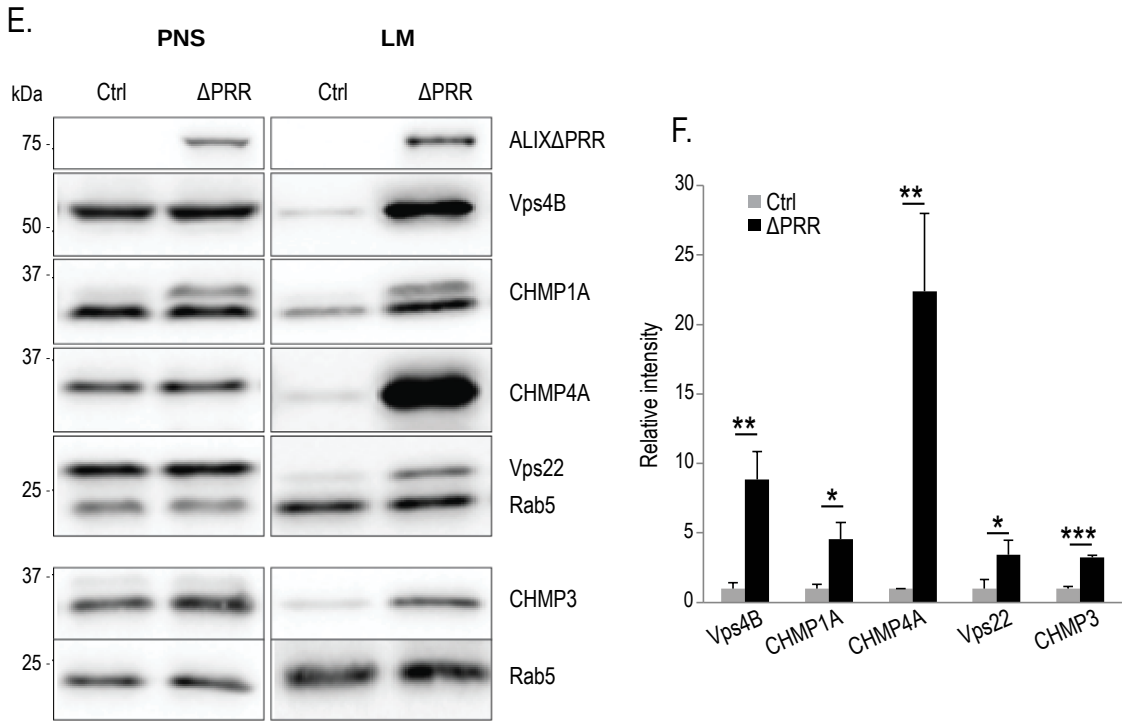

Larios et al., **Figure 5**

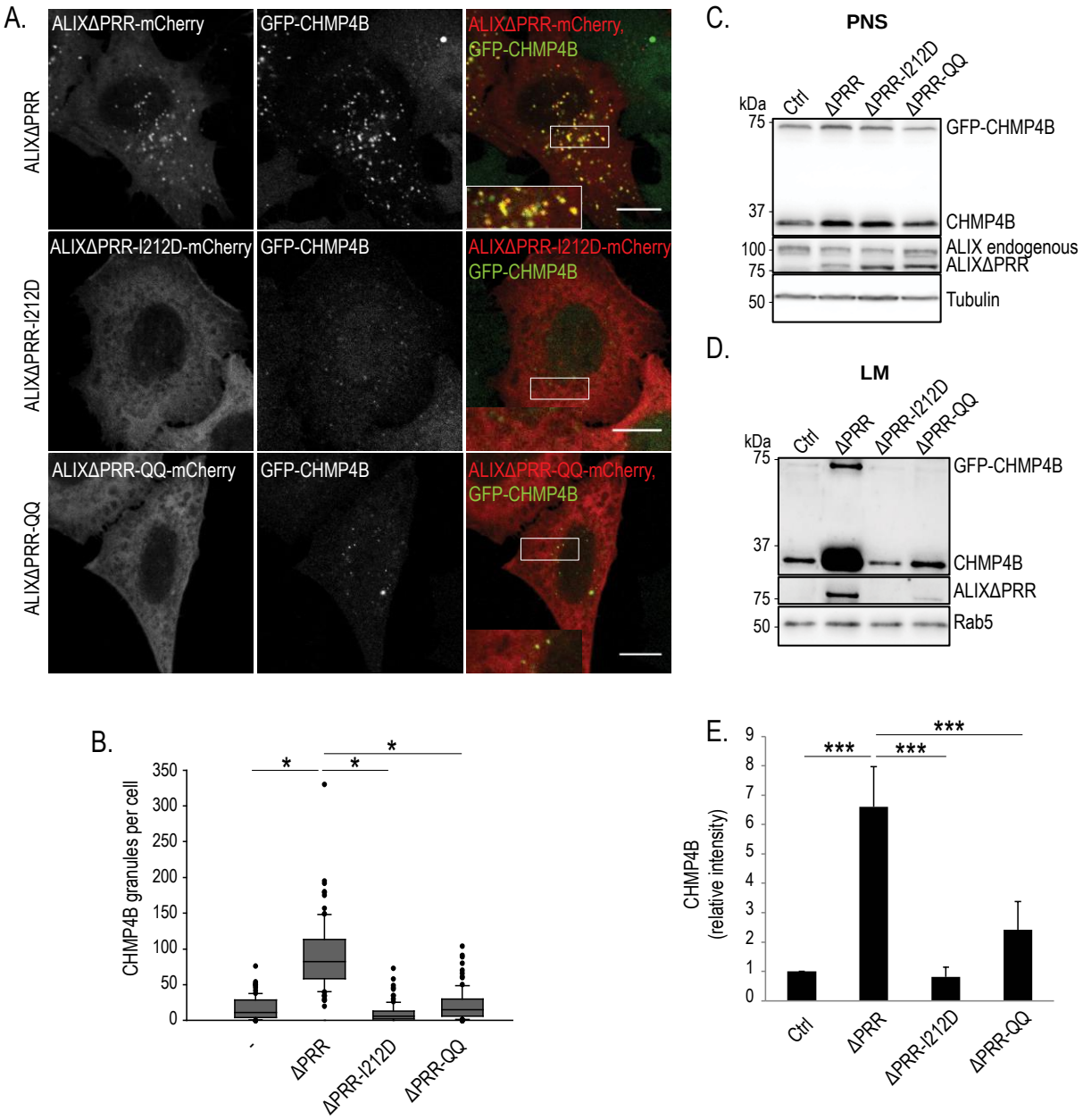

Larios et al., **Figure 6**

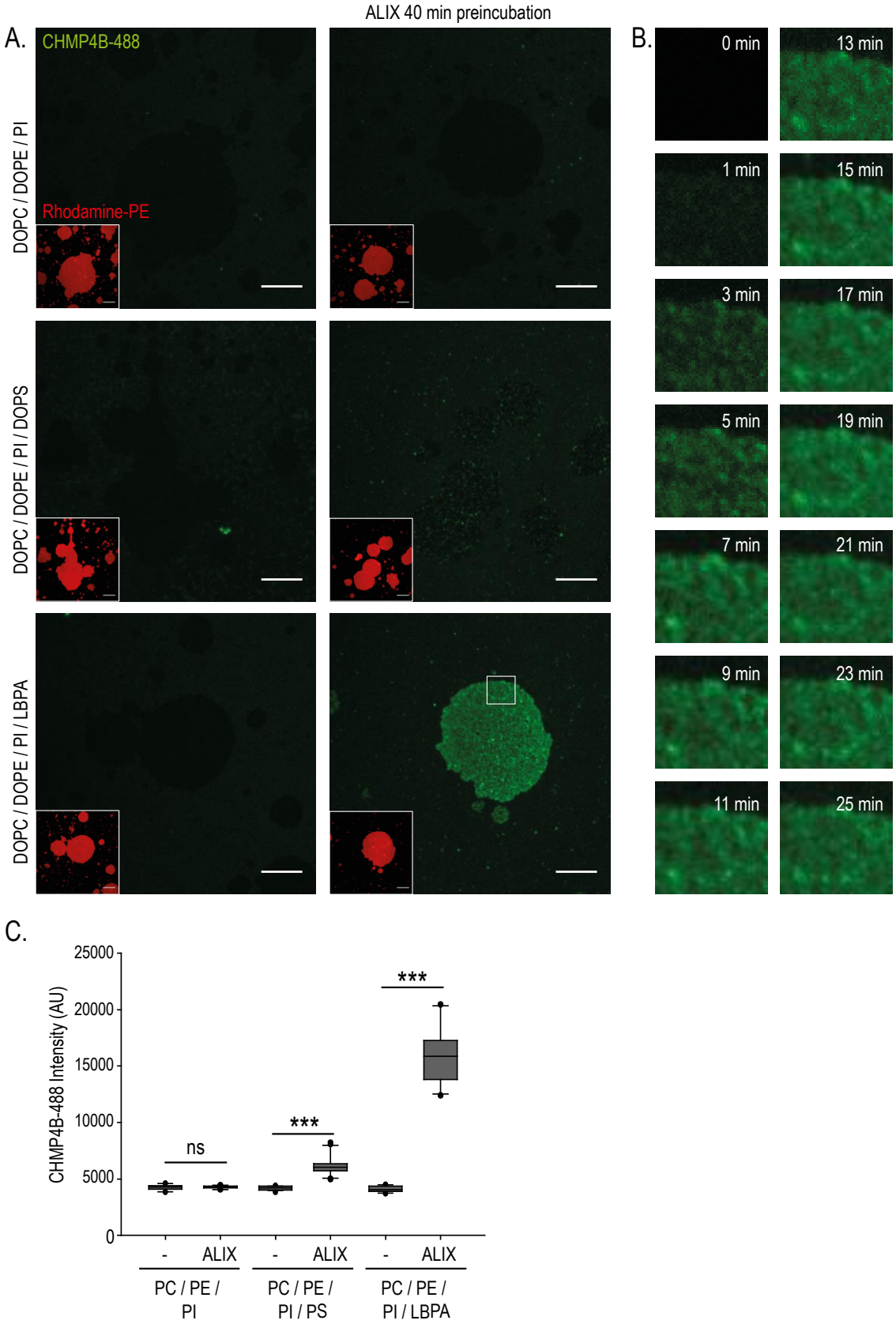

Larios et al., **Figure 7**

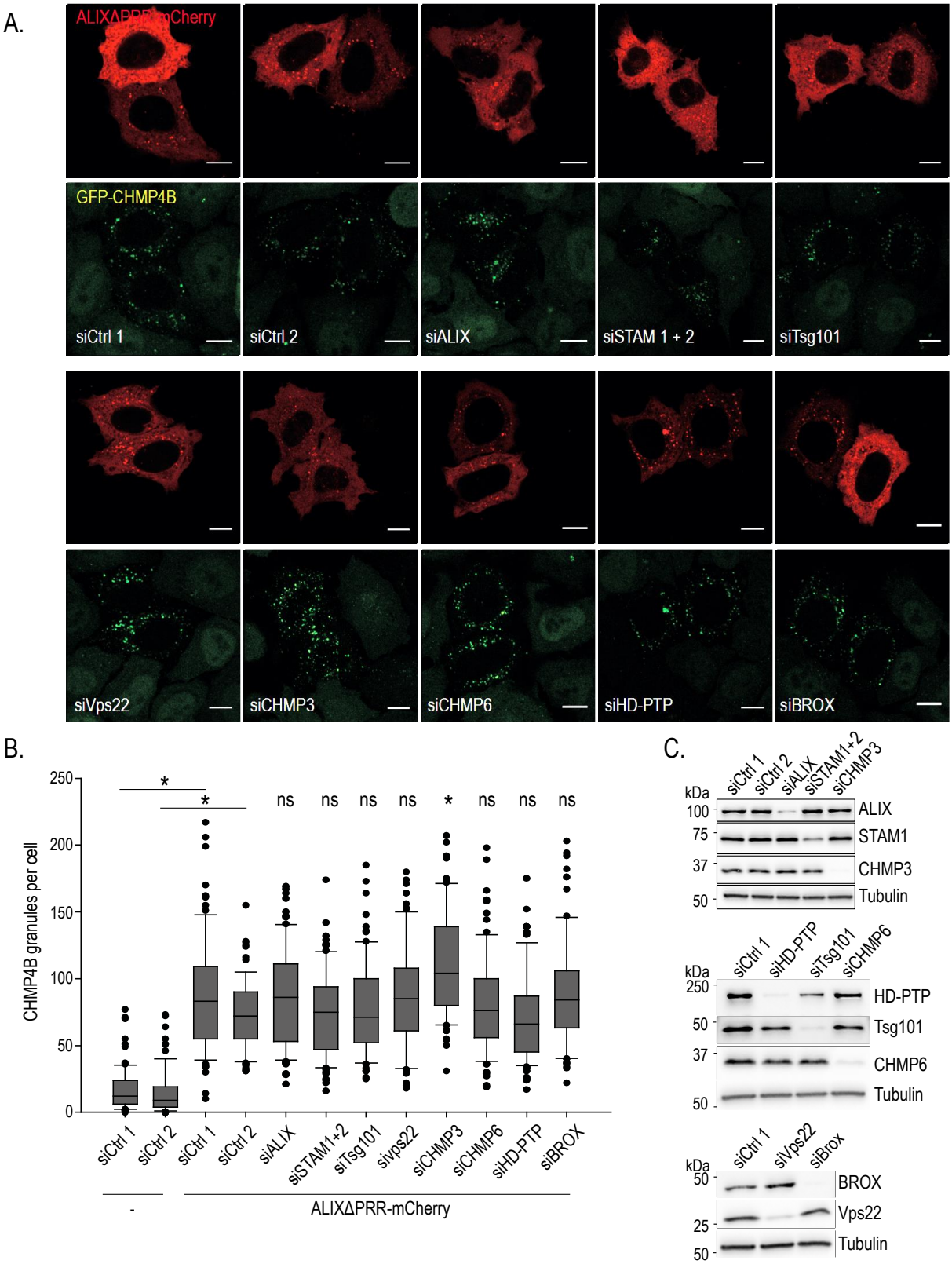

Larios et al., **Figure 8**

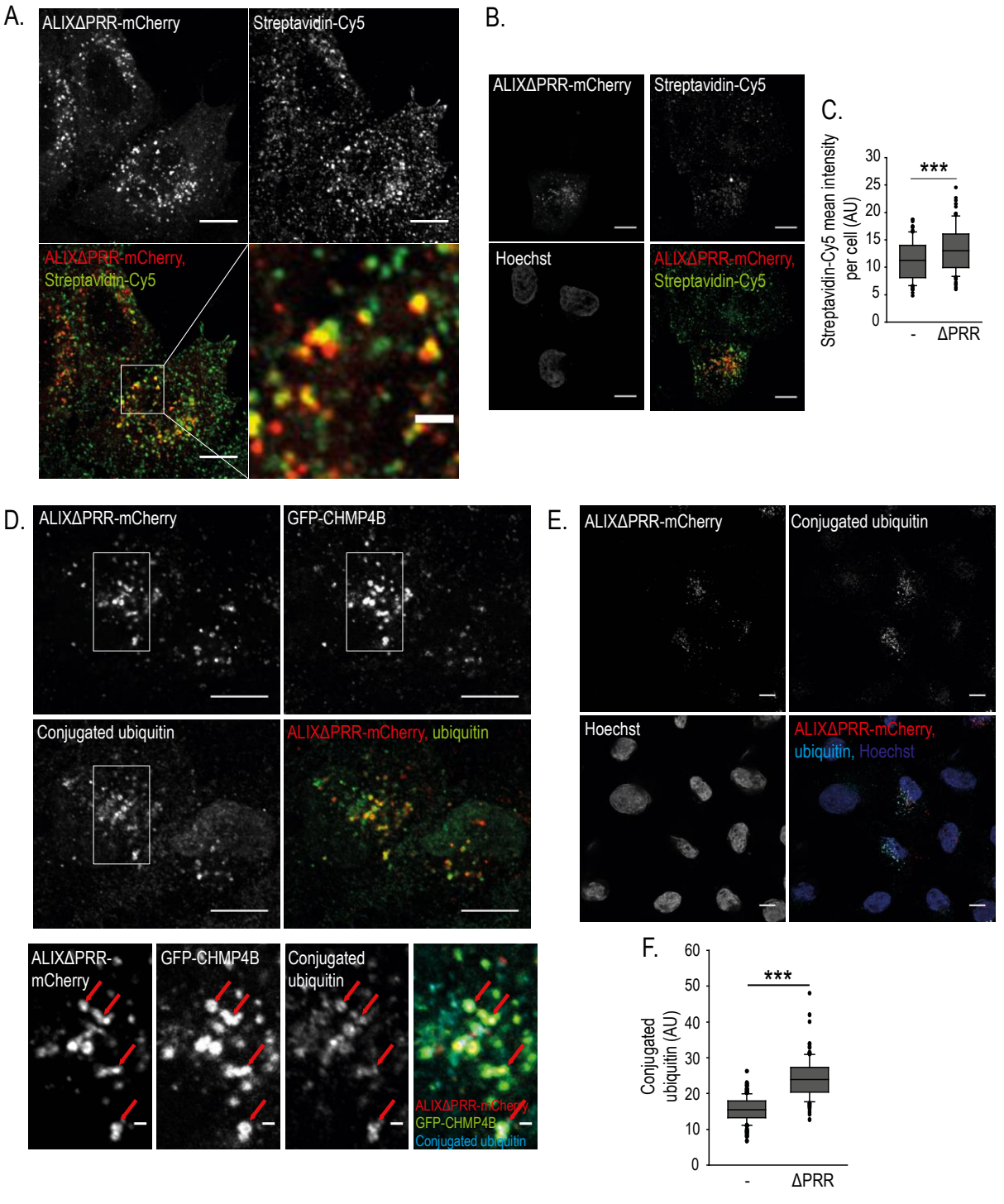

Larios et al., **Figure 9**

A.

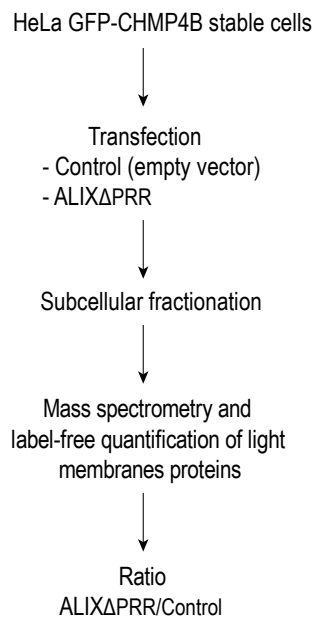

B.

Transmembrane proteins (55)

IL13RA1, TMEM248, JPH1, P2RX5, ATRN, EMP3, GRAMD1A, SLC19A2, SLC26A11, SLC37A3, SLC8B1, SORCS2, OLR1, APLP2, ATP6V1D, CRIM1, CLIC1, SERINC3, APP, SERINC1, TMEM59, ITM2B, KDELR1, LIFR, NDFIP1, IFITM3, SDC4, LDLR, LTBR, GPR56, LRP10, GPR107, REEP6, CLIC4, ANTXR1, KCNN4, MARCH6, RNF149, BACE2, CD46, TNFRSF-12A, LGR4, LAPTM4B, NDFIP2, UST, TGFBR1, IGF2R, ADCY6, ADIPOR1, M6PR, SGCE, TMEM50A, CD81, NCSTN, CD320

Ub-linked (21)

UEVLD, TRAF2, STUB1, WWP2, USP8, KEAP1, ITCH, UBE2N, MARCH6, RNF149, NDFIP2, SQSTM1, PSMD2, SKP1, CDKN2A, TRAF4, KLHL13, KCTD10, RNF167, RAD23B, TOLLIP

Autophagy (6)

GABARALP2, GABARAP, SQSTM1, TOLLIP, TMEM59, ULK3

Endosome, endocytosis, actin binding and depolymerization (26)

KIAA0196, ARPC2, ARPC3, SNX5, ACTR3, WDR1, CAP1, COTL1, CFL1, CFL2, DSTN, TPM3, TWF1, ARL5B, NDFIP1, NDFP2, VAC14, GOLPH3, ITM2B, IFITM3, MITD1, OSBPL11, PLEKHB2, SQSTM1, SPAST, TMEM59

C.

ESCRT proteins	ALIXΔPRR/Control	
ESCRT-0	Experiment 1	Experiment 2
Hgs (HRS)	2.68	2.18
STAM1	-	2.06
STAM2	-	+
ESCRT-I		
Tsg101	+	1.97
Vps37A	-	-
Vps37B	-	+
Vps37C	-	1.2
Vps37D	-	-
Vps28	-	+
MVB12A	-	-
MVB12B	-	-
UBAP1	-	-
ESCRT-II		
Vps36	-	-
Snf8 (Vps22)	-	-
Vps25	-	-

ESCRT proteins	ALIXΔPRR/Control	
ESCRT-III	Experiment 1	Experiment 2
CHMP6	-	+
CHMP4A	+	+
CHMP4B	18.11	11.49
CHMP4C	+	+
CHMP3	5.43	5.74
CHMP2A	9.24	3.67
CHMP2B	+	7.51
CHMP1A	4.41	3.8
CHMP1B	4.12	2.85
CHMP5	-	2.38
CHMP7	-	-
ESCRT-associated		
VPS4A	2.87	3.4
VPS4B	+	10.6
VTA1 (LIP5)	+	4.29
IST1	3.27	2.67
ALIX	34.4	28.56
PTPN23 (HD-PTP)	-	1.5
BROX	-	2.47
PDCD6 (ALG2)	1.05	1.08

Larios et al., **Figure S1**

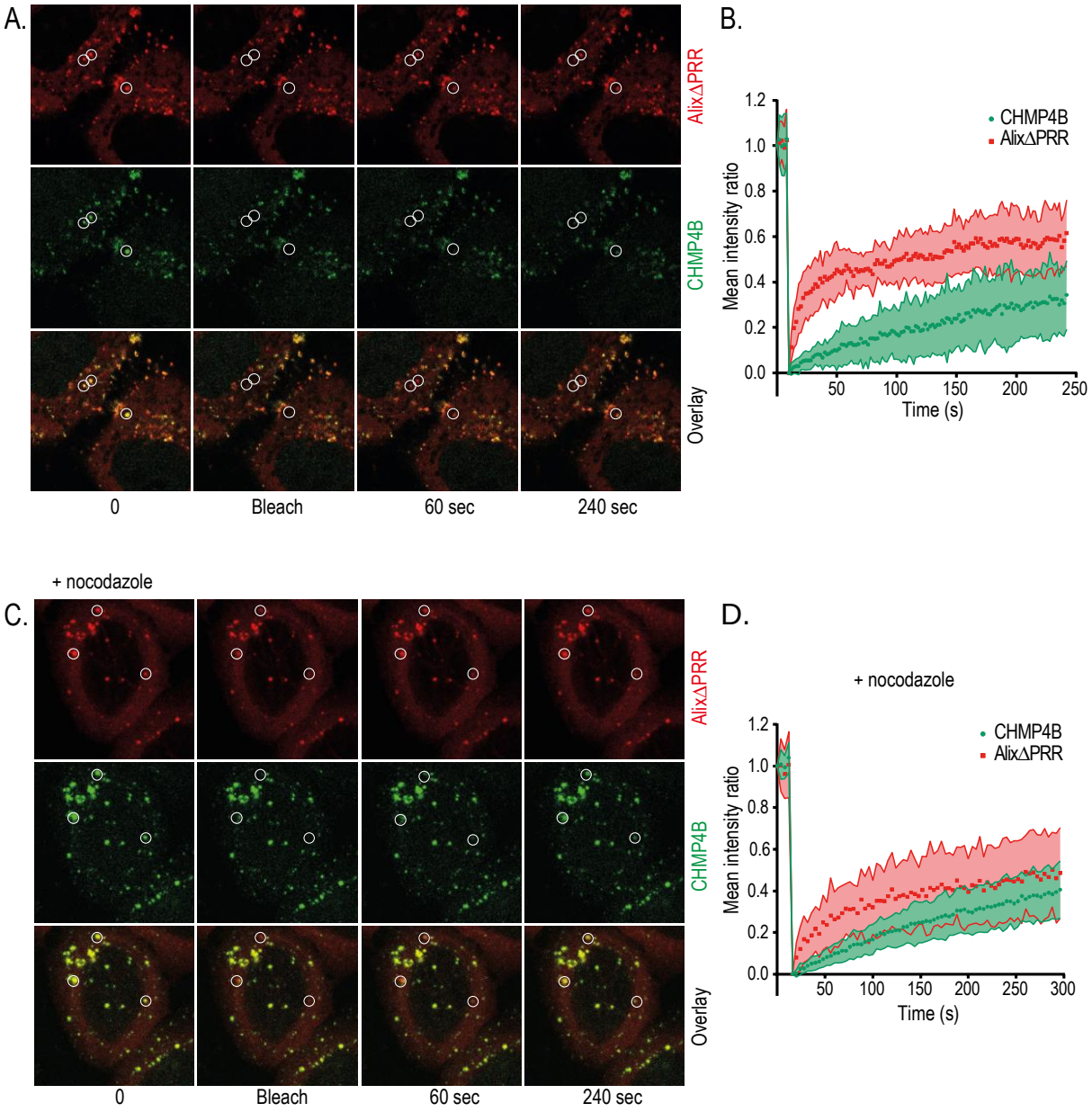

Larios et al., **Figure S2**

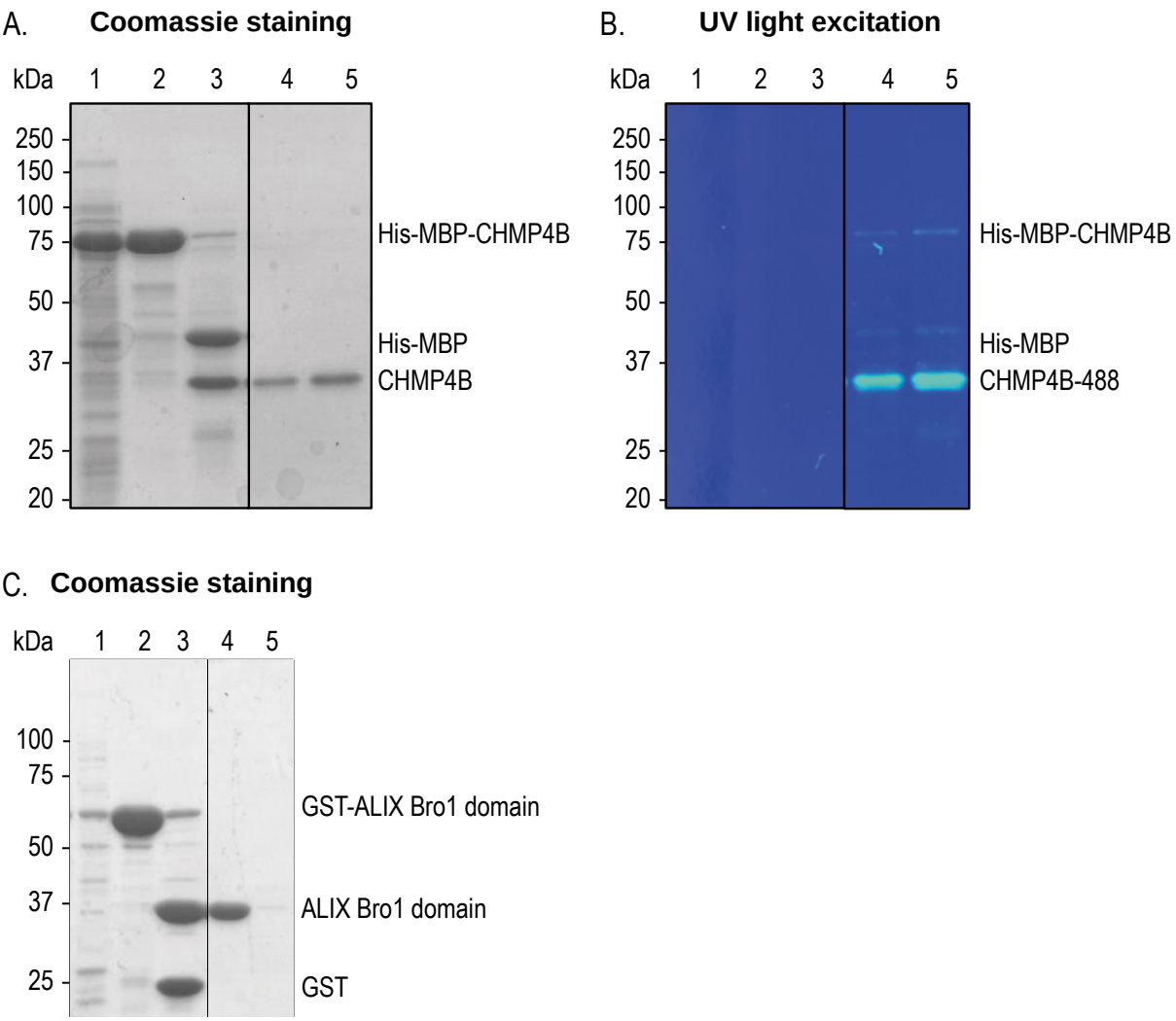

Larios et al., **Figure S3**

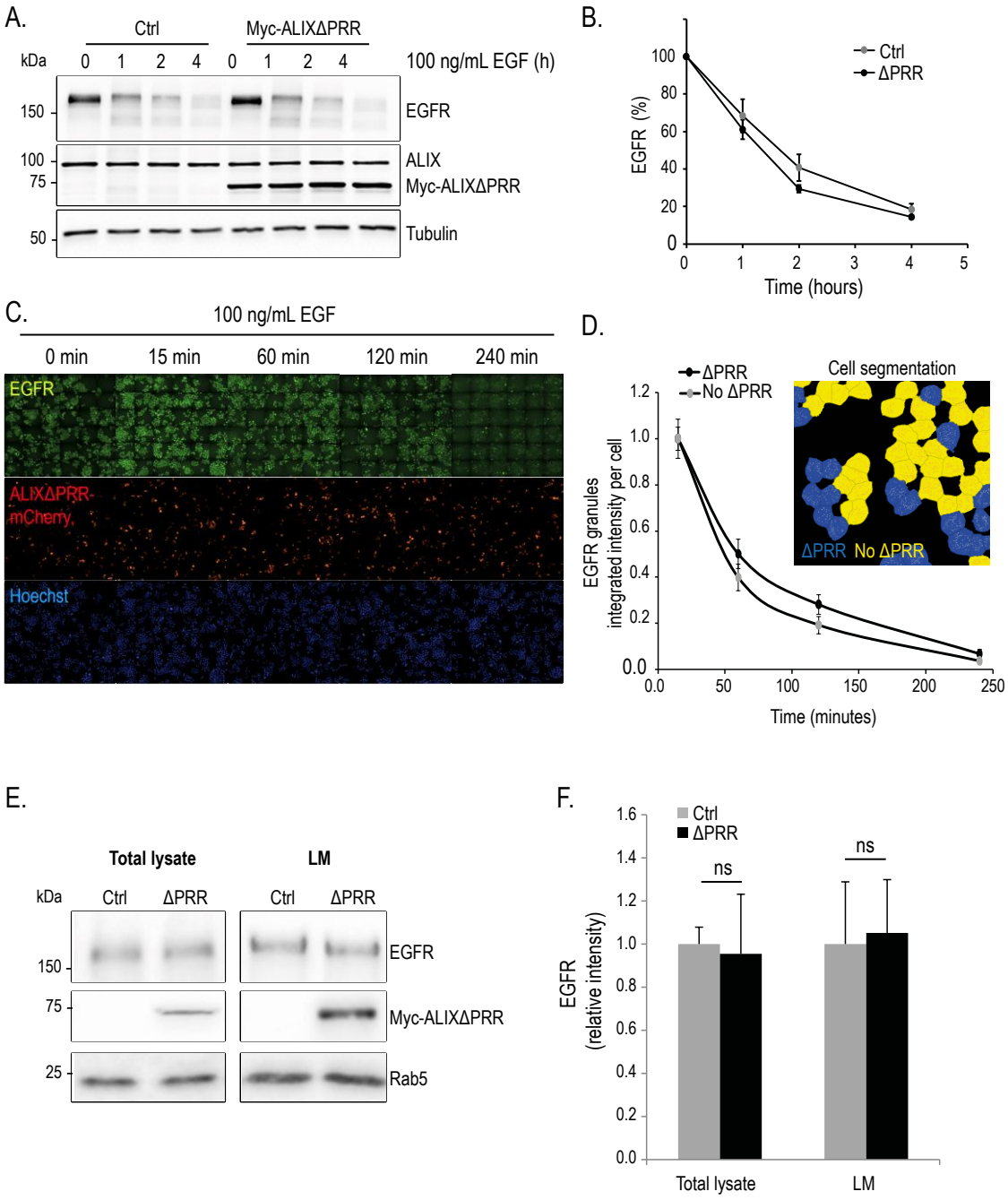

Larios et al., **Figure S4**

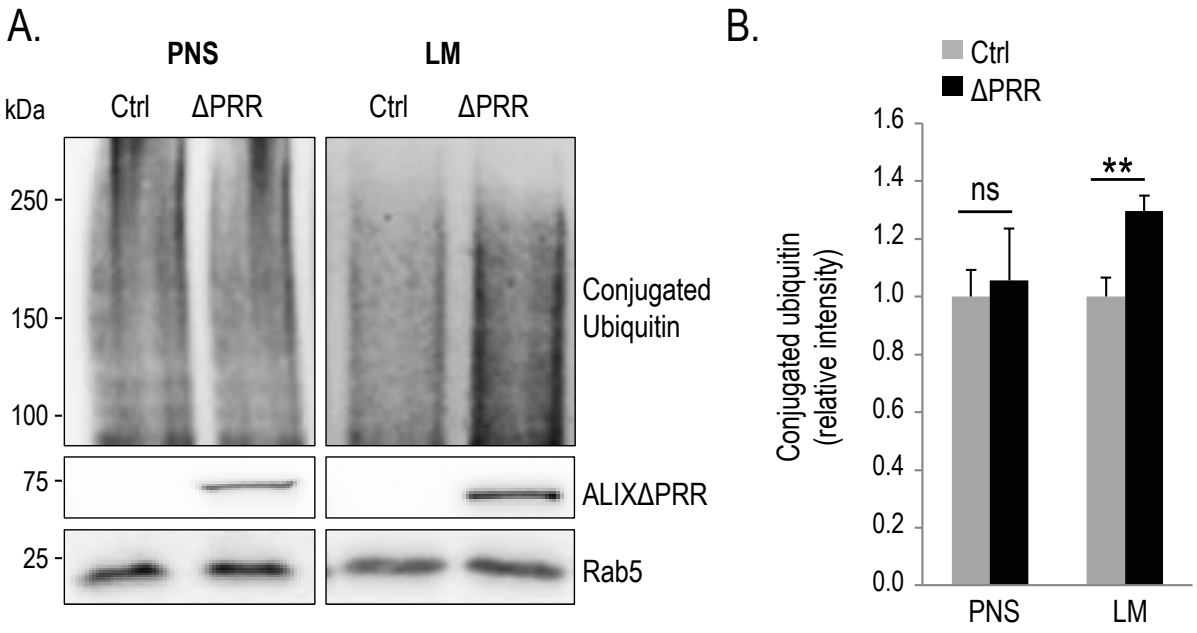

Larios et al., **Figure S5**

	A	B	Mean	Protein
1	---	++++		ARL5B
2	---	++++		CALML5
3	---	++++		CC2D1A
4	---	++++		DHX30
5	---	++++		IL13RA1
6	---	++++		LGALS7
7	---	++++		SERPINB
8	---	++++		SERPINB
9	---	++++		SNX5
10	---	++++		SPAST
11	---	++++		TMEM248
12	---	++++		TWF1
13	+++	++++		CHMP4C
14	---	+++		CALCOC
15	---	+++		CC2D1B
16	---	+++		CHMP4A
17	---	+++		CHMP6
18	---	+++		COG8
19	+	+++		JPH1
20	+++	4.29	4.29	VTA1
21	+++	7.51	7.51	CHMP2B
22	---	+++		KRT2
23	---	+++		LAMA1
24	---	+++		NT5C3A
25	---	+++		P2RX5
26	+	+++		TJP2
27	---	+++		UEVLD
28	---	++		ATRN
29	---	++		BAG5
30	---	++		DKC1
31	---	++		EMP3
32	---	++		GDA
33	---	++		GRAMD1
34	---	++		PITPNB
35	---	++		PRMT1
36	---	++		PXDN
37	---	++		RNF121;RNF175
38	---	++		MAMDC2
39	---	++		SHC1
40	++	197	197	TSG101
41	---	++		SLC19A2
42	---	++		SLC26A11
43	---	++		SLC37A3
44	---	++		SLC8B1
45	---	++		SORCS2
46	---	++		SUN1
47	---	++		TIMM23;TIMM23B
48	---	++		VPS37B
49	---	++		CRIP1
50	34	28.6	3148	PDCD6IP
51	18	11.5	14.8	CHMP4B
52	---	10.6	10.6	VPS4B
53	---	6.73	6.73	CD2AP
54	9.2	3.67	6.46	CHMP2A
55	5.4	5.74	5.58	CHMP3
56	4.9	3.75	4.35	TRAF2
57	4.4	3.8	4.1	CHMP1A
58	5.8	1.82	3.83	OLR1
59	4.1	2.85	3.48	CHMP1B
60	2.9	3.4	3.13	VPS4A
61	3.3	2.67	2.97	IST1
62	4.2	1.47	2.83	PRSS23
63	---	2.8	2.8	DYNC2H1

	A	B	Mean	Protein
64	2.71	---	2.71	AGA
65	2.77	2.26	2.52	DYNLL1
66	---	2.47	2.47	BROX
67	---	2.44	2.44	MITD1
68	2.68	2.18	2.43	HGS
69	2.69	2.12	2.4	DSTN
70	---	2.38	2.38	CHMP5
71	3.2	1.5	2.35	CCT6A
72	2.79	1.87	2.33	APLP2
73	3.47	1.16	2.31	ATP6V1D
74	---	2.3	2.3	CRIM1
75	2.57	1.95	2.26	CFL1
76	2.26	---	2.26	GSPT1
77	---	2.25	2.25	GABARA
78	2.16	2.28	2.22	CLIC1
79	---	2.22	2.22	SERINC3
80	---	2.19	2.19	HIST2H2
81	2.28	1.98	2.13	FTH1
82	---	2.12	2.12	CAB39
83	2.78	1.38	2.08	STUB1
84	---	2.06	2.06	STAM
85	---	2.03	2.03	ULK3
86	---	196	196	WBP2
87	2.35	1.56	196	EDIL3
88	2.49	1.42	1.95	CYR61
89	2.07	176	191	APP
90	2.41	1.38	189	WWP2
91	2.25	1.52	1.88	SERINC1
92	---	185	185	TAX1BP1
93	2.47	1.21	184	USP8
94	---	1.82	1.82	EFEMP1
95	2.08	149	178	TMEM59
96	2.16	14	178	SQSTM1
97	1.52	2.04	178	ITM2B
98	1.83	1.73	178	CAPN7
99	---	178	178	TIMP3
100	2.04	151	177	WDR1
101	---	176	176	KDELR1
102	1.46	2.02	174	SFN
103	1.97	146	171	LIFR
104	---	171	171	ADCK1;C
105	---	171	171	COTL1
106	---	17	17	PSMB1
107	---	168	168	TRAF4
108	---	168	168	NDFIP1
109	---	167	167	FTL
110	---	167	167	IFITM3
111	---	166	166	AP1S3
112	---	165	165	SDC4
113	1.91	138	164	LDLR
114	1.77	151	164	LTBR;MIF
115	2.07	1.2	163	PEF1
116	175	148	162	CLU
117	1.4	1.82	161	CAP1
118	---	161	161	PRPS1P
119	1.54	166	1.6	GPR56
120	---	158	158	KEAP1
121	---	158	158	VAC14
122	---	158	158	LRP10
123	---	157	157	ITCH
124	---	156	156	TSN
125	1.87	126	156	GPR107
126	---	156	156	PLEKHB2

	A	B	Mean	Protein
127	186	126	156	GOLPH3
128	---	156	156	CPNE1
129	172	137	154	YWHAE
130	---	153	153	REEP6
131	---	153	153	CFL2
132	171	135	153	CLIC4
133	---	153	153	KIF23
134	181	122	152	TRIM14
135	162	141	151	ANTXR1
136	---	1.51	1.51	KCNN4
137	---	15	15	UBE2N;UBE2
138	---	15	15	BZW2
139	---	15	15	PTPN23
140	149	---	149	TPM3;TPM1
141	166	132	149	DNAJA1
142	---	149	149	GCC2
143	---	149	149	PRKCA
144	---	149	149	CDKN2A
145	---	148	148	MARCH6
146	---	148	148	RNF149
147	---	148	148	KIAA0196
148	---	148	148	APOM
149	138	156	147	NUDC
150	14	154	147	BACE2
151	154	14	147	CD46
152	161	133	147	JAK1
153	---	147	147	TNFRSF12A
154	---	147	147	LGR4
155	172	121	146	PGAM1
156	147	146	146	GDI2
157	---	1.46	1.46	LOXL2
158	---	146	146	LAPTM4B
159	---	146	146	NDFIP2
160	16	13	145	PSMD2
161	1.55	136	145	LGALS1
162	1.53	136	145	ACTR3
163	---	145	145	UST
164	---	145	145	CTNNAL1
165	1.54	134	144	CCT2
166	149	139	144	TGFBR1
167	168	12	144	IGF2R
168	147	141	144	ARPC2
169	168	1.2	144	HSPA4
170	---	143	143	ADCY6
171	---	143	143	FXR1
172	---	143	143	WNT5A
173	142	144	143	ARPC3
174	---	143	143	TOLLIP
175	162	1.23	143	PSAP
176	143	---	143	GABARAPL2
177	---	142	142	ADIPOR1
178	---	142	142	ST13;ST13P4
179	---	142	142	SKP1
180	---	142	142	CTPS1
181	1.6	1.3	141	YWHAQ
182	1.6	1.2	141	M6PR
183	---	1.4	141	SGCE
184	1.6	1.2	141	RAD23B
185	---	1.4	141	TMEM50A
186	1.5	1.3	141	YWHAZ
187	---	1.4	141	CD81
188	1.1	1.7	141	NCSTN
189	1.6	1.2	14	CD320

Larios et al., **Figure S6**

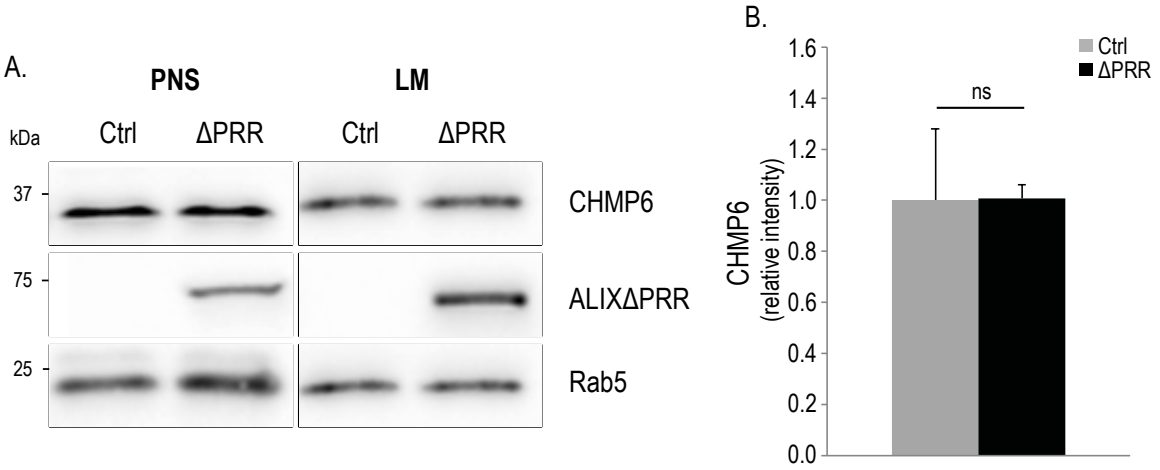

Larios et al., **Figure S7**

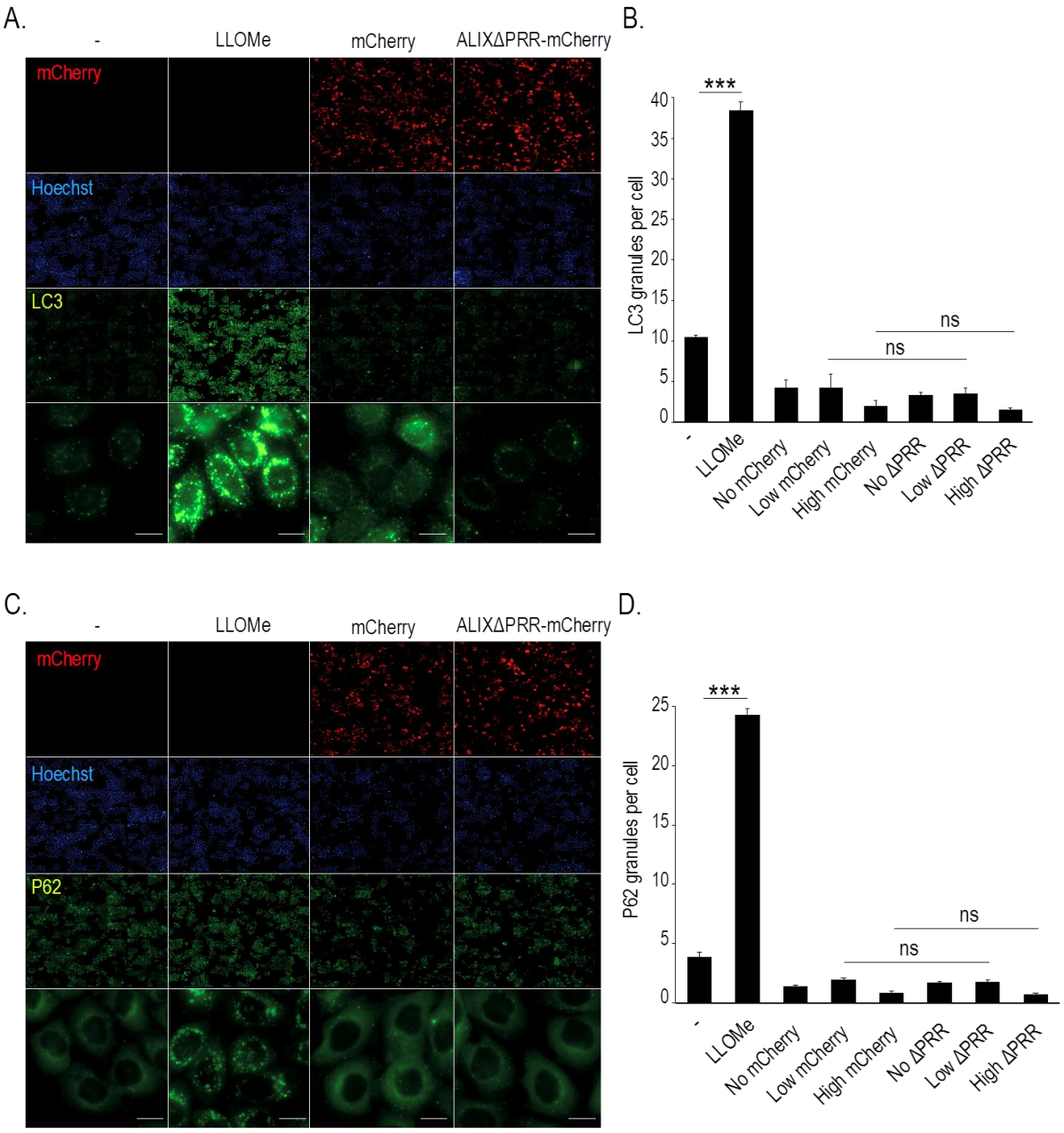

2. Ongoing Research

In this section, I present the current work I performed for the identification and characterization of ALIX-dependent cargo sorting in endosomes. In addition, I show some structural aspects of the recombinant purified proteins CHMP4B and ALIX BRO1.

2.1. Identification and characterization of ALIX-dependent cargo sorting in endosomes

Within the mass spectrometry list of proteins accumulated in endosomes by ALIXΔPRR expression (Fig S4. Results, section 1), 55 corresponded to transmembrane proteins (Fig 9, Results, section 1), which suggest that ALIX participates in endosomal sorting. As discussed before, endosomal EGFR levels were not affected by ALIXΔPRR expression, which was confirmed by western blot (Fig S2. Results, section 1).

2.1.1. CI-M6PR and ANTXR1 endosomal accumulation in ALIXΔPRR expressing cells

The ESCRT proteins play a role in the sorting of acid hydrolases (e.g CPY, CPS) from Golgi to lysosomes (Bankaitis et al. 1986; Rothman and Stevens 1986). In mammals, M6PRs bind to hydrolytic enzymes in the biosynthetic pathway and target them to lysosomes. Cation-independent mannose 6-phosphate receptor (CI-M6PR, also called insulin-like growth factor 2 receptor, IGFR2) cellular levels and distribution are regulated by ESCRTs and the ESCRT-associated protein ubiquitin-specific-processing protease 8 (USP8) (Raiborg et al. 2008; MacDonald et al. 2014), however, a role of ALIX in M6PR trafficking has not been explored. ALIXΔPRR expression induced a 1.4 fold increase in endosomal CI-M6PR (Fig 9 and Fig S4, Results, section 1). This accumulation was not evident by western blot analysis of the endosomal fractions (Fig 16A-B), which may well be due to the high sensitivity of mass spectrometry compared to western blot technique. Similarly, the mass spectrometry results showed that the anthrax toxin receptor 1 (ANTXR1) accumulates in endosomes upon ALIXΔPRR expression (Fig S4. Results, section 1), which is not observed by western blot (Fig 16C-D). ANTXR1 allows the entry of the anthrax toxin into host cells (Bradley et al. 2001) and ALIX is known to participate in the endosome to cytosol delivery of

the anthrax toxin during cell intoxication (Abrami et al. 2013), which makes ANTXR1 an interesting candidate for further studies.

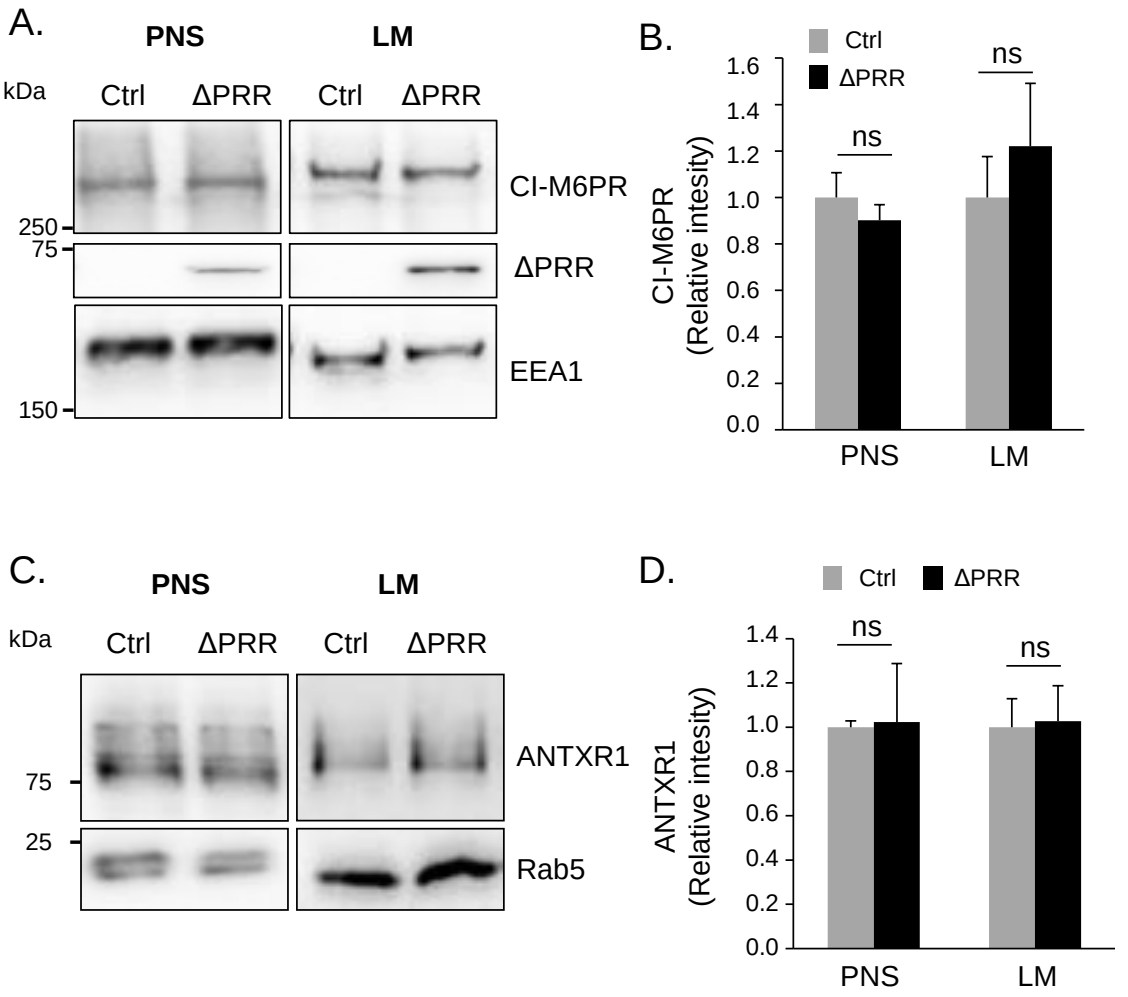

Figure 16. ALIXΔPRR expression does not affect CI-M6PR nor ANTXR1 endosomal levels. (A-D). HeLa GFP-CHMP4B cells transfected for 18 h with ALIXΔPRR (ΔPRR) or an empty vector as control (Ctrl) were fractionated by flotation in a sucrose density gradient. The post-nuclear supernatant (PNS) and the light membranes (LM) were analyzed by western blotting using antibodies against CI-M6PR (A) and ANTXR1 (C) and ALIX, as well as EEA1 and RAB5 (equal loading controls) (A). The relative amounts of CI-M6PR (B) and ANTXR1 (D) in PNS and LM fractions was quantified by densitometry, using EEA1 and RAB5 intensity for the normalization of CI-M6PR and ANTXR1 signal, respectively. Boxes, mean; bars, ± SD (*n* = 3); ns: not significant.

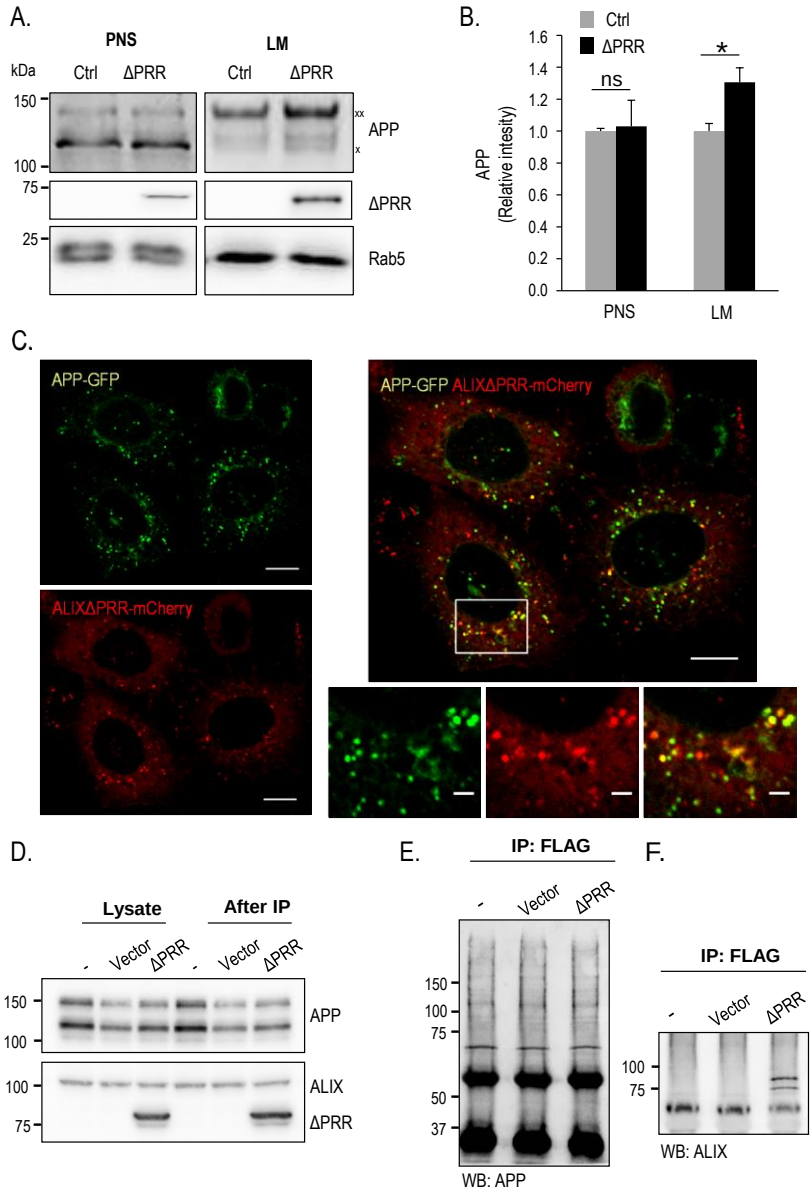

Figure 17. ALIXΔPRR expression induces APP endosomal accumulation. (A-B). HeLa GFP-CHMP4B cells transfected for 18 h with ALIXΔPRR (ΔPRR) or an empty vector as control (ctrl) were fractionated by flotation in a sucrose density gradient. The post-nuclear supernatant (PNS) and the light membranes (LM) were analyzed by western blotting using antibodies against APP and ALIX, as well as RAB5 (equal loading controls) (A). The relative amounts of APP in LM fractions was quantified by densitometry (B), using RAB5 intensity for the normalization of APP signal. Boxes, mean; bars, ± SD (n = 3); ctrl vs ΔPRR, *$p < 0.05$; ns: not significant; x: unglycosylated APP; xx: glycosylated APP. **(C).** HeLa-MZ cells stably expressing APP-GFP transfected with ALIXΔPRR-mCherry. The boxed area is shown in higher magnification. Scale bar: 10 µm and 2 µm (magnified area). **(D-F).** Lysates from HeLa GFP-CHMP4B cells co-transfected with ALIXΔPRR (ΔPRR) and ubiquitin-FLAG or an empty vector (vector) together with ubiquitin-FLAG, were incubated with an antibody against FLAG epitope for immunoprecipitation (IP). A control condition without transfection was included (-). The lysates (D, before and after IP) and the immunoprecipitated proteins (E and F) were analyzed by western blotting using antibodies against APP and ALIX.

2.1.2. APP endosomal accumulation in ALIXΔPRR expressing cells

The sorting of two proteins belonging to the amyloid precursor protein (APP) family, APP and amyloid-like protein 2 precursor (APLP2), was impaired by ALIXΔPRR expression (Fig S4. Results, section 1). Three transmembrane proteins form part of the APP family in mammals: APP, APLP1 and APLP2. They are highly express in neurons and participate in numerous neuronal and synaptic processes (Muller and Zheng 2012). However, the mechanisms of action remain unknown and often controversial. Furthermore, deposition of the amyloid beta (Aβ) peptide, which is produced by the proteolytic processing of APP, is a hallmark feature of Alzheimer's disease (Murphy and LeVine 2010). APP has been localized to MVEs, and its sorting into ILVs (Morel et al. 2013), lysosomal delivery and Aβ levels are regulated by HRS (ESCRT-0) and TSG101 (ESCRT-I) (Edgar et al. 2015). Interestingly, two transmembrane proteins which participate in APP processing, beta-site APP cleaving enzyme 2 (BACE2) and Nicastrin (NCSTN), were also accumulated upon ALIXΔPRR expression suggesting that ALIX could be involved in APP cleavage (Fig S4, Results, section 1).

The APP endosomal accumulation upon ALIXΔPRR expression was confirmed by western blot analysis of the endosomal fractions (Fig 17A-B). In addition, endosomal APP-GFP colocalized with ALIXΔPRR-mCherry in HeLa cells (Fig 17C). However, ALIXΔPRR expression did not affect APP-GFP distribution between EEs and LEs, which was analyzed by high throughput fluorescence microscopy (Fig 18). APP ubiquitination has been shown to regulate the sorting of the protein into ILVs, its cleavage and the secretion of APP fragments in exosomes (Williamson et al. 2017). APP ubiquitination levels were evaluated by immunoprecipitation of cells expressing ubiquitin-FLAG and ALIXΔPRR (Fig 17D-E). Although APP ubiquitination was not detected, two bands (75 kDa and 100 kDa approximately) corresponding to ubiquitinated ALIXΔPRR were observed (Fig 17D-E), which suggest that ALIXΔPRR ubiquitination might be involved in endosomal cargo sorting.

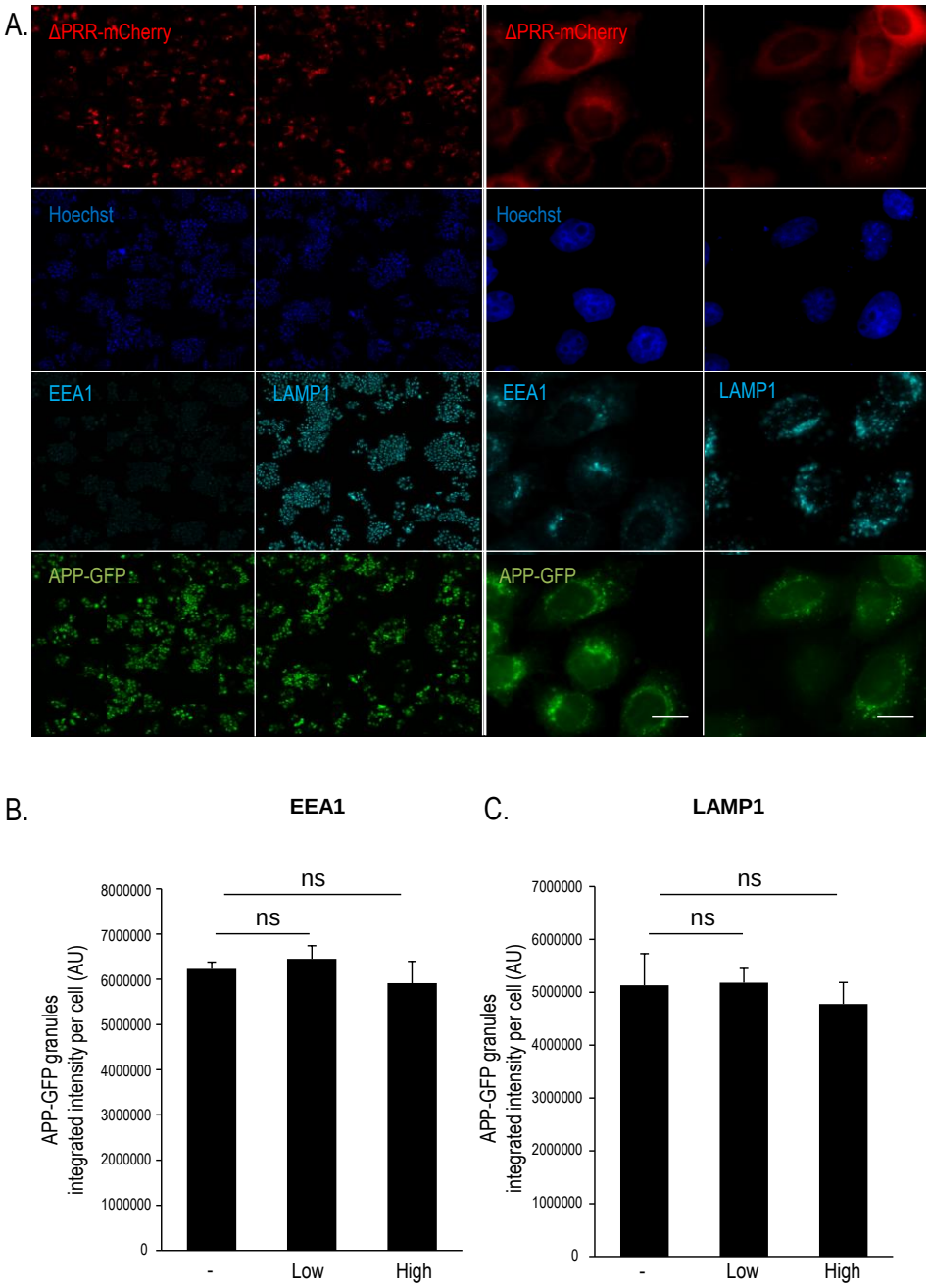

Figure 18. ALIXΔPRR expression does not affect APP distribution in early nor late endosomes. (A-C). HeLa-MZ cells stably expressing APP-GFP were transfected with ALIXΔPRR-mCherry (ΔPRR-mCherry) for 18 h. After fixation, cells were labeled with an antibody against EEA1 or LAMP1 and processed for quadruple-channel immunofluorescence microscopy (A). Each row represents the imaged area obtained from one 96-well plate. Nuclear staining, Hoechst, is shown in blue. A higher magnification is shown in the last two columns. Cells were segmented and the nucleus, cytoplasm, together with EEA1, LAMP1 and APP-GFP granules were identified. ALIXΔPRR-mCherry transfected cells were classify in three groups according to their mCherry signal intensity: no expression (-), low expression (low) and high expression (high). For each condition, approximately 35000 cells were analyzed, and the average APP-GFP intensity within EEA1 (B) or LAMP1 (C) compartments was quantified. Boxes, mean; bars, ± SD. ns: not significant. Scale bar: 10 µm.

2.1.3. ALIXΔPRR is secreted in exosomes

ALIX participates in the biogenesis of exosomes and contributes to exosomal cargo sorting (Baietti et al. 2012). Our results showing that ALIXΔPRR expression induces the accumulation of APP in endosomes, led us to evaluate the participation of ALIX in protein packing into exosomes. ALIXΔPRR was secreted in exosomes when expressed in HeLa cells (Fig 19). The percentage of secreted ALIXΔPRR (approximately 0.4%) from the total cell lysate was at least 20 times higher than the endogenous full length protein (Fig 19B). Contrary to ALIX, full length APP-GFP was not detected in exosomes (control or ALIXΔPRR transfected cells) and the exosomal levels of APP carboxy-terminal fragment (CTF), which correspond to an APP membrane-associated cleavage product, does not seem to be affected by the expression of ALIXΔPRR (Fig 19B). Furthermore, the exosomal sorting of CD63, an endosome-resident tetraspanin that is packed into exosomes and has been classically used as an exosome marker, was not impaired upon ALIXΔPRR expression (Fig 19B-C).

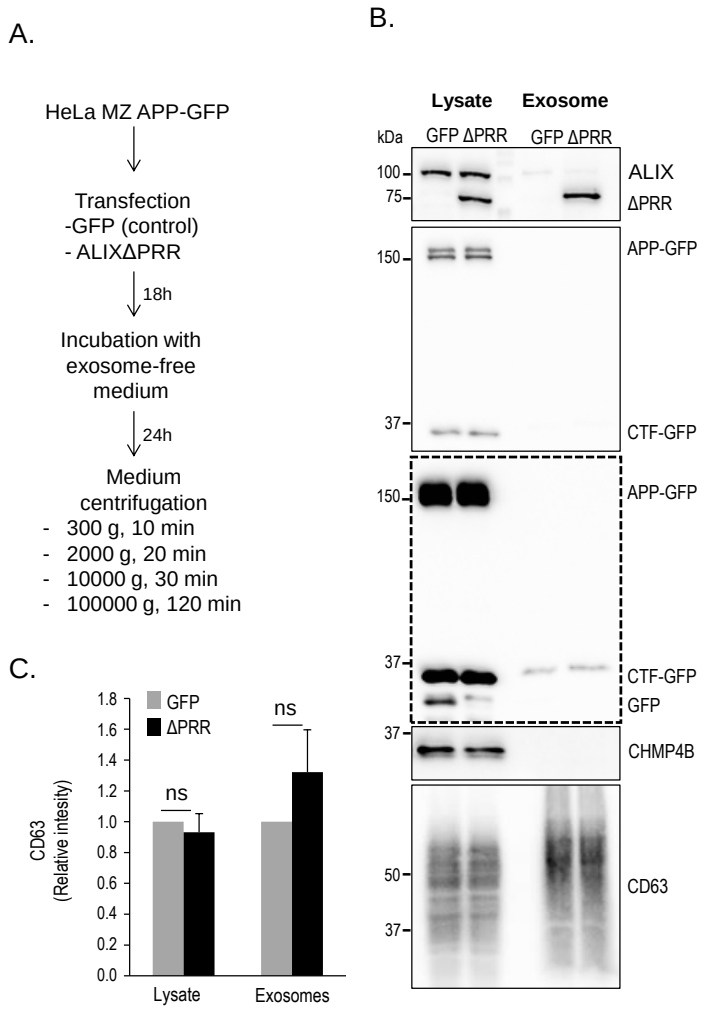

Figure 19. ALIXΔPRR is secreted in exosomes to the cellular medium. (A-C) HeLa-MZ cells stably expressing APP-GFP (HeLa-MZ APP-GFP) were transfected for 18 h with ALIXΔPRR (ΔPRR) or GFP as a control and incubated with an exosome-free medium for 24 h. The cell medium was collected and exosomes were obtained by differential centrifugation (A). The cell lysate and the exosome samples were analyzed by western blotting using antibodies against ALIX, GFP, CHMP4B and CD63 (B). Same amount of protein was loaded for each condition. Lysate and exosomal CD63 were quantified by densitometry (C). Boxes, mean; bars, ± SD (*n* = 4); ns: not significant. Dashed box: APP signal, more exposure. CTF: C-terminal fragment.

2.2. CHMP4B forms circular and spiral-shaped polymers that are modify by ALIX BRO1 domain

Human full length CHMP4B (FL-CHMP4B) has not been characterized *in vitro* before. Several studies use “active” forms of CHMPs, which lack the auto-inhibitory C-terminal region, in order to trigger the polymerization of the proteins [for review of *in vitro* CHMP structures see (Chiaruttini and Roux 2017)]. Recombinant CHMP4BΔC (CHMP4B lacking the C-terminal region) and CHMP4BΔC-ALIX (CHMP4B lacking the C-terminal region, but with the ALIX-interacting region intact) form multiple structures in solution, from ring-shaped to curly or spiral-shaped polymers (Pires et al. 2009). Recombinant FL-CHMP4B (Fig S1. results, section 1) analyzed by negative staining transmission electron microscopy (Fig 20A-C), formed filaments that curl into 50 nm ring-shaped structures in addition to spiral polymers. Furthermore, addition of recombinant ALIX BRO1 (Fig S1. Results, section 1) induced a two-fold increase in CHMP4B ring thickness (Fig 20D-E), which resembles the double ring structures described for SNF7 during MVE formation (Henne et al. 2012)

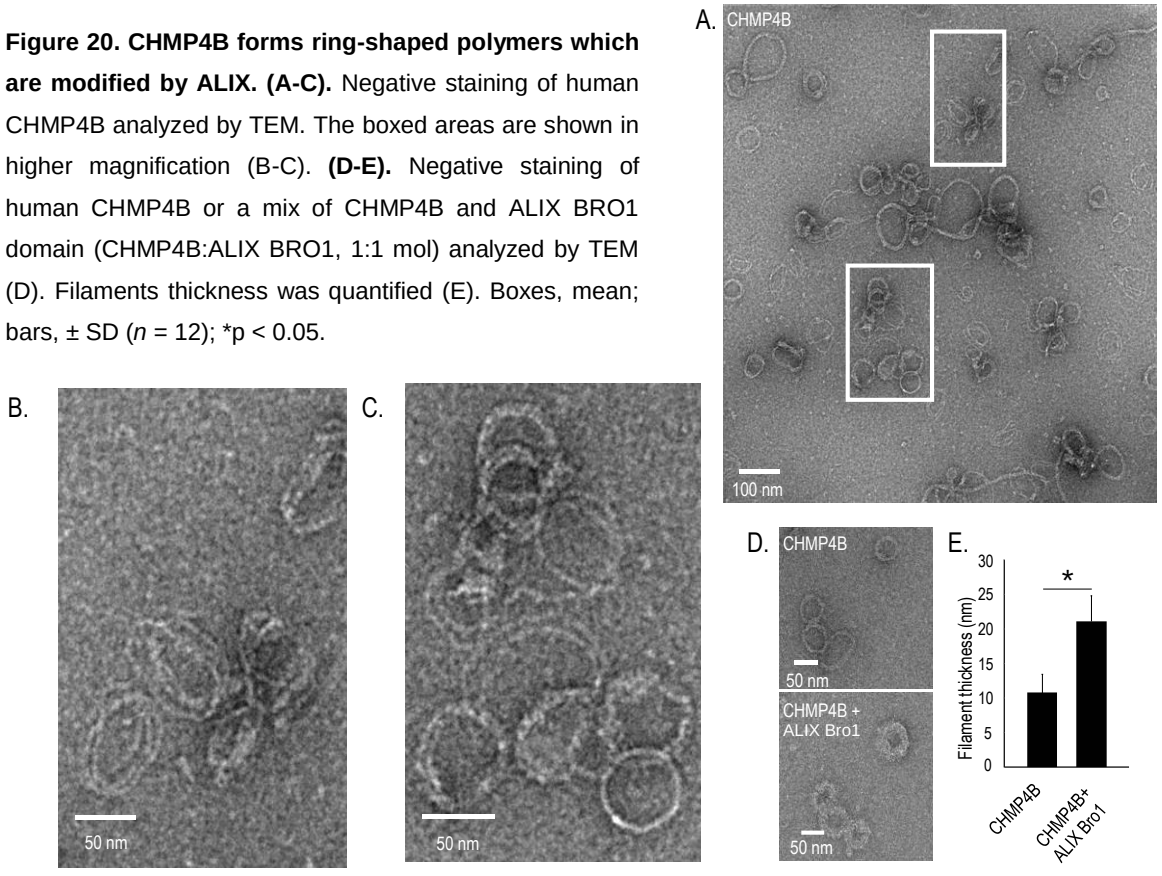

Figure 20. CHMP4B forms ring-shaped polymers which are modified by ALIX. (A-C). Negative staining of human CHMP4B analyzed by TEM. The boxed areas are shown in higher magnification (B-C). **(D-E).** Negative staining of human CHMP4B or a mix of CHMP4B and ALIX BRO1 domain (CHMP4B:ALIX BRO1, 1:1 mol) analyzed by TEM (D). Filaments thickness was quantified (E). Boxes, mean; bars, ± SD (n = 12); *p < 0.05.

2.3. Materials and Methods

Cells, Antibodies and Reagents

We obtained HeLa-MZ cells from Marino Zerial (MPI-CBG, Dresden) and HeLa Kyoto cells stably expressing GFP-CHMP4B from Anthony Hyman (MPI-CBG, Dresden) (Poser et al. 2008). HeLa-MZ cells stably expressing APP-GFP were generated with ViraPower lentiviral packing mix (Thermo Fisher Scientific, Waltham, MA) according to manufacturer's instructions. All cells were grown in Minimum Essential Media Eagle (MEM) (Sigma-Aldrich, St. Louis, MO) supplemented with 10% fetal bovine serum (FBS) (Thermo Fisher Scientific, Waltham, MA), 1% MEM Non-Essential Amino Acids (Thermo Fisher Scientific, Waltham, MA), 2 mM L- Glutamine (Thermo Fisher Scientific, Waltham, MA), 100 µg/mL penicillin and 100 units/mL streptomycin (Thermo Fisher Scientific, Waltham, MA) in a 37 °C, 5% CO_2 incubator. HeLa Kyoto cells stably expressing GFP-CHMP4B and HeLa-MZ cells stably expressing APP-GFP, were additionally supplemented with 0.5 mg/mL Geneticin (Millipore, Billerica, MA) and 3 µg/mL Blasticidin (Thermo Fisher Scientific, Waltham, MA), respectively.

The anti-RAB5 monoclonal antibody was a gift from Reinhard Jahn (Göttingen, Germany). The antibodies against CI-M6PR (EPR6599), CHMP4B (ab105767), CD63 (ab59479) were obtained from Abcam (Cambridge, UK), against GFP (11814460001) from Roche (Basel, Switzerland), against APP (A8717), ANTXR1 (SAB2501028) and FLAG from Sigma-Aldrich (St. Louis, MO), against EEA1 (ALX-210-239-C100) from Enzo Life Sciences (Farmingdale, NY), against Lamp1 (D2D11) from Cell Signaling Technology (Danvers, MA) against ALIX (pab0204) from Covalab (Villeurbanne, France). The Cy5-conjugated fluorescent antibodies were from Jackson ImmunoResearch (West Grove, PA) and the peroxidase-conjugated secondary antibodies from Bio-Rad Laboratories (Hercules, CA). Ni-NTA Agarose, 7 kDa MWCO Zeba Spin Desalting Columns and Hoechst 33342 were from Thermo Fisher Scientific (Waltham, MA). MBPTrap HD 5 mL columns, Glutathione Sepharose 4B and Dextrin Sepharose High Performance were from GE Healthcare (Anaheim, CA). The cOmplete Protease Inhibitor Cocktail was from Roche (Basel, Switzerland). Restriction enzymes were obtained from New England Biolabs (Ipswich, MA). Other reagents and chemicals were obtained from Sigma-Aldrich (St. Louis, MO).

Plasmids and Transfection

Ubiquitin-FLAG plasmid was obtained from Ivan Dikic (Frankfurt, Germany), APP-GFP from Addgene (no. 69924) and pEGFP-C2 from Clontech (Mountain View, CA). Myc-ALIXΔPRR-mCherry plasmid was generated by cloning ALIX ALIXΔPRR cDNA (ALIX BRO1 domain and V-domain, which corresponds to the first 702 amino acids) into a pCMV-Tag3C vector (Agilent Technologies, Santa Clara, CA) using *XhoI* site. Then, the mCherry cDNA was cloned in ALIX C-terminus using *XhoI* and *ApaI* sites. The CHMP4B expression plasmid for recombinant protein purification was generated by replacing SNF7 from pMBP-HIS2-SNF7 plasmid (Addgene no. 21492) for the CHMP4B cDNA, using BamHI and NotI sites. Before cloning CHMP4B into the plasmid, a silent mutation was generated in the CHMP4B sequence in order to remove an internal BamHI cutting site. The primers used for the mutation were the following: forward, AACTGGGCTGGGTCCATGTAACCAGCTTTCTTG and reverse, CAAGAAAGCTGGTTACATGGACCCAGCCCAGTT. The ALIX BRO1 domain plasmid for recombinant protein production was generated by cloning the BRO1 domain (1-359 amino acids) into a pGEX-6P-2 vector.

DNA was transfected in cells according to the manufacturer's instructions using FuGENE HD (Promega Corporation, Madison, WI). Experiments were performed after 18 h transfection with DNA.

Recombinant protein purification

Human CHMP4B was expressed in bacteria and purified as described (Mierzwa et al. 2017). Briefly, pMBP-HIS2-CHMP4B was expressed in *Escherichia coli* Rosetta cells. At OD_{600nm}=0.7, protein expression was induced with 0.5 mM IPTG for 3 h at 30 °C. Bacteria were lysed and sonicated in lysis buffer containing 20 mM Hepes pH 8, 100 mM NaCl, 1% Triton X-100, and cOmplete Protease Inhibitor Cocktail at 4 °C. The fusion protein 6xHis-MBP-CHMP4B was purified by affinity chromatography using an MBPTrap HP 5 mL column. The column was first washed with 20 mM Hepes pH 8, 250 mM NaCl, 0.1% Triton X-100, followed by a second wash with 20 mM Hepes pH 8 and proteins bound to the column were eluted in 20 mM Hepes pH 8, 10 mM maltose. The 6xHis-MBP region was removed by cleavage with TEV protease, followed by incubation with Ni-NTA Agarose resin and with Dextrin Sepharose media. CHMP4B fluorescent-labeling was performed by incubating the protein with Alexa Fluor 488 TFP ester in a 1:2 molar ratio (protein:dye), in the presence of 100 mM $NaHCO_3$ pH 9, 1h at room temperature. The free dye was removed by overnight

dialysis against 20 mM Hepes pH 8 at 4 °C, using a membrane of 12–14 kDa MWCO, followed by size-exclusion chromatography using 7 kDa MWCO Zeba Spin Desalting Columns. Finally, the protein was centrifuge at 100,000 g for 10 min, 4 °C. The supernatant was aliquoted, snap frozen using liquid N_2 and stored at -80 °C.

Human ALIX BRO1 domain was expressed and purified from *Escherichia coli* Rosetta cells transformed with the pGEX-ALIX BRO1 domain. At OD_{600nm}=0.5, protein expression was induced with 0.4 mM IPTG for 18 h at 18 °C. Bacteria were lysed and sonicated in lysis buffer containing PBS, 1 mM EDTA, 1 mM DTT, 1% Triton X-100, and cOmplete Protease Inhibitor Cocktail at 4 °C. The lysate was centrifuged at 10,000 g for 30 min at 4 °C and the supernatant was filtered through a 0.22 µm filter. The lysate was incubated with Glutathione Sepharose beads for 2 h at 4 °C. The beads were first washed with PBS, followed by a second wash with 50 mM Tris pH 7.5, 150 mM NaCl, 1 mM EDTA and 1 mM DTT. ALIX BRO1 domain was release from the Glutathione Sepharose beads by the cleavage of GST-ALIX BRO1 domain using PreScission protease. The supernatant was loaded into a size-exclusion chromatography Zeba Spin Desalting Column (7 kDa MWCO) for buffer exchange. The final buffer was 25 mM Hepes pH 7.4, 0.3 mM BAPTA, 0.3 mM NTA and 0.3 mM HEDTA. After centrifugation at 100,000 g for 10 min, 4 °C, the supernatant was aliquoted, snap frozen using liquid N_2 and stored at -80 °C.

Fluorescent light microscopy

Immunofluorescence was performed after fixing cells grown on glass coverslips, or directly in 96-well dish plates for high throughput microscopy, for 20 min with 3% PFA in PBS. All steps of the immunofluorescence procedure were performed at room temperature. After fixation, cells were incubated for 45 min in 1% fish skin gelatin, 0.1% saponin in PBS, followed by 30 min incubation with the primary antibody in 1% fish gelatin in PBS. After washing the primary antibody with PBS, the cells were incubated for 30 min with the secondary antibody (Cy5-conjugated fluorescent antibody) in 1% fish gelatin in PBS, followed by PBS washes. The cells were mounted in Mowiol 40-88 medium containing 10 µg/mL Hoechst and imaged with a Zeiss 700 confocal microscope (Carl Zeiss AG; Oberkochen, Germany) using a 63x objective. For high throughput microscopy, 96-well plates were imaged with an ImageXpress Micro Confocal High-content microscope (Molecular Devices; CA, USA) (used in the widefield mode) using a 40x objective.

Image analysis

High throughput image analysis was performed using custom module editor MetaXpress software, from Molecular Devices (CA, USA). Briefly, cells were segmented and the nucleus, cytoplasm and granules (LAMP1, EEA1, APP-GFP) were identified. The average APP-GFP intensity within EEA1 and LAMP1 was quantified in cells expressing ALIXΔPRR-mCherry and compared with non-expressing cells.

Immunoprecipitation

HeLa Kyoto cells stably expressing GFP-CHMP4B were transfected with pCMV-Tag3C and ubiquitin-FLAG or ALIXΔPRR together with ubiquitin-FLAG for 18 h. Cells were collected and lysed with 0.5% Triton X-100 in PBS. The cell lysate was centrifuged at 14000 rpm for 5 min and 1.5 mg of supernatant was incubated with 50 µL of protein G agarose beads for 1 h at 4°C (lysate pre-clearance). Then, the supernatant was incubated with 30 µg of anti-FLAG antibody for 2 h at 4°C, followed by incubation with 50 µL of protein G agarose beads for 1 h at 4°C. The beads were washed three times with 0.5% Triton X-100 in PBS and resuspended in Laemmli sample buffer.

Exosomes Isolation

Exosome isolation was carried out by differential centrifugation as described (Thery et al. 2006). Briefly, two square dishes (500cm^2 square growth area) of 80% confluency HeLa-MZ cells stably expressing APP-GFP were transfected with Myc-ALIXΔPRR or pEGFP-C2 for 18 h. Then, cells were washed with PBS and incubated for 24 h with an exosome-free medium (Thery et al. 2006). The medium was collected and centrifuged at 300 g for 10 min at 4°C. In order to remove cell debris, the supernatant was centrifuged two more times at 2000 g for 20 min and 10000 g for 30 min at 4°C. Exosomes were sedimented by high-speed centrifugation at 100000 g for 2 h at 4°C. The pellet was washed with PBS, re-sedimented by centrifugation at 100000 g for 2 h at 4°C and finally resuspended in 80 µL of PBS.

Negative staining and electron microscopy

5 µL of recombinant CHMP4B (2.7 µM, 100 mM NaCl, 20 mM Hepes pH 8) or a mix of CHMP4B and ALIX BRO1 domain (each protein at a final concentration of 2.7 µM) was placed on a plasma pre-cleaned carbon grid [CF300H-CU-UL, from Electron Microscopy

Sciences (Hatfield, PA)]. The excess of liquid was removed with a Whatman filter paper and the grid was incubated 1 s and 30 s in 2% uranyl acetate. The excess of liquid was removed, the grid was dried at RT and it was imaged with a Tecnai G2 Sphera (FEI; Hillsboro, OR) transmission electron microscope.

Other experimental procedures

Subcellular fractionation was carried out by flotation in sucrose gradients as described (Muriel et al. 2017). Cell lysis was performed with 50 mM Tris, pH 7.4, 1% NP-40, 0.25% sodium deoxycholate, 150 mM NaCl, 1mM EDTA, 1mM PMSF, 1 µg/mL aprotinin, 1 µg/mL leupeptin, 1 µg/mL pepstatin. Before loading the samples for SDS-PAGE, they were mixed with Laemmli sample buffer. Western blot analysis was preformed using WesternBright ECL from Advansta (Menlo Park, CA)

Discussion

The ESCRT machinery plays an important role in the sorting of proteins to the vacuole/lysosome. In addition to ESCRTs participation in the delivery of proteins from the biosynthetic route to the vacuole/lysosomes, they coordinate the lysosomal sorting and degradation of transmembrane proteins coming from the plasma membrane. More specifically, ESCRT binding to the limiting membrane of endosomes promotes the sorting of cargo proteins into ILVs, which is important for the efficient lysosomal degradation of proteins. ESCRT endosomal association and cargo sorting is a highly regulated process, in which temporal and spatial membrane recruitment of ESCRTs are coordinated. In mammals, the ESCRT-associated protein, ALIX, has been suggested to facilitate protein targeting to lysosomes, but the mechanism remains poorly understood. In order to address this open question, we first analyzed the *in vivo* and *in vitro* participation of ALIX in the recruitment of ESCRT proteins to lipid membranes, and then aimed to identify new cargo proteins which follow an ALIX-dependent endosomal sorting.

The discussion of the first part of the results of the thesis (results, section 1, paper in preparation: Regulation of ESCRT Endosomal Recruitment by the Lipid-binding Protein ALIX) was already presented. Here I discuss the ongoing research (Results, section 2) and I present a model for ALIX-LBPA-dependent ILV formation and cargo sorting.

1. ALIXΔPRR expression induces endosomal accumulation of specific transmembrane proteins and could participate in exosome biogenesis

Two proteins from the APP family, APP and APLP2, appear in the mass spectrometry list of transmembrane proteins accumulated in endosomes by ALIXΔPRR expression. In addition, APP proteases BACE and NCSTN, and two other transmembrane proteins that regulate APP cleavage, transmembrane protein 59 (TMEM59) (Ullrich et al. 2010) and integral membrane protein 2B (ITM2B) (Fotinopoulou et al. 2005), are also accumulated upon ALIXΔPRR expression. The latter observation, together with the well-studied link between APP cleavage, which results in the accumulation of neurotoxic extracellular Aβ plaques, and Alzheimer´s disease (Reiss et al. 2018) led us to study a possible role of ALIX

in APP endosomal sorting. ALIXΔPRR expression affects APP endosomal levels, but does not seems to impair the protein distribution between early and late endosomes. In addition, even though we do not see a direct effect on APP endosomal localization, we consider that other aspects should be evaluated in future studies, like APP cleavage and Aβ production, which has been shown already to take place in endosomes (Haass et al. 1992; Koo and Squazzo 1994; Zhang and Song 2013).

PAR1 and P2Y1 are YP(X)nL motif-containing proteins, which confers them the capacity to directly bind to ALIX V-domain (Dores et al. 2012; Dores et al. 2016). Four proteins containing YP(X)nL motifs are accumulated in endosomes upon ALIXΔPRR expression: TMEM59, chloride intracellular channel protein 1 (CLIC1), NEDD4 family-interacting protein 2 (NDFIP2) and LDLR. As we mentioned before TMEM59 regulates APP cleavage and is also involved in endosomal autophagy (Boada-Romero et al. 2013). CLIC1 is a chloride channel which participates in macrophages phagosomal acidification (Jiang et al. 2012). NDFIP2 interacts and regulates the activity of several HECT-type E3 ligases (Mund and Pelham 2009), and therefore its endosomal sorting could also be important for the ubiquitination and ILV delivery of other protein cargos. All of them traffic through endosomes, and are interesting candidates for further studies.

In addition to ILV and cargo delivery to lysosomes for degradation, MVEs can fuse with the plasma membrane and release ILVs to the extracellular medium as exosomes. The syndecan-syntenin-ALIX complex has been suggested as one of the mechanisms for exosome biogenesis (Baietti et al. 2012). Syndecan 4 (SDC4) is accumulated in endosomes upon ALIXΔPRR expression (mass spectrometry), which suggest that ALIXΔPRR could promote the sorting and secretion of proteins in exosomes by the syndecan-syntenin-ALIX pathway. Furthermore, we find high amounts of ALIXΔPRR present in exosomes compared with the endogenous full length ALIX, which may be due to the lack of the auto-inhibitory PRR. The tetraspanin CD81, which is a protein enriched in exosomes and has been largely used as an exosomal marker, is also accumulated in endosomes isolated from ALIXΔPRR expressing cells. APP and APP cleavage products are present in multivesicular structures and are secreted in exosomes (Rajendran et al. 2006; Vingtdeux et al. 2007; Miranda et al. 2018). We could not detect APP-GFP in exosomes, and the levels of APP-CTF do not seem affected by ALIXΔPRR expression. Thus, ALIXΔPRR expression might regulate exosome formation, and could be used as a tool to identify the cargo proteins which follow the ALIX-dependent pathway for exosome biogenesis and secretion.

2. ALIX recruits actin remodeling factors and autophagy proteins to endosomes

Actin polymerization plays an important role in endosomes movement and maturation, protein sorting and MVE biogenesis (Durrbach et al. 1996; Taunton et al. 2000; Derivery et al. 2009; Gomez and Billadeau 2009; Morel et al. 2009; Duleh and Welch 2010; Puthenveedu et al. 2010; Carnell et al. 2011; Derivery et al. 2012; Muriel et al. 2016). AnnexinA2, a lipid-binding protein, is a nucleation factor for actin recruitment and polymerization on the endosomal membranes (Morel et al. 2009), and the WASP and SCAR homologue (WASH) complex regulates actin branching in this compartment by the activation of the actin nucleation complex Arp 2/3 (Derivery et al. 2009; Derivery and Gautreau 2010). ALIX has also been suggested to regulate cortical actin and endosomal distribution, however the mechanism of action is still unknown (Cabezas et al. 2005). ALIXΔPRR expression induces the endosomal accumulation of three subunits of the Arp 2/3 complex, actin-related protein 2/3 complex subunits 2 and 3 (ARPC2 and ARPC3) and actin-related protein 3 (ACTR3). Furthermore, WD repeat-containing protein 1 (WDR1), cofilin 1 and 2 (CFL1, 2) and destrin (DSTN), which are actin-depolymerizing factors (Nishida et al. 1985; Yonezawa et al. 1985; Yeoh et al. 2002; Ono 2017) are also increased upon ALIXΔPRR expression. Thus, this suggests that ALIX could be an important factor for actin filament remodeling on endosomal membranes.

Two LC3 homologs, gamma-aminobutyric acid type A receptor associated protein (GABARAP) and GABARAP like 2 (GABARAPL2), sequestosome 1 (SQSTM1), tool-interacting protein (TOLLIP), TMEM59 and Unc-51-like kinase 3 (ULK3), are accumulated in endosomes upon ALIXΔPRR expression, and are known to participate in autophagy (Kabeya et al. 2004; Bjorkoy et al. 2005; Young et al. 2009; Chakrama et al. 2010; Weidberg et al. 2010; Boada-Romero et al. 2013; Shimizu et al. 2014). Furthermore, ESCRT proteins and ALIX have been suggested to play a role during autophagy (Rusten and Simonsen 2008; Murrow et al. 2015). Basal autophagy (number of autophagosomes) is not affected in ALIXΔPRR expressing cells, which might suggest that the autophagy proteins that we find accumulated in endosomes, could be playing functions unrelated to autophagy, as it has been shown for GABARAP, ULK3, TOLLIP and TMEM59 (Burns et al. 2000; Katoh et al. 2004b; Ullrich et al. 2010; Zhu et al. 2012; Caballe et al. 2015; Schaaf et al. 2016).

3. Model for endosomal ESCRT-III recruitment and cargo sorting by ALIX and LBPA

Our results provide first insights into the molecular mechanism of how ALIX and its interaction with LBPA/BMP regulate the endosomal ESCRT pathway. We propose a model in which initially cytosolic ALIX is "activated" prior to its recruitment to LBPA/BMP-containing endosomes. ALIX PRR acts as an auto-inhibitory region for the BRO1 domain interaction with CHMP4 (Zhou et al. 2009), and presumably also LBPA. ALIX "open or active" conformation can be induced by phosphorylation of the PRR or the interaction with ALG-2 (Sun et al. 2015; Sun et al. 2016). After ALIX activation, the flexible loop present in ALIX BRO1 domain is partially inserted into the cytoplasmic leaflet of the lipid bilayer (Bissig et al. 2013). This interaction could stabilize LBPA/BMP at the limiting membrane of late endosomes, which is normally found accumulated in the lumen of the compartment (Kobayashi et al. 1998), and induce the formation of membrane domains rich in LBPA/BMP. This negatively-charged lipid has membrane deformation properties, and participates in ILV formation (Matsuo et al. 2004). In addition, SNF7/CHMP4 membrane nucleation is faster in concave (negatively-curved) negatively-charged membrane surfaces (Lee et al. 2015). Thus, two factors will promote CHMP4 endosomal recruitment in the ALIX-LBPA/BMP pathway; the first one is the direct interaction of CHMP4 with ALIX BRO1 domain, and the second one is the negative membrane curvature induced by LBPA/BMP membrane domains. Right after CHMP4 nucleation, ALIX-CHMP4 interaction could activate CHMP4 polymerization on membranes, as it is for BRO1-SNF7 in yeast (Tang et al. 2016), and consequently induce membrane deformation. In this regard, membrane remodeling depends on a dynamic subunit turnover in ESCRT-III assemblies (Adell et al. 2017; Mierzwa et al. 2017), which indicates that VPS4 could also participate in the ALIX-LBPA/BMP pathway (Fig. 22).

In our model, cargo protein sorting into ILVs can be achieved by different mechanisms. First, ALIX V-domain could interact directly with the YP(X)nL motif of transmembrane (e.g PAR1 and P2Y1) proteins (and non-transmembrane proteins e.g. syntenin), acting as a bridge between the cargo and the ESCRT-III machinery. Second, ALIX could indirectly bind to the cargo by the assistance of other proteins. A third possibility is the direct interaction of ALIX V-domain to the conjugated ubiquitin in the cargo. Any of these possible interactions will presumably promote the clustering of the cargo protein in specific membrane regions enriched in LBPA/BMP and ESCRT-III, and trigger its sorting into ILVs.

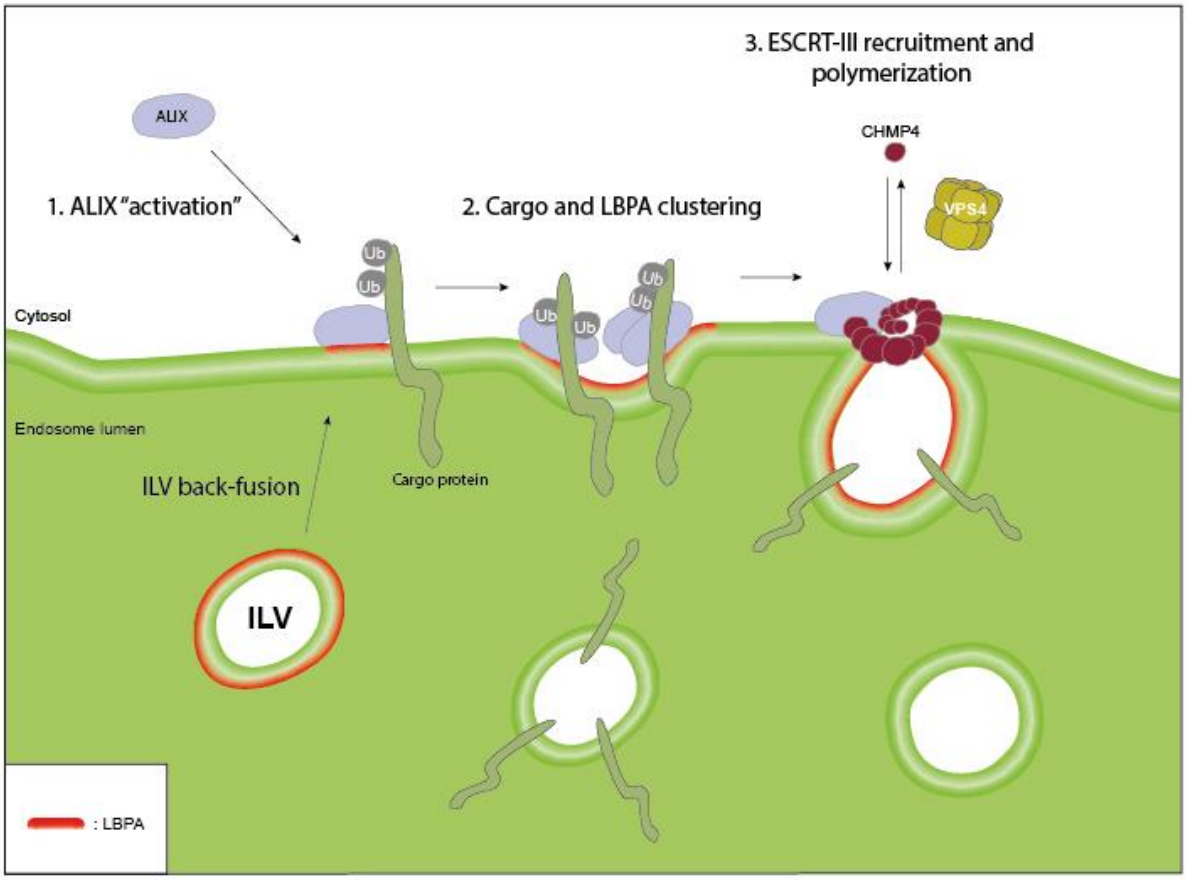

Figure 21. Model for ALIX-LBPA-dependent ESCRT recruitment and cargo sorting into ILVs. 1. ALIX is "activated" and interacts with LBPA and specific cargo proteins on the limiting membrane of late endosomes. 2. LBPA micro-domains are formed, which promotes membrane invagination. 3. ALIX, together with the negative membrane curvature, facilitates ESCRT-III recruitment, nucleation and polymerization on the membranes, which is necessary for cargo sorting into ILVs. ILV: intraluminal vesicle; Ub: ubiquitin.

4. Conclusion

The evidence presented in this thesis elucidates a role for ALIX in a non-canonical ESCRT-III endosomal recruitment. We showed that ALIX recruits ESCRT-III proteins, primarily CHMP4, in an LBPA dependent and ESCRT-0, -I, –II, and CHMP6 independent manner. Furthermore, data provides evidence that ALIX participates in the endosomal sorting of ubiquitinated cargo, as shown by accumulation of transmembrane and ubiquitinated proteins in endosomes in the presence of ALIX lacking its PRR.

Abbreviations

AAA-ATPase	ATPase associated with diverse cellular activities
ACTR3	Actin-related protein 3
AIP4	Atrophin-1-interacting protein 4
ALIX	Apoptosis-linked gene 2-interacting protein X
ANTXR1	Anthrax toxin receptor 1
APLP	Amyloid-like protein precursor
APP	Amyloid precursor protein
ARF6	Adenosine 5′-diphosphate (ADP)-ribosylation factor 6
ARPC	Actin-related protein 2/3 complex
ARRDC3	Arrestin domain-containing protein 3
ATG	Autophagy-related
ATP	Adenosine triphosphate
ATP8A1	Phospholipid-transporting ATPase IA
Aβ	Amyloid beta
BACE	Beta-site APP cleaving enzyme
BMP	Bismonoacyl glycerophosphate
BRO1	Bro domain-containing protein 1
BROX	BRO1 domain- and CAAX motif-containing protein
Cbl	Casitas B-lineage lymphoma
CCR5	C-C chemokine receptor type 5
CD4	Cluster of differentiation 4
CEP55	Centrosomal protein of 55 kDa
CFL	Cofilin
CFTR	Cystic fibrosis transmembrane conductance regulator

CHMP	Charged multivesicular body protein
CI-M6PR	Cation-independent mannose 6-phosphate receptor
CLIC1	Chloride intracellular channel protein 1
CORVET	Class C core endosome vacuole tethering
CTF	Carboxy-terminal fragment
CXCR4	C-X-C chemokine receptor type 4
DID2	DOA4-independent degradation protein 2
DOA4	Degradation of alpha 4
DOPC	1, 2-Dioleoyl-sn-glycerol-3-phosphocholine
DOPE	1, 2-Dioleoyl-sn-glycerol-3-phosphoethanolamine
DOPS	1, 2-Dioleoyl-sn-glycerol-3-phospho-L-serine
DOR	δ-opioid receptor
DSTN	Destrin
DUB	Deubiquitinating enzyme
EAP45	ELL-associated protein of 45 kDa
ECV	Endosomal carrier vesicle
EE	Early endosome
EEA1	Endosome antigen 1
EGF	Epidermal growth factor
EGFR	EGF receptor
EIAV	Equine infectious anemia virus
ENaC	Epithelial Na(+) channel
ENT	Epsin
EphR	Ephrin receptor
EPS15	Epidermal growth factor receptor substrate 15
ER	Endoplasmic reticulum
ERC	Endocytic recycling compartment

ESCRT	Endosomal sorting complexes required for transport
FGFR	Fibroblast growth factor receptor
FRAP	Fluorescence recovery after photobleaching
FYVE	Fab1p, YOTB, Vac1p, EEA1
GABARAP	Gamma-aminobutyric acid type A receptor associated protein
GABARAPL2	GABARAP like 2
GAP	GTPase-activating protein
GASP1	G-protein coupled receptor-associated sorting protein 1
GDP	Guanosine diphosphate
GEF	GDP-GTP exchange factor
GLUE	GRAM-like ubiquitin-binding in EAP45
GP73	Serum Golgi protein 73
GPCR	G-protein-coupled receptor
GTP	Guanosine triphosphate
GUV	Giant unilamellar vesicles
HD-PTP	His domain-containing protein tyrosine phosphatase
HECT	Homologous to E6-AP carboxyl terminus
HIV-1	Human immunodeficiency virus type 1
HOPS	Homotypic vacuole fusion and protein sorting
HRS	Hepatocyte growth factor-regulated tyrosine kinase substrate
HSE1	Has symptoms of class E mutant
HSP70	Heat Shock Protein 70
IGF-IR	Insulin-like growth factor 1
IGFR2	Insulin-like growth factor 2 receptor, IGFR2
IL-2Rβ	Interleukin-2 receptor subunit beta
ILV	Intraluminal vesicle
IST1	Increased sodium tolerance 1

ITM2B	Integral membrane protein 2B
KSHV	Kaposi’s sarcoma-associated herpes virus
LBPA	Lysobisphosphatic acid
LDL	Low-density lipoprotein
LDLR	Low-density lipoprotein receptor
LE	Late endosome
MHC	Major histocompatibility complex
MIM	MIT-interacting motif
MIT	Microtubule interacting and transport domain
MTOC	Microtubule-organizing center
MVB	Multivesciular body
MVB12	Multivesicular body sorting factor 12
MVE	Multivesicular endosome
NCC	Nuclear chloride ion channel
NCSTN	Nicastrin
NDFIP2	NEDD4 family-interacting protein 2
NEDD4	Neural precursor cell expressed developmentally down-regulated protein 4
NEDL	NEDD4-like E3 ubiquitin-protein ligase
Nef	Negative factor
NPC	Niemann-Pick type C
P2Y1	P2Y purinoreceptor 1
PAR1	Protease-activated receptor 1
PDGFR	Platelet-derived growth factor receptor
PDGFRB	platelet-derived growth factor receptor beta
PDZ	PSD-95, Discs Large, Zo-1
PEST	Proline-, glutamic acid-, serine-, and threonine-rich
PI	L-α-phosphatidylinositol

PI	Phosphatidylinositide
PI3K	Phosphatidyilinositol-3 kinase
PIKfyve	Phosphatidylinositol-3-phosphate 5-kinase type III
PLD2	Phospholipase D2
PRR	Proline rich region
PtdIns	Phosphatidylinositol
PtdSer	Phosphatidylserine
PX	Phox homology
RAB	Rab-related protein in brain
RBR	Ring between ring fingers
RE	Recycling endosome
RILP	RAB-interacting lysosomal protein
RING	Really interesting new gene
RSP5	Reverses SPT-phenotype protein 5
RTK	Receptor tyrosine kinase
SARA	Smad anchor for receptor activation
SDC4	Syndecan 4
SM	Sec1/Munc-18
SMases	Sphingomyelinases
SMURF	SMAD ubiquitination regulatory factor
SNARE	Soluble N-ethylmaleimide-sensitive factor attachment protein receptor
SNF7	Sucrose non fermenting protein 7
SPH	Sphingomyelins
SQSTM1	Sequestosome 1
STAM	Signal transducing adapter molecule
TGFβR	Transforming growth factor β/bone morphogenetic protein receptor
TGN	Trans-Golgi network

TGN38	TGN integral protein 38
TMEM59	Transmembrane protein 59
TOLLIP	Tool-interacting protein
TSG101	Tumor susceptibility gene 101
UBPY	Ubiquitin isopeptidase Y
ULK3	Unc-51-like kinase 3
USP8	Ubiquitin-specific-processing protease 8
UV	Ultraviolet
VAMP4	Vesicle-associated protein 4
VEGFR	Vascular endothelial growth factor receptor
VPS	Vacuolar protein sorting
VSV	Vesicular stomatitis virus
VTI1A	Vesicle transport through interaction with t-SNAREs 1A
WASH	WASP and SCAR homolog
WDR1	WD repeat-containing protein 1
WWP	WW domain containing E3 ubiquitin protein ligase
YAP	Yes-associated protein
YPT7	Yeast protein two 7
β2-AR	Beta-2 adrenergic receptor

Bibliography

Abrami L, Brandi L, Moayeri M, Brown MJ, Krantz BA, Leppla SH, van der Goot FG. 2013. Hijacking multivesicular bodies enables long-term and exosome-mediated long-distance action of anthrax toxin. *Cell Rep* **5**: 986-996.

Abrami L, Lindsay M, Parton RG, Leppla SH, van der Goot FG. 2004. Membrane insertion of anthrax protective antigen and cytoplasmic delivery of lethal factor occur at different stages of the endocytic pathway. *J Cell Biol* **166**: 645-651.

Adell MA, Vogel GF, Pakdel M, Muller M, Lindner H, Hess MW, Teis D. 2014. Coordinated binding of Vps4 to ESCRT-III drives membrane neck constriction during MVB vesicle formation. *J Cell Biol* **205**: 33-49.

Adell MAY, Migliano SM, Upadhyayula S, Bykov YS, Sprenger S, Pakdel M, Vogel GF, Jih G, Skillern W, Behrouzi R et al. 2017. Recruitment dynamics of ESCRT-III and Vps4 to endosomes and implications for reverse membrane budding. *Elife* **6**.

Alam SL, Sun J, Payne M, Welch BD, Blake BK, Davis DR, Meyer HH, Emr SD, Sundquist WI. 2004. Ubiquitin interactions of NZF zinc fingers. *EMBO J* **23**: 1411-1421.

Ali N, Zhang L, Taylor S, Mironov A, Urbe S, Woodman P. 2013. Recruitment of UBPY and ESCRT exchange drive HD-PTP-dependent sorting of EGFR to the MVB. *Curr Biol* **23**: 453-461.

Amorim NA, da Silva EM, de Castro RO, da Silva-Januario ME, Mendonca LM, Bonifacino JS, da Costa LJ, daSilva LL. 2014. Interaction of HIV-1 Nef protein with the host protein Alix promotes lysosomal targeting of CD4 receptor. *J Biol Chem* **289**: 27744-27756.

Anderson RG, Brown MS, Beisiegel U, Goldstein JL. 1982. Surface distribution and recycling of the low density lipoprotein receptor as visualized with antireceptor antibodies. *J Cell Biol* **93**: 523-531.

Anderson RG, Brown MS, Goldstein JL. 1977. Role of the coated endocytic vesicle in the uptake of receptor-bound low density lipoprotein in human fibroblasts. *Cell* **10**: 351-364.

Babst M, Katzmann DJ, Estepa-Sabal EJ, Meerloo T, Emr SD. 2002a. Escrt-III: an endosome-associated heterooligomeric protein complex required for mvb sorting. *Dev Cell* **3**: 271-282.

Babst M, Katzmann DJ, Snyder WB, Wendland B, Emr SD. 2002b. Endosome-associated complex, ESCRT-II, recruits transport machinery for protein sorting at the multivesicular body. *Dev Cell* **3**: 283-289.

Babst M, Odorizzi G, Estepa EJ, Emr SD. 2000. Mammalian tumor susceptibility gene 101 (TSG101) and the yeast homologue, Vps23p, both function in late endosomal trafficking. *Traffic* **1**: 248-258.

Babst M, Sato TK, Banta LM, Emr SD. 1997. Endosomal transport function in yeast requires a novel AAA-type ATPase, Vps4p. *EMBO J* **16**: 1820-1831.

Babst M, Wendland B, Estepa EJ, Emr SD. 1998. The Vps4p AAA ATPase regulates membrane association of a Vps protein complex required for normal endosome function. *EMBO J* **17**: 2982-2993.

Bache KG, Slagsvold T, Cabezas A, Rosendal KR, Raiborg C, Stenmark H. 2004. The growth-regulatory protein HCRP1/hVps37A is a subunit of mammalian ESCRT-I and mediates receptor down-regulation. *Mol Biol Cell* **15**: 4337-4346.

Bache KG, Stuffers S, Malerod L, Slagsvold T, Raiborg C, Lechardeur D, Walchli S, Lukacs GL, Brech A, Stenmark H. 2006. The ESCRT-III subunit hVps24 is required for degradation but not silencing of the epidermal growth factor receptor. *Mol Biol Cell* **17**: 2513-2523.

Baietti MF, Zhang Z, Mortier E, Melchior A, Degeest G, Geeraerts A, Ivarsson Y, Depoortere F, Coomans C, Vermeiren E et al. 2012. Syndecan-syntenin-ALIX regulates the biogenesis of exosomes. *Nat Cell Biol* **14**: 677-685.

Bajorek M, Schubert HL, McCullough J, Langelier C, Eckert DM, Stubblefield WM, Uter NT, Myszka DG, Hill CP, Sundquist WI. 2009. Structural basis for ESCRT-III protein autoinhibition. *Nat Struct Mol Biol* **16**: 754-762.

Balderhaar HJ, Lachmann J, Yavavli E, Brocker C, Lurick A, Ungermann C. 2013. The CORVET complex promotes tethering and fusion of Rab5/Vps21-positive membranes. *Proc Natl Acad Sci U S A* **110**: 3823-3828.

Balla T, Bondeva T, Varnai P. 2000. How accurately can we image inositol lipids in living cells? *Trends Pharmacol Sci* **21**: 238-241.

Bankaitis VA, Johnson LM, Emr SD. 1986. Isolation of yeast mutants defective in protein targeting to the vacuole. *Proc Natl Acad Sci U S A* **83**: 9075-9079.

Belgareh-Touze N, Leon S, Erpapazoglou Z, Stawiecka-Mirota M, Urban-Grimal D, Haguenauer-Tsapis R. 2008. Versatile role of the yeast ubiquitin ligase Rsp5p in intracellular trafficking. *Biochem Soc Trans* **36**: 791-796.

Benmerah A, Gagnon J, Begue B, Megarbane B, Dautry-Varsat A, Cerf-Bensussan N. 1995. The tyrosine kinase substrate eps15 is constitutively associated with the plasma membrane adaptor AP-2. *J Cell Biol* **131**: 1831-1838.

Bethani I, Lang T, Geumann U, Sieber JJ, Jahn R, Rizzoli SO. 2007. The specificity of SNARE pairing in biological membranes is mediated by both proof-reading and spatial segregation. *EMBO J* **26**: 3981-3992.

Bilodeau PS, Urbanowski JL, Winistorfer SC, Piper RC. 2002. The Vps27p Hse1p complex binds ubiquitin and mediates endosomal protein sorting. *Nat Cell Biol* **4**: 534-539.

Bishop N, Horman A, Woodman P. 2002. Mammalian class E vps proteins recognize ubiquitin and act in the removal of endosomal protein-ubiquitin conjugates. *J Cell Biol* **157**: 91-101.

Bissig C, Gruenberg J. 2014. ALIX and the multivesicular endosome: ALIX in Wonderland. *Trends Cell Biol* **24**: 19-25.

Bissig C, Hurbain I, Raposo G, van Niel G. 2017. PIKfyve activity regulates reformation of terminal storage lysosomes from endolysosomes. *Traffic* **18**: 747-757.

Bissig C, Lenoir M, Velluz MC, Kufareva I, Abagyan R, Overduin M, Gruenberg J. 2013. Viral infection controlled by a calcium-dependent lipid-binding module in ALIX. *Dev Cell* **25**: 364-373.

Bjorkoy G, Lamark T, Brech A, Outzen H, Perander M, Overvatn A, Stenmark H, Johansen T. 2005. p62/SQSTM1 forms protein aggregates degraded by autophagy and has a protective effect on huntingtin-induced cell death. *J Cell Biol* **171**: 603-614.

Blumental-Perry A, Haney CJ, Weixel KM, Watkins SC, Weisz OA, Aridor M. 2006. Phosphatidylinositol 4-phosphate formation at ER exit sites regulates ER export. *Dev Cell* **11**: 671-682.

Boada-Romero E, Letek M, Fleischer A, Pallauf K, Ramon-Barros C, Pimentel-Muinos FX. 2013. TMEM59 defines a novel ATG16L1-binding motif that promotes local activation of LC3. *EMBO J* **32**: 566-582.

Bowers K, Lottridge J, Helliwell SB, Goldthwaite LM, Luzio JP, Stevens TH. 2004. Protein-protein interactions of ESCRT complexes in the yeast Saccharomyces cerevisiae. *Traffic* **5**: 194-210.

Bowers K, Piper SC, Edeling MA, Gray SR, Owen DJ, Lehner PJ, Luzio JP. 2006. Degradation of endocytosed epidermal growth factor and virally ubiquitinated major histocompatibility complex class I is independent of mammalian ESCRTII. *J Biol Chem* **281**: 5094-5105.

Bowers K, Stevens TH. 2005. Protein transport from the late Golgi to the vacuole in the yeast Saccharomyces cerevisiae. *Biochim Biophys Acta* **1744**: 438-454.

Bradley KA, Mogridge J, Mourez M, Collier RJ, Young JA. 2001. Identification of the cellular receptor for anthrax toxin. *Nature* **414**: 225-229.

Brown MS, Goldstein JL. 1975. Lipoprotein receptors and genetic control of cholesterol metabolism in cultured human cells. *Naturwissenschaften* **62**: 385-389.

Bucci C, Parton RG, Mather IH, Stunnenberg H, Simons K, Hoflack B, Zerial M. 1992. The small GTPase rab5 functions as a regulatory factor in the early endocytic pathway. *Cell* **70**: 715-728.

Buchkovich NJ, Henne WM, Tang S, Emr SD. 2013. Essential N-terminal insertion motif anchors the ESCRT-III filament during MVB vesicle formation. *Dev Cell* **27**: 201-214.

Burns K, Clatworthy J, Martin L, Martinon F, Plumpton C, Maschera B, Lewis A, Ray K, Tschopp J, Volpe F. 2000. Tollip, a new component of the IL-1RI pathway, links IRAK to the IL-1 receptor. *Nat Cell Biol* **2**: 346-351.

Caballe A, Wenzel DM, Agromayor M, Alam SL, Skalicky JJ, Kloc M, Carlton JG, Labrador L, Sundquist WI, Martin-Serrano J. 2015. ULK3 regulates cytokinetic abscission by phosphorylating ESCRT-III proteins. *Elife* **4**: e06547.

Cabezas A, Bache KG, Brech A, Stenmark H. 2005. Alix regulates cortical actin and the spatial distribution of endosomes. *J Cell Sci* **118**: 2625-2635.

Cabrera M, Arlt H, Epp N, Lachmann J, Griffith J, Perz A, Reggiori F, Ungermann C. 2013. Functional separation of endosomal fusion factors and the class C core vacuole/endosome tethering (CORVET) complex in endosome biogenesis. *J Biol Chem* **288**: 5166-5175.

Cantalupo G, Alifano P, Roberti V, Bruni CB, Bucci C. 2001. Rab-interacting lysosomal protein (RILP): the Rab7 effector required for transport to lysosomes. *EMBO J* **20**: 683-693.

Carlton JG, Agromayor M, Martin-Serrano J. 2008. Differential requirements for Alix and ESCRT-III in cytokinesis and HIV-1 release. *Proc Natl Acad Sci U S A* **105**: 10541-10546.

Carlton JG, Martin-Serrano J. 2007. Parallels between cytokinesis and retroviral budding: a role for the ESCRT machinery. *Science* **316**: 1908-1912.

Carnell M, Zech T, Calaminus SD, Ura S, Hagedorn M, Johnston SA, May RC, Soldati T, Machesky LM, Insall RH. 2011. Actin polymerization driven by WASH causes V-ATPase retrieval and vesicle neutralization before exocytosis. *J Cell Biol* **193**: 831-839.

Carstea ED, Morris JA, Coleman KG, Loftus SK, Zhang D, Cummings C, Gu J, Rosenfeld MA, Pavan WJ, Krizman DB et al. 1997. Niemann-Pick C1 disease gene: homology to mediators of cholesterol homeostasis. *Science* **277**: 228-231.

Cashikar AG, Shim S, Roth R, Maldazys MR, Heuser JE, Hanson PI. 2014. Structure of cellular ESCRT-III spirals and their relationship to HIV budding. *Elife* **3**.

Cauvin C, Echard A. 2015. Phosphoinositides: Lipids with informative heads and mastermind functions in cell division. *Biochim Biophys Acta* **1851**: 832-843.

Chakrama FZ, Seguin-Py S, Le Grand JN, Fraichard A, Delage-Mourroux R, Despouy G, Perez V, Jouvenot M, Boyer-Guittaut M. 2010. GABARAPL1 (GEC1) associates with autophagic vesicles. *Autophagy* **6**: 495-505.

Chavrier P, Parton RG, Hauri HP, Simons K, Zerial M. 1990. Localization of low molecular weight GTP binding proteins to exocytic and endocytic compartments. *Cell* **62**: 317-329.

Chevallier J, Chamoun Z, Jiang G, Prestwich G, Sakai N, Matile S, Parton RG, Gruenberg J. 2008. Lysobisphosphatidic acid controls endosomal cholesterol levels. *J Biol Chem* **283**: 27871-27880.

Chiaruttini N, Redondo-Morata L, Colom A, Humbert F, Lenz M, Scheuring S, Roux A. 2015. Relaxation of Loaded ESCRT-III Spiral Springs Drives Membrane Deformation. *Cell* **163**: 866-879.

Chiaruttini N, Roux A. 2017. Dynamic and elastic shape transitions in curved ESCRT-III filaments. *Curr Opin Cell Biol* **in press**.

Christ L, Raiborg C, Wenzel EM, Campsteijn C, Stenmark H. 2017. Cellular Functions and Molecular Mechanisms of the ESCRT Membrane-Scission Machinery. *Trends Biochem Sci* **42**: 42-56.

Christ L, Wenzel EM, Liestol K, Raiborg C, Campsteijn C, Stenmark H. 2016. ALIX and ESCRT-I/II function as parallel ESCRT-III recruiters in cytokinetic abscission. *J Cell Biol* **212**: 499-513.

Christoforidis S, McBride HM, Burgoyne RD, Zerial M. 1999. The Rab5 effector EEA1 is a core component of endosome docking. *Nature* **397**: 621-625.

Clague MJ, Heride C, Urbe S. 2015. The demographics of the ubiquitin system. *Trends Cell Biol* **25**: 417-426.

Clarke CJ, Snook CF, Tani M, Matmati N, Marchesini N, Hannun YA. 2006. The extended family of neutral sphingomyelinases. *Biochemistry* **45**: 11247-11256.

Colombo M, Moita C, van Niel G, Kowal J, Vigneron J, Benaroch P, Manel N, Moita LF, Thery C, Raposo G. 2013. Analysis of ESCRT functions in exosome biogenesis, composition and secretion highlights the heterogeneity of extracellular vesicles. *J Cell Sci* **126**: 5553-5565.

Coonrod EM, Stevens TH. 2010. The yeast vps class E mutants: the beginning of the molecular genetic analysis of multivesicular body biogenesis. *Mol Biol Cell* **21**: 4057-4060.

daSilva LL, Sougrat R, Burgos PV, Janvier K, Mattera R, Bonifacino JS. 2009. Human immunodeficiency virus type 1 Nef protein targets CD4 to the multivesicular body pathway. *J Virol* **83**: 6578-6590.

Davies BA, Azmi IF, Payne J, Shestakova A, Horazdovsky BF, Babst M, Katzmann DJ. 2010. Coordination of substrate binding and ATP hydrolysis in Vps4-mediated ESCRT-III disassembly. *Mol Biol Cell* **21**: 3396-3408.

Davis CG, Goldstein JL, Sudhof TC, Anderson RG, Russell DW, Brown MS. 1987. Acid-dependent ligand dissociation and recycling of LDL receptor mediated by growth factor homology region. *Nature* **326**: 760-765.

Davis NG, Horecka JL, Sprague GF, Jr. 1993. Cis- and trans-acting functions required for endocytosis of the yeast pheromone receptors. *J Cell Biol* **122**: 53-65.

Denais CM, Gilbert RM, Isermann P, McGregor AL, te Lindert M, Weigelin B, Davidson PM, Friedl P, Wolf K, Lammerding J. 2016. Nuclear envelope rupture and repair during cancer cell migration. *Science* **352**: 353.

Derivery E, Gautreau A. 2010. Generation of branched actin networks: assembly and regulation of the N-WASP and WAVE molecular machines. *Bioessays* **32**: 119-131.

Derivery E, Helfer E, Henriot V, Gautreau A. 2012. Actin polymerization controls the organization of WASH domains at the surface of endosomes. *PLoS One* **7**: e39774.

Derivery E, Sousa C, Gautier JJ, Lombard B, Loew D, Gautreau A. 2009. The Arp2/3 activator WASH controls the fission of endosomes through a large multiprotein complex. *Dev Cell* **17**: 712-723.

Deshaies RJ, Joazeiro CA. 2009. RING domain E3 ubiquitin ligases. *Annu Rev Biochem* **78**: 399-434.

Dikic I, Wakatsuki S, Walters KJ. 2009. Ubiquitin-binding domains - from structures to functions. *Nat Rev Mol Cell Biol* **10**: 659-671.

Dores MR, Chen B, Lin H, Soh UJ, Paing MM, Montagne WA, Meerloo T, Trejo J. 2012. ALIX binds a YPX(3)L motif of the GPCR PAR1 and mediates ubiquitin-independent ESCRT-III/MVB sorting. *J Cell Biol* **197**: 407-419.

Dores MR, Grimsey NJ, Mendez F, Trejo J. 2016. ALIX Regulates the Ubiquitin-Independent Lysosomal Sorting of the P2Y1 Purinergic Receptor via a YPX3L Motif. *PLoS One* **11**: e0157587.

Dores MR, Lin H, N JG, Mendez F, Trejo J. 2015. The alpha-arrestin ARRDC3 mediates ALIX ubiquitination and G protein-coupled receptor lysosomal sorting. *Mol Biol Cell* **26**: 4660-4673.

Dores MR, Trejo J. 2014. Atypical regulation of G protein-coupled receptor intracellular trafficking by ubiquitination. *Curr Opin Cell Biol* **27**: 44-50.

Dove SK, Dong K, Kobayashi T, Williams FK, Michell RH. 2009. Phosphatidylinositol 3,5-bisphosphate and Fab1p/PIKfyve underPPIn endo-lysosome function. *Biochem J* **419**: 1-13.

Dowlatshahi DP, Sandrin V, Vivona S, Shaler TA, Kaiser SE, Melandri F, Sundquist WI, Kopito RR. 2012. ALIX is a Lys63-specific polyubiquitin binding protein that functions in retrovirus budding. *Dev Cell* **23**: 1247-1254.

Doyotte A, Mironov A, McKenzie E, Woodman P. 2008. The Bro1-related protein HD-PTP/PTPN23 is required for endosomal cargo sorting and multivesicular body morphogenesis. *Proc Natl Acad Sci U S A* **105**: 6308-6313.

Doyotte A, Russell MR, Hopkins CR, Woodman PG. 2005. Depletion of TSG101 forms a mammalian "Class E" compartment: a multicisternal early endosome with multiple sorting defects. *J Cell Sci* **118**: 3003-3017.

Duleh SN, Welch MD. 2010. WASH and the Arp2/3 complex regulate endosome shape and trafficking. *Cytoskeleton (Hoboken)* **67**: 193-206.

Dumas JJ, Merithew E, Sudharshan E, Rajamani D, Hayes S, Lawe D, Corvera S, Lambright DG. 2001. Multivalent endosome targeting by homodimeric EEA1. *Mol Cell* **8**: 947-958.

Dupre S, Haguenauer-Tsapis R. 2001. Deubiquitination step in the endocytic pathway of yeast plasma membrane proteins: crucial role of Doa4p ubiquitin isopeptidase. *Mol Cell Biol* **21**: 4482-4494.

Dupre S, Urban-Grimal D, Haguenauer-Tsapis R. 2004. Ubiquitin and endocytic internalization in yeast and animal cells. *Biochim Biophys Acta* **1695**: 89-111.

Durrbach A, Louvard D, Coudrier E. 1996. Actin filaments facilitate two steps of endocytosis. *J Cell Sci* **109 (Pt 2)**: 457-465.

Duval M, Bedard-Goulet S, Delisle C, Gratton JP. 2003. Vascular endothelial growth factor-dependent down-regulation of Flk-1/KDR involves Cbl-mediated ubiquitination. Consequences on nitric oxide production from endothelial cells. *J Biol Chem* **278**: 20091-20097.

Edgar JR, Willen K, Gouras GK, Futter CE. 2015. ESCRTs regulate amyloid precursor protein sorting in multivesicular bodies and intracellular amyloid-beta accumulation. *J Cell Sci* **128**: 2520-2528.

Egner R, Kuchler K. 1996. The yeast multidrug transporter Pdr5 of the plasma membrane is ubiquitinated prior to endocytosis and degradation in the vacuole. *FEBS Lett* **378**: 177-181.

Erpapazoglou Z, Dhaoui M, Pantazopoulou M, Giordano F, Mari M, Leon S, Raposo G, Reggiori F, Haguenauer-Tsapis R. 2012. A dual role for K63-linked ubiquitin chains in multivesicular body biogenesis and cargo sorting. *Molecular Biology of the Cell* **23**: 2170-2183.

Eugster A, Pecheur EI, Michel F, Winsor B, Letourneur F, Friant S. 2004. Ent5p is required with Ent3p and Vps27p for ubiquitin-dependent protein sorting into the multivesicular body. *Mol Biol Cell* **15**: 3031-3041.

Fairn GD, Schieber NL, Ariotti N, Murphy S, Kuerschner L, Webb RI, Grinstein S, Parton RG. 2011. High-resolution mapping reveals topologically distinct cellular pools of phosphatidylserine. *J Cell Biol* **194**: 257-275.

Falguieres T, Luyet PP, Bissig C, Scott CC, Velluz MC, Gruenberg J. 2008. In vitro budding of intralumenal vesicles into late endosomes is regulated by Alix and Tsg101. *Mol Biol Cell* **19**: 4942-4955.

Fasen K, Cerretti DP, Huynh-Do U. 2008. Ligand binding induces Cbl-dependent EphB1 receptor degradation through the lysosomal pathway. *Traffic* **9**: 251-266.

Filimonenko M, Stuffers S, Raiborg C, Yamamoto A, Malerod L, Fisher EM, Isaacs A, Brech A, Stenmark H, Simonsen A. 2007. Functional multivesicular bodies are required for autophagic clearance of protein aggregates associated with neurodegenerative disease. *J Cell Biol* **179**: 485-500.

Fisher RD, Chung HY, Zhai Q, Robinson H, Sundquist WI, Hill CP. 2007. Structural and biochemical studies of ALIX/AIP1 and its role in retrovirus budding. *Cell* **128**: 841-852.

Foot N, Henshall T, Kumar S. 2017. Ubiquitination and the Regulation of Membrane Proteins. *Physiol Rev* **97**: 253-281.

Fotinopoulou A, Tsachaki M, Vlavaki M, Poulopoulos A, Rostagno A, Frangione B, Ghiso J, Efthimiopoulos S. 2005. BRI2 interacts with amyloid precursor protein (APP) and regulates amyloid beta (Abeta) production. *J Biol Chem* **280**: 30768-30772.

Friand V, David G, Zimmermann P. 2015. Syntenin and syndecan in the biogenesis of exosomes. *Biol Cell* **107**: 331-341.

Friant S, Pecheur EI, Eugster A, Michel F, Lefkir Y, Nourrisson D, Letourneur F. 2003. Ent3p Is a PtdIns(3,5)P2 effector required for protein sorting to the multivesicular body. *Dev Cell* **5**: 499-511.

Funderburk SF, Wang QJ, Yue Z. 2010. The Beclin 1-VPS34 complex--at the crossroads of autophagy and beyond. *Trends Cell Biol* **20**: 355-362.

Gahloth D, Levy C, Walker L, Wunderley L, Mould AP, Taylor S, Woodman P, Tabernero L. 2017. Structural Basis for Specific Interaction of TGF beta Signaling Regulators SARA/Endofin with HD-PTP. *Structure* **25**: 1011-+.

Garrus JE, von Schwedler UK, Pornillos OW, Morham SG, Zavitz KH, Wang HE, Wettstein DA, Stray KM, Cote M, Rich RL et al. 2001. Tsg101 and the vacuolar protein sorting pathway are essential for HIV-1 budding. *Cell* **107**: 55-65.

Ghossoub R, Lembo F, Rubio A, Gaillard CB, Bouchet J, Vitale N, Slavik J, Machala M, Zimmermann P. 2014. Syntenin-ALIX exosome biogenesis and budding into multivesicular bodies are controlled by ARF6 and PLD2. *Nat Commun* **5**: 3477.

Gillooly DJ, Morrow IC, Lindsay M, Gould R, Bryant NJ, Gaullier JM, Parton RG, Stenmark H. 2000. Localization of phosphatidylinositol 3-phosphate in yeast and mammalian cells. *EMBO J* **19**: 4577-4588.

Gillooly DJ, Raiborg C, Stenmark H. 2003. Phosphatidylinositol 3-phosphate is found in microdomains of early endosomes. *Histochem Cell Biol* **120**: 445-453.

Gomez TS, Billadeau DD. 2009. A FAM21-containing WASH complex regulates retromer-dependent sorting. *Dev Cell* **17**: 699-711.

Grice GL, Nathan JA. 2016. The recognition of ubiquitinated proteins by the proteasome. *Cell Mol Life Sci* **73**: 3497-3506.

Grootjans JJ, Reekmans G, Ceulemans H, David G. 2000. Syntenin-syndecan binding requires syndecan-synteny and the co-operation of both PDZ domains of syntenin. *J Biol Chem* **275**: 19933-19941.

Gu M, LaJoie D, Chen OS, von Appen A, Ladinsky MS, Redd MJ, Nikolova L, Bjorkman PJ, Sundquist WI, Ullman KS et al. 2017. LEM2 recruits CHMP7 for ESCRT-mediated nuclear envelope closure in fission yeast and human cells. *Proc Natl Acad Sci U S A* **114**: E2166-E2175.

Guizetti J, Gerlich DW. 2012. ESCRT-III polymers in membrane neck constriction. *Trends Cell Biol* **22**: 133-140.

Guizetti J, Schermelleh L, Mantler J, Maar S, Poser I, Leonhardt H, Muller-Reichert T, Gerlich DW. 2011. Cortical constriction during abscission involves helices of ESCRT-III-dependent filaments. *Science* **331**: 1616-1620.

Haass C, Koo EH, Mellon A, Hung AY, Selkoe DJ. 1992. Targeting of cell-surface beta-amyloid precursor protein to lysosomes: alternative processing into amyloid-bearing fragments. *Nature* **357**: 500-503.

Hanson PI, Roth R, Lin Y, Heuser JE. 2008. Plasma membrane deformation by circular arrays of ESCRT-III protein filaments. *J Cell Biol* **180**: 389-402.

Hawryluk MJ, Keyel PA, Mishra SK, Watkins SC, Heuser JE, Traub LM. 2006. Epsin 1 is a polyubiquitin-selective clathrin-associated sorting protein. *Traffic* **7**: 262-281.

Helenius A, Mellman I, Wall D, Hubbard A. 1983. Endosomes. *Trends in Biochemical Sciences* **8**: 245-250.

Henne WM, Buchkovich NJ, Zhao Y, Emr SD. 2012. The endosomal sorting complex ESCRT-II mediates the assembly and architecture of ESCRT-III helices. *Cell* **151**: 356-371.

Henry AG, White IJ, Marsh M, von Zastrow M, Hislop JN. 2011. The role of ubiquitination in lysosomal trafficking of delta-opioid receptors. *Traffic* **12**: 170-184.

Hicke L, Riezman H. 1996. Ubiquitination of a yeast plasma membrane receptor signals its ligand-stimulated endocytosis. *Cell* **84**: 277-287.

Hiroyama M, Exton JH. 2005. Localization and regulation of phospholipase D2 by ARF6. *J Cell Biochem* **95**: 149-164.

Hislop JN, Marley A, Von Zastrow M. 2004. Role of mammalian vacuolar protein-sorting proteins in endocytic trafficking of a non-ubiquitinated G protein-coupled receptor to lysosomes. *J Biol Chem* **279**: 22522-22531.

Horiuchi H, Lippe R, McBride HM, Rubino M, Woodman P, Stenmark H, Rybin V, Wilm M, Ashman K, Mann M et al. 1997. A novel Rab5 GDP/GTP exchange factor complexed to Rabaptin-5 links nucleotide exchange to effector recruitment and function. *Cell* **90**: 1149-1159.

Hsu C, Morohashi Y, Yoshimura S, Manrique-Hoyos N, Jung S, Lauterbach MA, Bakhti M, Gronborg M, Mobius W, Rhee J et al. 2010. Regulation of exosome secretion by Rab35 and its GTPase-activating proteins TBC1D10A-C. *J Cell Biol* **189**: 223-232.

Huang F, Goh LK, Sorkin A. 2007. EGF receptor ubiquitination is not necessary for its internalization. *Proc Natl Acad Sci U S A* **104**: 16904-16909.

Huang F, Kirkpatrick D, Jiang X, Gygi S, Sorkin A. 2006. Differential regulation of EGF receptor internalization and degradation by multiubiquitination within the kinase domain. *Mol Cell* **21**: 737-748.

Huotari J, Helenius A. 2011. Endosome maturation. *EMBO J* **30**: 3481-3500.

Hutagalung AH, Novick PJ. 2011. Role of Rab GTPases in membrane traffic and cell physiology. *Physiol Rev* **91**: 119-149.

Iavello A, Frech VS, Gai C, Deregibus MC, Quesenberry PJ, Camussi G. 2016. Role of Alix in miRNA packaging during extracellular vesicle biogenesis. *Int J Mol Med* **37**: 958-966.

Ichioka F, Kobayashi R, Katoh K, Shibata H, Maki M. 2008. Brox, a novel farnesylated Bro1 domain-containing protein that associates with charged multivesicular body protein 4 (CHMP4). *FEBS J* **275**: 682-692.

Ichioka F, Takaya E, Suzuki H, Kajigaya S, Buchman VL, Shibata H, Maki M. 2007. HD-PTP and Alix share some membrane-traffic related proteins that interact with their Bro1 domains or proline-rich regions. *Arch Biochem Biophys* **457**: 142-149.

Im YJ, Wollert T, Boura E, Hurley JH. 2009. Structure and function of the ESCRT-II-III interface in multivesicular body biogenesis. *Dev Cell* **17**: 234-243.

Jiang L, Salao K, Li H, Rybicka JM, Yates RM, Luo XW, Shi XX, Kuffner T, Tsai VW, Husaini Y et al. 2012. Intracellular chloride channel protein CLIC1 regulates macrophage function through modulation of phagosomal acidification. *J Cell Sci* **125**: 5479-5488.

Jimenez AJ, Maiuri P, Lafaurie-Janvore J, Divoux S, Piel M, Perez F. 2014. ESCRT machinery is required for plasma membrane repair. *Science* **343**: 1247136.

Joshi A, Munshi U, Ablan SD, Nagashima K, Freed EO. 2008. Functional replacement of a retroviral late domain by ubiquitin fusion. *Traffic* **9**: 1972-1983.

Kabeya Y, Mizushima N, Yamamoto A, Oshitani-Okamoto S, Ohsumi Y, Yoshimori T. 2004. LC3, GABARAP and GATE16 localize to autophagosomal membrane depending on form-II formation. *J Cell Sci* **117**: 2805-2812.

Kamentsky L, Jones TR, Fraser A, Bray MA, Logan DJ, Madden KL, Ljosa V, Rueden C, Eliceiri KW, Carpenter AE. 2011. Improved structure, function and compatibility for CellProfiler: modular high-throughput image analysis software. *Bioinformatics* **27**: 1179-1180.

Katoh K, Shibata H, Hatta K, Maki M. 2004a. CHMP4b is a major binding partner of the ALG-2-interacting protein Alix among the three CHMP4 isoforms. *Arch Biochem Biophys* **421**: 159-165.

Katoh K, Shibata H, Suzuki H, Nara A, Ishidoh K, Kominami E, Yoshimori T, Maki M. 2003. The ALG-2-interacting protein Alix associates with CHMP4b, a human homologue of yeast Snf7 that is involved in multivesicular body sorting. *J Biol Chem* **278**: 39104-39113.

Katoh Y, Shiba Y, Mitsuhashi H, Yanagida Y, Takatsu H, Nakayama K. 2004b. Tollip and Tom1 form a complex and recruit ubiquitin-conjugated proteins onto early endosomes. *J Biol Chem* **279**: 24435-24443.

Katzmann DJ, Babst M, Emr SD. 2001. Ubiquitin-dependent sorting into the multivesicular body pathway requires the function of a conserved endosomal protein sorting complex, ESCRT-I. *Cell* **106**: 145-155.

Katzmann DJ, Stefan CJ, Babst M, Emr SD. 2003. Vps27 recruits ESCRT machinery to endosomes during MVB sorting. *J Cell Biol* **162**: 413-423.

Keren-Kaplan T, Attali I, Estrin M, Kuo LS, Farkash E, Jerabek-Willemsen M, Blutraich N, Artzi S, Peri A, Freed EO et al. 2013. Structure-based in silico identification of ubiquitin-binding domains provides insights into the ALIX-V:ubiquitin complex and retrovirus budding. *EMBO J* **32**: 538-551.

Kharitidi D, Apaja PM, Manteghi S, Suzuki K, Malitskaya E, Roldan A, Gingras MC, Takagi J, Lukacs GL, Pause A. 2015. Interplay of Endosomal pH and Ligand Occupancy in Integrin alpha5beta1 Ubiquitination, Endocytic Sorting, and Cell Migration. *Cell Rep* **13**: 599-609.

Kieffer C, Skalicky JJ, Morita E, De Domenico I, Ward DM, Kaplan J, Sundquist WI. 2008. Two distinct modes of ESCRT-III recognition are required for VPS4 functions in lysosomal protein targeting and HIV-1 budding. *Dev Cell* **15**: 62-73.

Kim J, Sitaraman S, Hierro A, Beach BM, Odorizzi G, Hurley JH. 2005. Structural basis for endosomal targeting by the Bro1 domain. *Dev Cell* **8**: 937-947.

Kobayashi T, Stang E, Fang KS, de Moerloose P, Parton RG, Gruenberg J. 1998. A lipid associated with the antiphospholipid syndrome regulates endosome structure and function. *Nature* **392**: 193-197.

Kolling R, Hollenberg CP. 1994. The ABC-transporter Ste6 accumulates in the plasma membrane in a ubiquitinated form in endocytosis mutants. *EMBO J* **13**: 3261-3271.

Koo EH, Squazzo SL. 1994. Evidence that production and release of amyloid beta-protein involves the endocytic pathway. *J Biol Chem* **269**: 17386-17389.

Kowal J, Tkach M, Thery C. 2014. Biogenesis and secretion of exosomes. *Curr Opin Cell Biol* **29**: 116-125.

Kranz A, Kinner A, Kolling R. 2001. A family of small coiled-coil-forming proteins functioning at the late endosome in yeast. *Mol Biol Cell* **12**: 711-723.

Krick R, Henke S, Tolstrup J, Thumm M. 2008. Dissecting the localization and function of Atg18, Atg21 and Ygr223c. *Autophagy* **4**: 896-910.

Kummel D, Ungermann C. 2014. Principles of membrane tethering and fusion in endosome and lysosome biogenesis. *Curr Opin Cell Biol* **29**: 61-66.

Langdon WY, Hartley JW, Klinken SP, Ruscetti SK, Morse HC, 3rd. 1989a. v-cbl, an oncogene from a dual-recombinant murine retrovirus that induces early B-lineage lymphomas. *Proc Natl Acad Sci U S A* **86**: 1168-1172.

Langdon WY, Hyland CD, Grumont RJ, Morse HC, 3rd. 1989b. The c-cbl proto-oncogene is preferentially expressed in thymus and testis tissue and encodes a nuclear protein. *J Virol* **63**: 5420-5424.

Langelier C, von Schwedler UK, Fisher RD, De Domenico I, White PL, Hill CP, Kaplan J, Ward D, Sundquist WI. 2006. Human ESCRT-II complex and its role in human immunodeficiency virus type 1 release. *J Virol* **80**: 9465-9480.

Lawe DC, Chawla A, Merithew E, Dumas J, Carrington W, Fogarty K, Lifshitz L, Tuft R, Lambright D, Corvera S. 2002. Sequential roles for phosphatidylinositol 3-phosphate and Rab5 in tethering and fusion of early endosomes via their interaction with EEA1. *J Biol Chem* **277**: 8611-8617.

Le Blanc I, Luyet PP, Pons V, Ferguson C, Emans N, Petiot A, Mayran N, Demaurex N, Faure J, Sadoul R et al. 2005. Endosome-to-cytosol transport of viral nucleocapsids. *Nat Cell Biol* **7**: 653-664.

Lebrand C, Corti M, Goodson H, Cosson P, Cavalli V, Mayran N, Faure J, Gruenberg J. 2002. Late endosome motility depends on lipids via the small GTPase Rab7. *EMBO J* **21**: 1289-1300.

Lee IH, Kai H, Carlson LA, Groves JT, Hurley JH. 2015. Negative membrane curvature catalyzes nucleation of endosomal sorting complex required for transport (ESCRT)-III assembly. *Proc Natl Acad Sci U S A* **112**: 15892-15897.

Lee J, Oh KJ, Lee D, Kim BY, Choi JS, Ku B, Kim SJ. 2016. Structural Study of the HD-PTP Bro1 Domain in a Complex with the Core Region of STAM2, a Subunit of ESCRT-0. *PLoS One* **11**: e0149113.

Lee JA, Beigneux A, Ahmad ST, Young SG, Gao FB. 2007. ESCRT-III dysfunction causes autophagosome accumulation and neurodegeneration. *Curr Biol* **17**: 1561-1567.

Leung KF, Dacks JB, Field MC. 2008. Evolution of the multivesicular body ESCRT machinery; retention across the eukaryotic lineage. *Traffic* **9**: 1698-1716.

Levine TP, Munro S. 2002. Targeting of Golgi-specific pleckstrin homology domains involves both PtdIns 4-kinase-dependent and -independent components. *Curr Biol* **12**: 695-704.

Levkowitz G, Waterman H, Ettenberg SA, Katz M, Tsygankov AY, Alroy I, Lavi S, Iwai K, Reiss Y, Ciechanover A et al. 1999. Ubiquitin ligase activity and tyrosine phosphorylation underlie suppression of growth factor signaling by c-Cbl/Sli-1. *Mol Cell* **4**: 1029-1040.

Levkowitz G, Waterman H, Zamir E, Kam Z, Oved S, Langdon WY, Beguinot L, Geiger B, Yarden Y. 1998. c-Cbl/Sli-1 regulates endocytic sorting and ubiquitination of the epidermal growth factor receptor. *Genes Dev* **12**: 3663-3674.

Liscum L, Ruggiero RM, Faust JR. 1989. The intracellular transport of low density lipoprotein-derived cholesterol is defective in Niemann-Pick type C fibroblasts. *J Cell Biol* **108**: 1625-1636.

Lorente-Rodriguez A, Barlowe C. 2011. Requirement for Golgi-localized PI(4)P in fusion of COPII vesicles with Golgi compartments. *Mol Biol Cell* **22**: 216-229.

Luhtala N, Odorizzi G. 2004. Bro1 coordinates deubiquitination in the multivesicular body pathway by recruiting Doa4 to endosomes. *J Cell Biol* **166**: 717-729.

Ma H, Wardega P, Mazaud D, Klosowska-Wardega A, Jurek A, Engstrom U, Lennartsson J, Heldin CH. 2015. Histidine-domain-containing protein tyrosine phosphatase regulates platelet-derived growth factor receptor intracellular sorting and degradation. *Cell Signal* **27**: 2209-2219.

MacDonald E, Urbe S, Clague MJ. 2014. USP8 controls the trafficking and sorting of lysosomal enzymes. *Traffic* **15**: 879-888.

Maejima I, Takahashi A, Omori H, Kimura T, Takabatake Y, Saitoh T, Yamamoto A, Hamasaki M, Noda T, Isaka Y et al. 2013. Autophagy sequesters damaged lysosomes to control lysosomal biogenesis and kidney injury. *EMBO J* **32**: 2336-2347.

Mageswaran SK, Dixon MG, Curtiss M, Keener JP, Babst M. 2014. Binding to any ESCRT can mediate ubiquitin-independent cargo sorting. *Traffic* **15**: 212-229.

Mageswaran SK, Johnson NK, Odorizzi G, Babst M. 2015. Constitutively active ESCRT-II suppresses the MVB-sorting phenotype of ESCRT-0 and ESCRT-I mutants. *Mol Biol Cell* **26**: 554-568.

Malerod L, Stuffers S, Brech A, Stenmark H. 2007. Vps22/EAP30 in ESCRT-II mediates endosomal sorting of growth factor and chemokine receptors destined for lysosomal degradation. *Traffic* **8**: 1617-1629.

Marley A, von Zastrow M. 2010. Dysbindin promotes the post-endocytic sorting of G protein-coupled receptors to lysosomes. *PLoS One* **5**: e9325.

Marmor MD, Yarden Y. 2004. Role of protein ubiquitylation in regulating endocytosis of receptor tyrosine kinases. *Oncogene* **23**: 2057-2070.

Martin-Serrano J, Yarovoy A, Perez-Caballero D, Bieniasz PD. 2003. Divergent retroviral late-budding domains recruit vacuolar protein sorting factors by using alternative adaptor proteins. *Proc Natl Acad Sci U S A* **100**: 12414-12419.

Martin-Serrano J, Zang T, Bieniasz PD. 2001. HIV-1 and Ebola virus encode small peptide motifs that recruit Tsg101 to sites of particle assembly to facilitate egress. *Nat Med* **7**: 1313-1319.

Matsudaira T, Mukai K, Noguchi T, Hasegawa J, Hatta T, Iemura SI, Natsume T, Miyamura N, Nishina H, Nakayama J et al. 2017. Endosomal phosphatidylserine is critical for the YAP signalling pathway in proliferating cells. *Nat Commun* **8**: 1246.

Matsuo H, Chevallier J, Mayran N, Le Blanc I, Ferguson C, Faure J, Blanc NS, Matile S, Dubochet J, Sadoul R et al. 2004. Role of LBPA and Alix in multivesicular liposome formation and endosome organization. *Science* **303**: 531-534.

Maziere JC, Maziere C, Mora L, Lageron A, Polonovski C, Polonovski J. 1986. [Changes in the biosynthesis, esterification and efflux of cholesterol in fibroblasts in culture from patients with Niemann-Pick disease type C]. *C R Seances Soc Biol Fil* **180**: 669-676.

McCullough J, Fisher RD, Whitby FG, Sundquist WI, Hill CP. 2008. ALIX-CHMP4 interactions in the human ESCRT pathway. *Proc Natl Acad Sci U S A* **105**: 7687-7691.

Meng B, Ip NC, Prestwood LJ, Abbink TE, Lever AM. 2015. Evidence that the endosomal sorting complex required for transport-II (ESCRT-II) is required for efficient human immunodeficiency virus-1 (HIV-1) production. *Retrovirology* **12**: 72.

Meyer HH, Wang Y, Warren G. 2002. Direct binding of ubiquitin conjugates by the mammalian p97 adaptor complexes, p47 and Ufd1-Npl4. *EMBO J* **21**: 5645-5652.

Michelet X, Djeddi A, Legouis R. 2010. Developmental and cellular functions of the ESCRT machinery in pluricellular organisms. *Biol Cell* **102**: 191-202.

Mierzwa B, Chiaruttini N, Redondo-Morata L, Moser von Filseck J, König J, Larios J, Poser I, Müller-Reichert T, Scheuring S, Roux A et al. 2017. Dynamic subunit turnover in ESCRT-III assemblies is regulated by Vps4 to mediate membrane remodelling during cytokinesis. *Nature Cell Biology* **in press**.

Miranda AM, Lasiecka ZM, Xu Y, Neufeld J, Shahriar S, Simoes S, Chan RB, Oliveira TG, Small SA, Di Paolo G. 2018. Neuronal lysosomal dysfunction releases exosomes harboring APP C-terminal fragments and unique lipid signatures. *Nat Commun* **9**: 291.

Miyake S, Mullane-Robinson KP, Lill NL, Douillard P, Band H. 1999. Cbl-mediated negative regulation of platelet-derived growth factor receptor-dependent cell proliferation. A critical role for Cbl tyrosine kinase-binding domain. *J Biol Chem* **274**: 16619-16628.

Mohapatra B, Ahmad G, Nadeau S, Zutshi N, An W, Scheffe S, Dong L, Feng D, Goetz B, Arya P et al. 2013. Protein tyrosine kinase regulation by ubiquitination: critical roles of Cbl-family ubiquitin ligases. *Biochim Biophys Acta* **1833**: 122-139.

Morel E, Chamoun Z, Lasiecka ZM, Chan RB, Williamson RL, Vetanovetz C, Dall'Armi C, Simoes S, Point Du Jour KS, McCabe BD et al. 2013. Phosphatidylinositol-3-phosphate regulates sorting and processing of amyloid precursor protein through the endosomal system. *Nat Commun* **4**: 2250.

Morel E, Parton RG, Gruenberg J. 2009. Annexin A2-dependent polymerization of actin mediates endosome biogenesis. *Dev Cell* **16**: 445-457.

Morita E, Sandrin V, Chung HY, Morham SG, Gygi SP, Rodesch CK, Sundquist WI. 2007. Human ESCRT and ALIX proteins interact with proteins of the midbody and function in cytokinesis. *EMBO J* **26**: 4215-4227.

Muller UC, Zheng H. 2012. Physiological functions of APP family proteins. *Cold Spring Harb Perspect Med* **2**: a006288.

Mund T, Pelham HR. 2009. Control of the activity of WW-HECT domain E3 ubiquitin ligases by NDFIP proteins. *EMBO Rep* **10**: 501-507.

Muriel O, Scott CC, Larios J, Mercier V, Gruenberg J. 2017. In Vitro Polymerization of F-actin on Early Endosomes. *J Vis Exp*.

Muriel O, Tomas A, Scott CC, Gruenberg J. 2016. Moesin and cortactin control actin-dependent multivesicular endosome biogenesis. *Mol Biol Cell* **27**: 3305-3316.

Murphy MP, LeVine H, 3rd. 2010. Alzheimer's disease and the amyloid-beta peptide. *J Alzheimers Dis* **19**: 311-323.

Murrow L, Debnath J. 2015. ATG12-ATG3 connects basal autophagy and late endosome function. *Autophagy* **11**: 961-962.

Murrow L, Malhotra R, Debnath J. 2015. ATG12-ATG3 interacts with Alix to promote basal autophagic flux and late endosome function. *Nat Cell Biol* **17**: 300-310.

Myromslien FD, Grovdal LM, Raiborg C, Stenmark H, Madshus IH, Stang E. 2006. Both clathrin-positive and -negative coats are involved in endosomal sorting of the EGF receptor. *Exp Cell Res* **312**: 3036-3048.

Naureckiene S, Sleat DE, Lackland H, Fensom A, Vanier MT, Wattiaux R, Jadot M, Lobel P. 2000. Identification of HE1 as the second gene of Niemann-Pick C disease. *Science* **290**: 2298-2301.

Nickerson DP, West M, Odorizzi G. 2006. Did2 coordinates Vps4-mediated dissociation of ESCRT-III from endosomes. *J Cell Biol* **175**: 715-720.

Nielsen E, Christoforidis S, Uttenweiler-Joseph S, Miaczynska M, Dewitte F, Wilm M, Hoflack B, Zerial M. 2000. Rabenosyn-5, a novel Rab5 effector, is complexed with hVPS45 and recruited to endosomes through a FYVE finger domain. *J Cell Biol* **151**: 601-612.

Nikko E, Andre B. 2007. Split-ubiquitin two-hybrid assay to analyze protein-protein interactions at the endosome: application to Saccharomyces cerevisiae Bro1 interacting with ESCRT complexes, the Doa4 ubiquitin hydrolase, and the Rsp5 ubiquitin ligase. *Eukaryot Cell* **6**: 1266-1277.

Nishida E, Muneyuki E, Maekawa S, Ohta Y, Sakai H. 1985. An actin-depolymerizing protein (destrin) from porcine kidney. Its action on F-actin containing or lacking tropomyosin. *Biochemistry* **24**: 6624-6630.

Nour AM, Modis Y. 2014. Endosomal vesicles as vehicles for viral genomes. *Trends Cell Biol* **24**: 449-454.

Obita T, Saksena S, Ghazi-Tabatabai S, Gill DJ, Perisic O, Emr SD, Williams RL. 2007. Structural basis for selective recognition of ESCRT-III by the AAA ATPase Vps4. *Nature* **449**: 735-739.

Odorizzi G, Babst M, Emr SD. 1998. Fab1p PtdIns(3)P 5-kinase function essential for protein sorting in the multivesicular body. *Cell* **95**: 847-858.

Odorizzi G, Katzmann DJ, Babst M, Audhya A, Emr SD. 2003. Bro1 is an endosome-associated protein that functions in the MVB pathway in Saccharomyces cerevisiae. *J Cell Sci* **116**: 1893-1903.

Ohya T, Miaczynska M, Coskun U, Lommer B, Runge A, Drechsel D, Kalaidzidis Y, Zerial M. 2009. Reconstitution of Rab- and SNARE-dependent membrane fusion by synthetic endosomes. *Nature* **459**: 1091-1097.

Oikawa T, Yamaguchi H, Itoh T, Kato M, Ijuin T, Yamazaki D, Suetsugu S, Takenawa T. 2004. PtdIns(3,4,5)P3 binding is necessary for WAVE2-induced formation of lamellipodia. *Nat Cell Biol* **6**: 420-426.

Okazaki S, Kato R, Uchida Y, Taguchi T, Arai H, Wakatsuki S. 2012. Structural basis of the strict phospholipid binding specificity of the pleckstrin homology domain of human evectin-2. *Acta Crystallogr D Biol Crystallogr* **68**: 117-123.

Olmos Y, Hodgson L, Mantell J, Verkade P, Carlton JG. 2015. ESCRT-III controls nuclear envelope reformation. *Nature* **522**: 236-239.

Olmos Y, Perdrix-Rosell A, Carlton JG. 2016. Membrane Binding by CHMP7 Coordinates ESCRT-III-Dependent Nuclear Envelope Reformation. *Curr Biol* **26**: 2635-2641.

Ono S. 2017. Functions of actin-interacting protein 1 (AIP1)/WD repeat protein 1 (WDR1) in actin filament dynamics and cytoskeletal regulation. *Biochem Biophys Res Commun*.

Ostrowicz CW, Brocker C, Ahnert F, Nordmann M, Lachmann J, Peplowska K, Perz A, Auffarth K, Engelbrecht-Vandre S, Ungermann C. 2010. Defined subunit arrangement and rab interactions are required for functionality of the HOPS tethering complex. *Traffic* **11**: 1334-1346.

Ostrowski M, Carmo NB, Krumeich S, Fanget I, Raposo G, Savina A, Moita CF, Schauer K, Hume AN, Freitas RP et al. 2010. Rab27a and Rab27b control different steps of the exosome secretion pathway. *Nat Cell Biol* **12**: 19-30; sup pp 11-13.

Parkinson MD, Piper SC, Bright NA, Evans JL, Boname JM, Bowers K, Lehner PJ, Luzio JP. 2015. A non-canonical ESCRT pathway, including histidine domain phosphotyrosine phosphatase (HD-PTP), is used for down-regulation of virally ubiquitinated MHC class I. *Biochem J* **471**: 79-88.

Pashkova N, Gakhar L, Winistorfer SC, Sunshine AB, Rich M, Dunham MJ, Yu L, Piper RC. 2013. The yeast Alix homolog Bro1 functions as a ubiquitin receptor for protein sorting into multivesicular endosomes. *Dev Cell* **25**: 520-533.

Peplowska K, Markgraf DF, Ostrowicz CW, Bange G, Ungermann C. 2007. The CORVET tethering complex interacts with the yeast Rab5 homolog Vps21 and is involved in endo-lysosomal biogenesis. *Dev Cell* **12**: 739-750.

Piper RC, Cooper AA, Yang H, Stevens TH. 1995. VPS27 controls vacuolar and endocytic traffic through a prevacuolar compartment in Saccharomyces cerevisiae. *J Cell Biol* **131**: 603-617.

Piper RC, Dikic I, Lukacs GL. 2014. Ubiquitin-dependent sorting in endocytosis. *Cold Spring Harb Perspect Biol* **6**.

Pires R, Hartlieb B, Signor L, Schoehn G, Lata S, Roessle M, Moriscot C, Popov S, Hinz A, Jamin M et al. 2009. A crescent-shaped ALIX dimer targets ESCRT-III CHMP4 filaments. *Structure* **17**: 843-856.

Polo S, Sigismund S, Faretta M, Guidi M, Capua MR, Bossi G, Chen H, De Camilli P, Di Fiore PP. 2002. A single motif responsible for ubiquitin recognition and monoubiquitination in endocytic proteins. *Nature* **416**: 451-455.

Poser I, Sarov M, Hutchins JR, Heriche JK, Toyoda Y, Pozniakovsky A, Weigl D, Nitzsche A, Hegemann B, Bird AW et al. 2008. BAC TransgeneOmics: a high-throughput method for exploration of protein function in mammals. *Nat Methods* **5**: 409-415.

Price A, Wickner W, Ungermann C. 2000. Proteins needed for vesicle budding from the golgi complex are also required for the docking step of homotypic vacuole fusion. *Journal of Cell Biology* **148**: 1223-1229.

Puthenveedu MA, Lauffer B, Temkin P, Vistein R, Carlton P, Thorn K, Taunton J, Weiner OD, Parton RG, von Zastrow M. 2010. Sequence-dependent sorting of recycling proteins by actin-stabilized endosomal microdomains. *Cell* **143**: 761-773.

Raab M, Gentili M, de Belly H, Thiam H-R, Vargas P, Jimenez AJ, Lautenschlaeger F, Voituriez R, Lennon-Duménil A-M, Manel N et al. 2016. ESCRT III repairs nuclear envelope ruptures during cell migration to limit DNA damage and cell death. *Science* **352**: 359.

Raiborg C, Bache KG, Gillooly DJ, Madshus IH, Stang E, Stenmark H. 2002. Hrs sorts ubiquitinated proteins into clathrin-coated microdomains of early endosomes. *Nat Cell Biol* **4**: 394-398.

Raiborg C, Bache KG, Mehlum A, Stang E, Stenmark H. 2001a. Hrs recruits clathrin to early endosomes. *EMBO J* **20**: 5008-5021.

Raiborg C, Bremnes B, Mehlum A, Gillooly DJ, D'Arrigo A, Stang E, Stenmark H. 2001b. FYVE and coiled-coil domains determine the specific localisation of Hrs to early endosomes. *J Cell Sci* **114**: 2255-2263.

Raiborg C, Malerod L, Pedersen NM, Stenmark H. 2008. Differential functions of Hrs and ESCRT proteins in endocytic membrane trafficking. *Exp Cell Res* **314**: 801-813.

Raiborg C, Schink KO, Stenmark H. 2013. Class III phosphatidylinositol 3-kinase and its catalytic product PtdIns3P in regulation of endocytic membrane traffic. *FEBS J* **280**: 2730-2742.

Raiborg C, Wesche J, Malerod L, Stenmark H. 2006. Flat clathrin coats on endosomes mediate degradative protein sorting by scaffolding Hrs in dynamic microdomains. *J Cell Sci* **119**: 2414-2424.

Rajendran L, Honsho M, Zahn TR, Keller P, Geiger KD, Verkade P, Simons K. 2006. Alzheimer's disease beta-amyloid peptides are released in association with exosomes. *Proc Natl Acad Sci U S A* **103**: 11172-11177.

Raposo G, Nijman HW, Stoorvogel W, Liejendekker R, Harding CV, Melief CJ, Geuze HJ. 1996. B lymphocytes secrete antigen-presenting vesicles. *J Exp Med* **183**: 1161-1172.

Raposo G, Tenza D, Mecheri S, Peronet R, Bonnerot C, Desaymard C. 1997. Accumulation of major histocompatibility complex class II molecules in mast cell secretory granules and their release upon degranulation. *Mol Biol Cell* **8**: 2631-2645.

Raymond CK, Howald-Stevenson I, Vater CA, Stevens TH. 1992. Morphological classification of the yeast vacuolar protein sorting mutants: evidence for a prevacuolar compartment in class E vps mutants. *Mol Biol Cell* **3**: 1389-1402.

Razi M, Futter CE. 2006. Distinct roles for Tsg101 and Hrs in multivesicular body formation and inward vesiculation. *Mol Biol Cell* **17**: 3469-3483.

Reiss AB, Arain HA, Stecker MM, Siegart NM, Kasselman LJ. 2018. Amyloid toxicity in Alzheimer's disease. *Rev Neurosci*.

Richter C, West M, Odorizzi G. 2007. Dual mechanisms specify Doa4-mediated deubiquitination at multivesicular bodies. *EMBO J* **26**: 2454-2464.

Rieder SE, Banta LM, Kohrer K, McCaffery JM, Emr SD. 1996. Multilamellar endosome-like compartment accumulates in the yeast vps28 vacuolar protein sorting mutant. *Mol Biol Cell* **7**: 985-999.

Rieder SE, Emr SD. 1997. A novel RING finger protein complex essential for a late step in protein transport to the yeast vacuole. *Mol Biol Cell* **8**: 2307-2327.

Robinson JS, Klionsky DJ, Banta LM, Emr SD. 1988. Protein sorting in Saccharomyces cerevisiae: isolation of mutants defective in the delivery and processing of multiple vacuolar hydrolases. *Mol Cell Biol* **8**: 4936-4948.

Rohde G, Wenzel D, Haucke V. 2002. A phosphatidylinositol (4,5)-bisphosphate binding site within mu2-adaptin regulates clathrin-mediated endocytosis. *J Cell Biol* **158**: 209-214.

Rothman JH, Howald I, Stevens TH. 1989. Characterization of genes required for protein sorting and vacuolar function in the yeast Saccharomyces cerevisiae. *EMBO J* **8**: 2057-2065.

Rothman JH, Stevens TH. 1986. Protein sorting in yeast: mutants defective in vacuole biogenesis mislocalize vacuolar proteins into the late secretory pathway. *Cell* **47**: 1041-1051.

Rotin D, Kumar S. 2009. Physiological functions of the HECT family of ubiquitin ligases. *Nat Rev Mol Cell Biol* **10**: 398-409.

Roucourt B, Meeussen S, Bao J, Zimmermann P, David G. 2015. Heparanase activates the syndecan-syntenin-ALIX exosome pathway. *Cell Res* **25**: 412-428.

Rusten TE, Simonsen A. 2008. ESCRT functions in autophagy and associated disease. *Cell Cycle* **7**: 1166-1172.

Sachse M, Strous GJ, Klumperman J. 2004. ATPase-deficient hVPS4 impairs formation of internal endosomal vesicles and stabilizes bilayered clathrin coats on endosomal vacuoles. *J Cell Sci* **117**: 1699-1708.

Sachse M, Urbe S, Oorschot V, Strous GJ, Klumperman J. 2002. Bilayered clathrin coats on endosomal vacuoles are involved in protein sorting toward lysosomes. *Mol Biol Cell* **13**: 1313-1328.

Saksena S, Wahlman J, Teis D, Johnson AE, Emr SD. 2009. Functional reconstitution of ESCRT-III assembly and disassembly. *Cell* **136**: 97-109.

Savina A, Fader CM, Damiani MT, Colombo MI. 2005. Rab11 promotes docking and fusion of multivesicular bodies in a calcium-dependent manner. *Traffic* **6**: 131-143.

Schaaf MB, Keulers TG, Vooijs MA, Rouschop KM. 2016. LC3/GABARAP family proteins: autophagy-(un)related functions. *FASEB J* **30**: 3961-3978.

Scheffer LL, Sreetama SC, Sharma N, Medikayala S, Brown KJ, Defour A, Jaiswal JK. 2014. Mechanism of Ca(2)(+)-triggered ESCRT assembly and regulation of cell membrane repair. *Nat Commun* **5**: 5646.

Schink KO, Tan KW, Stenmark H. 2016. Phosphoinositides in Control of Membrane Dynamics. *Annu Rev Cell Dev Biol* **32**: 143-171.

Scott CC, Vacca F, Gruenberg J. 2014. Endosome maturation, transport and functions. *Semin Cell Dev Biol* **31**: 2-10.

Seals DF, Eitzen G, Margolis N, Wickner WT, Price A. 2000. A Ypt/Rab effector complex containing the Sec1 homolog Vps33p is required for homotypic vacuole fusion. *Proc Natl Acad Sci U S A* **97**: 9402-9407.

Sen A, Madhivanan K, Mukherjee D, Aguilar RC. 2012. The epsin protein family: coordinators of endocytosis and signaling. *Biomol Concepts* **3**: 117-126.

Sette P, Mu R, Dussupt V, Jiang J, Snyder G, Smith P, Xiao TS, Bouamr F. 2011. The Phe105 loop of Alix Bro1 domain plays a key role in HIV-1 release. *Structure* **19**: 1485-1495.

Shenoy SK, McDonald PH, Kohout TA, Lefkowitz RJ. 2001. Regulation of receptor fate by ubiquitination of activated beta 2-adrenergic receptor and beta-arrestin. *Science* **294**: 1307-1313.

Shields SB, Piper RC. 2011. How ubiquitin functions with ESCRTs. *Traffic* **12**: 1306-1317.

Shih SC, Katzmann DJ, Schnell JD, Sutanto M, Emr SD, Hicke L. 2002. Epsins and Vps27p/Hrs contain ubiquitin-binding domains that function in receptor endocytosis. *Nat Cell Biol* **4**: 389-393.

Shim S, Kimpler LA, Hanson PI. 2007. Structure/function analysis of four core ESCRT-III proteins reveals common regulatory role for extreme C-terminal domain. *Traffic* **8**: 1068-1079.

Shimizu M, Oguro-Ando A, Ohoto-Fujita E, Atomi Y. 2014. Toll-interacting protein pathway: degradation of an ubiquitin-binding protein. *Methods Enzymol* **534**: 323-330.

Simons K, Ehehalt R. 2002. Cholesterol, lipid rafts, and disease. *J Clin Invest* **110**: 597-603.

Simons K, Vaz WL. 2004. Model systems, lipid rafts, and cell membranes. *Annu Rev Biophys Biomol Struct* **33**: 269-295.

Simons M, Raposo G. 2009. Exosomes--vesicular carriers for intercellular communication. *Curr Opin Cell Biol* **21**: 575-581.

Simonsen A, Lippe R, Christoforidis S, Gaullier JM, Brech A, Callaghan J, Toh BH, Murphy C, Zerial M, Stenmark H. 1998. EEA1 links PI(3)K function to Rab5 regulation of endosome fusion. *Nature* **394**: 494-498.

Slagsvold T, Aasland R, Hirano S, Bache KG, Raiborg C, Trambaiolo D, Wakatsuki S, Stenmark H. 2005. Eap45 in mammalian ESCRT-II binds ubiquitin via a phosphoinositide-interacting GLUE domain. *J Biol Chem* **280**: 19600-19606.

Smit JJ, Sixma TK. 2014. RBR E3-ligases at work. *EMBO Rep* **15**: 142-154.

Sobo K, Le Blanc I, Luyet PP, Fivaz M, Ferguson C, Parton RG, Gruenberg J, van der Goot FG. 2007. Late endosomal cholesterol accumulation leads to impaired intra-endosomal trafficking. *PLoS One* **2**: e851.

Steinman RM, Mellman IS, Muller WA, Cohn ZA. 1983. Endocytosis and the recycling of plasma membrane. *J Cell Biol* **96**: 1-27.

Stoten CL, Carlton JG. 2018. ESCRT-dependent control of membrane remodelling during cell division. *Semin Cell Dev Biol* **74**: 50-65.

Strack B, Calistri A, Craig S, Popova E, Göttlinger HG. 2003. AIP1/ALIX Is a Binding Partner for HIV-1 p6 and EIAV p9 Functioning in Virus Budding. *Cell* **114**: 689-699.

Stringer DK, Piper RC. 2011. A single ubiquitin is sufficient for cargo protein entry into MVBs in the absence of ESCRT ubiquitination. *Journal of Cell Biology* **192**: 229-242.

Stuchell-Brereton MD, Skalicky JJ, Kieffer C, Karren MA, Ghaffarian S, Sundquist WI. 2007. ESCRT-III recognition by VPS4 ATPases. *Nature* **449**: 740-744.

Subra C, Laulagnier K, Perret B, Record M. 2007. Exosome lipidomics unravels lipid sorting at the level of multivesicular bodies. *Biochimie* **89**: 205-212.

Sun S, Sun L, Zhou X, Wu C, Wang R, Lin SH, Kuang J. 2016. Phosphorylation-Dependent Activation of the ESCRT Function of ALIX in Cytokinetic Abscission and Retroviral Budding. *Dev Cell* **36**: 331-343.

Sun S, Zhou X, Corvera J, Gallick GE, Lin SH, Kuang J. 2015. ALG-2 activates the MVB sorting function of ALIX through relieving its intramolecular interaction. *Cell Discov* **1**: 15018.

Swatek KN, Komander D. 2016. Ubiquitin modifications. *Cell Res* **26**: 399-422.

Tang S, Buchkovich NJ, Henne WM, Banjade S, Kim YJ, Emr SD. 2016. ESCRT-III activation by parallel action of ESCRT-I/II and ESCRT-0/Bro1 during MVB biogenesis. *Elife* **5**.

Tang S, Henne WM, Borbat PP, Buchkovich NJ, Freed JH, Mao Y, Fromme JC, Emr SD. 2015. Structural basis for activation, assembly and membrane binding of ESCRT-III Snf7 filaments. *Elife* **4**.

Tanowitz M, Von Zastrow M. 2002. Ubiquitination-independent trafficking of G protein-coupled receptors to lysosomes. *J Biol Chem* **277**: 50219-50222.

Taunton J, Rowning BA, Coughlin ML, Wu M, Moon RT, Mitchison TJ, Larabell CA. 2000. Actin-dependent propulsion of endosomes and lysosomes by recruitment of N-WASP. *J Cell Biol* **148**: 519-530.

Teis D, Saksena S, Emr SD. 2008. Ordered assembly of the ESCRT-III complex on endosomes is required to sequester cargo during MVB formation. *Dev Cell* **15**: 578-589.

Teis D, Saksena S, Judson BL, Emr SD. 2010. ESCRT-II coordinates the assembly of ESCRT-III filaments for cargo sorting and multivesicular body vesicle formation. *EMBO J* **29**: 871-883.

Teo H, Gill DJ, Sun J, Perisic O, Veprintsev DB, Vallis Y, Emr SD, Williams RL. 2006. ESCRT-I core and ESCRT-II GLUE domain structures reveal role for GLUE in linking to ESCRT-I and membranes. *Cell* **125**: 99-111.

Teo H, Perisic O, Gonzalez B, Williams RL. 2004. ESCRT-II, an endosome-associated complex required for protein sorting: crystal structure and interactions with ESCRT-III and membranes. *Dev Cell* **7**: 559-569.

Thery C, Amigorena S, Raposo G, Clayton A. 2006. Isolation and characterization of exosomes from cell culture supernatants and biological fluids. *Curr Protoc Cell Biol* **Chapter 3**: Unit 3 22.

Thery C, Boussac M, Veron P, Ricciardi-Castagnoli P, Raposo G, Garin J, Amigorena S. 2001. Proteomic analysis of dendritic cell-derived exosomes: a secreted subcellular compartment distinct from apoptotic vesicles. *J Immunol* **166**: 7309-7318.

Thery C, Regnault A, Garin J, Wolfers J, Zitvogel L, Ricciardi-Castagnoli P, Raposo G, Amigorena S. 1999. Molecular characterization of dendritic cell-derived exosomes. Selective accumulation of the heat shock protein hsc73. *J Cell Biol* **147**: 599-610.

Tomas A, Vaughan SO, Burgoyne T, Sorkin A, Hartley JA, Hochhauser D, Futter CE. 2015. WASH and Tsg101/ALIX-dependent diversion of stress-internalized EGFR from the canonical endocytic pathway. *Nat Commun* **6**: 7324.

Trajkovic K, Hsu C, Chiantia S, Rajendran L, Wenzel D, Wieland F, Schwille P, Brugger B, Simons M. 2008. Ceramide triggers budding of exosome vesicles into multivesicular endosomes. *Science* **319**: 1244-1247.

Uchida Y, Hasegawa J, Chinnapen D, Inoue T, Okazaki S, Kato R, Wakatsuki S, Misaki R, Koike M, Uchiyama Y et al. 2011. Intracellular phosphatidylserine is essential for retrograde membrane traffic through endosomes. *Proc Natl Acad Sci U S A* **108**: 15846-15851.

Ullrich O, Horiuchi H, Bucci C, Zerial M. 1994. Membrane association of Rab5 mediated by GDP-dissociation inhibitor and accompanied by GDP/GTP exchange. *Nature* **368**: 157-160.

Ullrich S, Munch A, Neumann S, Kremmer E, Tatzelt J, Lichtenthaler SF. 2010. The novel membrane protein TMEM59 modulates complex glycosylation, cell surface expression, and secretion of the amyloid precursor protein. *J Biol Chem* **285**: 20664-20674.

Umebayashi K, Stenmark H, Yoshimori T. 2008. Ubc4/5 and c-Cbl continue to ubiquitinate EGF receptor after internalization to facilitate polyubiquitination and degradation. *Mol Biol Cell* **19**: 3454-3462.

Usami Y, Popov S, Gottlinger HG. 2007. Potent rescue of human immunodeficiency virus type 1 late domain mutants by ALIX/AIP1 depends on its CHMP4 binding site. *J Virol* **81**: 6614-6622.

van Delft S, Schumacher C, Hage W, Verkleij AJ, van Bergen en Henegouwen PM. 1997. Association and colocalization of Eps15 with adaptor protein-2 and clathrin. *J Cell Biol* **136**: 811-821.

van Niel G, Charrin S, Simoes S, Romao M, Rochin L, Saftig P, Marks MS, Rubinstein E, Raposo G. 2011. The tetraspanin CD63 regulates ESCRT-independent and -dependent endosomal sorting during melanogenesis. *Dev Cell* **21**: 708-721.

Vietri M, Schink KO, Campsteijn C, Wegner CS, Schultz SW, Christ L, Thoresen SB, Brech A, Raiborg C, Stenmark H. 2015. Spastin and ESCRT-III coordinate mitotic spindle disassembly and nuclear envelope sealing. *Nature* **522**: 231-235.

Vingtdeux V, Hamdane M, Loyens A, Gele P, Drobeck H, Begard S, Galas MC, Delacourte A, Beauvillain JC, Buee L et al. 2007. Alkalizing drugs induce accumulation of amyloid precursor protein by-products in luminal vesicles of multivesicular bodies. *J Biol Chem* **282**: 18197-18205.

von Schwedler UK, Stuchell M, Müller B, Ward DM, Chung H-Y, Morita E, Wang HE, Davis T, He G-P, Cimbora DM et al. 2003. The Protein Network of HIV Budding. *Cell* **114**: 701-713.

Wang W, Struhl G. 2004. Drosophila Epsin mediates a select endocytic pathway that DSL ligands must enter to activate Notch. *Development* **131**: 5367-5380.

Weidberg H, Shvets E, Shpilka T, Shimron F, Shinder V, Elazar Z. 2010. LC3 and GATE-16/GABARAP subfamilies are both essential yet act differently in autophagosome biogenesis. *EMBO J* **29**: 1792-1802.

Welsch S, Habermann A, Jager S, Muller B, Krijnse-Locker J, Krausslich HG. 2006. Ultrastructural analysis of ESCRT proteins suggests a role for endosome-associated tubular-vesicular membranes in ESCRT function. *Traffic* **7**: 1551-1566.

Wemmer M, Azmi I, West M, Davies B, Katzmann D, Odorizzi G. 2011. Bro1 binding to Snf7 regulates ESCRT-III membrane scission activity in yeast. *J Cell Biol* **192**: 295-306.

Whitley P, Reaves BJ, Hashimoto M, Riley AM, Potter BV, Holman GD. 2003. Identification of mammalian Vps24p as an effector of phosphatidylinositol 3,5-bisphosphate-dependent endosome compartmentalization. *J Biol Chem* **278**: 38786-38795.

Williams RL, Urbe S. 2007. The emerging shape of the ESCRT machinery. *Nat Rev Mol Cell Biol* **8**: 355-368.

Williamson RL, Laulagnier K, Miranda AM, Fernandez MA, Wolfe MS, Sadoul R, Di Paolo G. 2017. Disruption of amyloid precursor protein ubiquitination selectively increases amyloid beta (Abeta) 40 levels via presenilin 2-mediated cleavage. *J Biol Chem* **292**: 19873-19889.

Wolfe BL, Marchese A, Trejo J. 2007. Ubiquitination differentially regulates clathrin-dependent internalization of protease-activated receptor-1. *J Cell Biol* **177**: 905-916.

Wollert T, Hurley JH. 2010. Molecular mechanism of multivesicular body biogenesis by ESCRT complexes. *Nature* **464**: 864-U873.

Wollert T, Wunder C, Lippincott-Schwartz J, Hurley JH. 2009. Membrane scission by the ESCRT-III complex. *Nature* **458**: 172-177.

Wolters N, Amerik A. 2015. The N-terminal domains determine cellular localization and functions of the Doa4 and Ubp5 deubiquitinating enzymes. *Biochem Biophys Res Commun* **467**: 570-576.

Wubbolts R, Leckie RS, Veenhuizen PT, Schwarzmann G, Mobius W, Hoernschemeyer J, Slot JW, Geuze HJ, Stoorvogel W. 2003. Proteomic and biochemical analyses of human B cell-derived exosomes. Potential implications for their function and multivesicular body formation. *J Biol Chem* **278**: 10963-10972.

Wurmser AE, Sato TK, Emr SD. 2000. New component of the vacuolar class C-Vps complex couples nucleotide exchange on the Ypt7 GTPase to SNARE-dependent docking and fusion. *J Cell Biol* **151**: 551-562.

Xiao J, Chen XW, Davies BA, Saltiel AR, Katzmann DJ, Xu Z. 2009. Structural basis of Ist1 function and Ist1-Did2 interaction in the multivesicular body pathway and cytokinesis. *Mol Biol Cell* **20**: 3514-3524.

Yamashiro DJ, Maxfield FR. 1987a. Acidification of Morphologically Distinct Endosomes in Mutant and Wild-Type Chinese-Hamster Ovary Cells. *Journal of Cell Biology* **105**: 2723-2733.

-. 1987b. Kinetics of endosome acidification in mutant and wild-type Chinese hamster ovary cells. *J Cell Biol* **105**: 2713-2721.

Yamashita Y, Kojima K, Tsukahara T, Agawa H, Yamada K, Amano Y, Kurotori N, Tanaka N, Sugamura K, Takeshita T. 2008. Ubiquitin-independent binding of Hrs mediates endosomal sorting of the interleukin-2 receptor beta-chain. *J Cell Sci* **121**: 1727-1738.

Yang B, Kumar S. 2010. Nedd4 and Nedd4-2: closely related ubiquitin-protein ligases with distinct physiological functions. *Cell Death Differ* **17**: 68-77.

Yang B, Stjepanovic G, Shen Q, Martin A, Hurley JH. 2015. Vps4 disassembles an ESCRT-III filament by global unfolding and processive translocation. *Nat Struct Mol Biol* **22**: 492-498.

Yeoh S, Pope B, Mannherz HG, Weeds A. 2002. Determining the differences in actin binding by human ADF and cofilin. *J Mol Biol* **315**: 911-925.

Yonezawa N, Nishida E, Sakai H. 1985. pH control of actin polymerization by cofilin. *J Biol Chem* **260**: 14410-14412.

Young ARJ, Narita M, Ferreira M, Kirschner K, Sadaie M, Darot JFJ, Tavare S, Arakawa S, Shimizu S, Watt FM et al. 2009. Autophagy mediates the mitotic senescence transition. *Gene Dev* **23**: 798-803.

Yu JW, Mendrola JM, Audhya A, Singh S, Keleti D, DeWald DB, Murray D, Emr SD, Lemmon MA. 2004. Genome-wide analysis of membrane targeting by S. cerevisiae pleckstrin homology domains. *Mol Cell* **13**: 677-688.

Zamborlini A, Usami Y, Radoshitzky SR, Popova E, Palu G, Gottlinger H. 2006. Release of autoinhibition converts ESCRT-III components into potent inhibitors of HIV-1 budding. *Proc Natl Acad Sci U S A* **103**: 19140-19145.

Zhai Q, Landesman MB, Chung HY, Dierkers A, Jeffries CM, Trewhella J, Hill CP, Sundquist WI. 2011. Activation of the retroviral budding factor ALIX. *J Virol* **85**: 9222-9226.

Zhang X, Song W. 2013. The role of APP and BACE1 trafficking in APP processing and amyloid-beta generation. *Alzheimers Res Ther* **5**: 46.

Zhou K, Blom T. 2015. Trafficking and Functions of Bioactive Sphingolipids: Lessons from Cells and Model Membranes. *Lipid Insights* **8**: 11-20.

Zhou X, Pan S, Sun L, Corvera J, Lee YC, Lin SH, Kuang J. 2009. The CHMP4b- and Src-docking sites in the Bro1 domain are autoinhibited in the native state of Alix. *Biochem J* **418**: 277-284.

Zhou X, Pan S, Sun L, Corvera J, Lin SH, Kuang J. 2008. The HIV-1 p6/EIAV p9 docking site in Alix is autoinhibited as revealed by a conformation-sensitive anti-Alix monoclonal antibody. *Biochem J* **414**: 215-220.

Zhou X, Si J, Corvera J, Gallick GE, Kuang J. 2010. Decoding the intrinsic mechanism that prohibits ALIX interaction with ESCRT and viral proteins. *Biochem J* **432**: 525-534.

Zhu L, Wang L, Luo X, Zhang Y, Ding Q, Jiang X, Wang X, Pan Y, Chen Y. 2012. Tollip, an intracellular trafficking protein, is a novel modulator of the transforming growth factor-beta signaling pathway. *J Biol Chem* **287**: 39653-39663.

Zick M, Wickner W. 2013. The tethering complex HOPS catalyzes assembly of the soluble SNARE Vam7 into fusogenic trans-SNARE complexes. *Molecular Biology of the Cell* **24**: 3746-3753.

Zimmermann P, Zhang Z, Degeest G, Mortier E, Leenaerts I, Coomans C, Schulz J, N'Kuli F, Courtoy PJ, David G. 2005. Syndecan recycling [corrected] is controlled by syntenin-PIP2 interaction and Arf6. *Dev Cell* **9**: 377-388.

Zitvogel L, Regnault A, Lozier A, Wolfers J, Flament C, Tenza D, Ricciardi-Castagnoli P, Raposo G, Amigorena S. 1998. Eradication of established murine tumors using a novel cell-free vaccine: dendritic cell-derived exosomes. *Nat Med* **4**: 594-600.